LOW DIMENSIONAL BAND-LIMITED FRAMELETS AND THEIR APPLICATIONS IN COLOUR IMAGE RESTORATION

HOU LIKUN

(B.Sc., USTC, China)

A THESIS SUBMITTED

FOR THE DEGREE OF DOCTOR OF PHILOSOPHY

DEPARTMENT OF MATHEMATICS

NATIONAL UNIVERSITY OF SINGAPORE

2013

To my parents

DECLARATION

I hereby declare that the thesis is my original work and it has been written by me in its entirety.

I have duly acknowledged all the sources of information which have been used in the thesis.

This thesis has also not been submitted for any degree in any university previously.

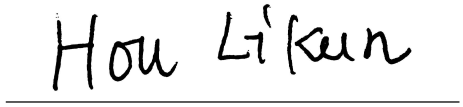

Hou Likun

April 2013

Acknowledgements

Firstly, I would like to express the sincerest thanks to my supervisor, Professor Shen Zuowei. Professor Shen is not only an outstanding figure in mathematical science, but also a person full of kindness and being supportive. In his research, he always sees through the fundamental things and has deep insight into the connections between different research fields. This way of thinking and doing mathematics has greatly influenced my research. Moreover, Professor Shen also encourages me to do research on my own, and helps me to cultivate self-confidence and independent thinking during our regular discussions. I feel a bit sorry for not meeting his expectations though. All in all, it could not be a greater honour to have him being my supervisor all through this PhD journey.

Secondly, I want to express great gratitude towards Professor Ji Hui for conducting our weekly seminars on image processing. Through those seminars I have gained a lot in both theoretical and applicational aspects. His profound knowledge, broad vision and critical thinking have greatly helped me in my research. Besides, it is a lifelong benefit to have the opportunity to do some research under his guidance as well. From him I got some valuable experiences, and under his

guidance I also learned the correct altitude towards doing research.

Thirdly, I want to thank the Department of Mathematics and National University Singapore for providing me good environment and scholarships for my research and study. I would also like to thank the Faculty of Science for funding me to attend the 8^{th} MPSGC in Thailand.

Lastly, I want to thank deeply to my friends and colleagues here for their encouragement and support. Many thanks to Dr. Pan Suqi, Dr. Jiang Kaifeng, Dr. Miao Weimin, Wang Kang, Li Jia, Gong Zheng, Zhou Junqi, Sun Xiang, Wang Yi, Ji Feng and Wu Bin. Without the company of you guys, this journey would be lonely and life would lose its colours.

Contents

Summary

This thesis consists of two major parts. The first part focuses on the theoretical study on the construction of band-limited framelets with good time-frequency localization property in low-dimensional Euclidean spaces. Based on the univariate Meyer's refinable function, this thesis provides a systematic approach to construct non-separable band-limited refinable functions, Riesz wavelets, orthonormal wavelets as well as wavelet tight frames (framelets) in 2D and 3D Euclidean spaces. With the newly constructed band-limited framelets in hand, the second part of the thesis focuses on the application of non-separable band-limited framelets and tensor-product spline framelets in colour image restoration. The main application explored in this thesis is on repairing over-exposed and under-exposed regions in regular digital colour photographs. By using wavelet tight frame based regularization methods and some tone mapping analogy, we develop in this thesis a comprehensive computational method to simultaneously (i) recover brightness values clipped due to over/under-exposure, (ii) enhance the contrast of under-exposed regions so that more visible image details could be revealed, and (iii) restore the chromatic values damaged due to over-exposure. Experimental results show that

the proposed method outperforms existing approaches in the test data set.

Basic Concepts and Notations

- In this thesis, we use $\mathbb{Z}$, $\mathbb{Z}^*$, $\mathbb{Z}^+$, $\mathbb{R}$ to denote the set of integers, nonnegative integers, positive integers, and real numbers respectively.

- For any positive integer N, we use $\mathbb{Z}_N$ to denote the quotient set $\mathbb{Z}/N\mathbb{Z}$ (or equivalently the set $\{0, 1, \cdots, N-1\}$).

- Cartesian product. Given n sets A_j, $j = 1, 2, \ldots, n$, we denote

$$A_1 \times A_2 \times \cdots \times A_n = \{(x_1, x_2, \ldots, x_n) : x_1 \in A_1, \ldots, x_n \in A_n\}.$$

  In particular, if $A_1 = A_2 = \cdots = A_n = A$, then we denote $A_1 \times A_2 \times \cdots \times A_n$ as A^n for simplicity.

- For any $d \in \mathbb{Z}^+$, we let $\mathbb{R}^d$ denote the d-dimensional Euclidean space with the inner product given by

$$x \cdot y = \sum_{j=1}^{d} x_j y_j, \text{ for } x = (x_1, \ldots, x_d) \text{ and } y = (y_1, \ldots, y_d) \in \mathbb{R}^d.$$

- For a countable index set $\mathcal{I}$, we let $\ell_p(\mathcal{I})$, $1 \leqslant p \leqslant \infty$, be the set of all complex-valued sequences on $\mathcal{I}$ such that

$$\|c\|_p := \begin{cases} \left(\sum_{k\in\mathcal{I}} |c(k)|^p\right)^{1/p} < \infty, & 1 \leqslant p < \infty; \\ \sup_{k\in\mathcal{I}} |c(k)| < \infty, & p = \infty. \end{cases}$$

- For any $n \in \mathbb{Z}^*$, we let $C^n(\mathbb{R}^d)$ denote the set of functions on $\mathbb{R}^d$ that have continuous derivatives up to order n, and $C^\infty(\mathbb{R}^d)$ denote the set $\bigcap_{n\in\mathbb{Z}^*} C^n(\mathbb{R}^d)$.

- $L_p(\mathbb{R}^d)$ $(1 \leqslant p \leqslant \infty)$ spaces. $L_p(\mathbb{R}^d)$ is the set of Lebesgue measurable functions on $\mathbb{R}^d$ such that

$$\|f\|_{L_p(\mathbb{R}^d)} := \begin{cases} \left(\int_{\mathbb{R}^d} |f(x)|^p dx\right)^{\frac{1}{p}} < \infty, & 1 \leqslant p < \infty; \\ \text{ess sup}\{|f(x)|, x \in \mathbb{R}^d\} < \infty, & p = \infty. \end{cases}$$

  In particular, when $p = 2$, the space $L_2(\mathbb{R}^d)$ is a Hilbert space with its norm induced by the inner product $\langle \cdot, \cdot \rangle$ defined as follows

$$\langle f, g\rangle = \int_{\mathbb{R}^d} f(x)\overline{g(x)}\, dx, \, \forall f, g \in L_2(\mathbb{R}^d),$$

  where $\overline{g(x)}$ is the complex conjugate of $g(x)$.

- Fourier transform. For any function $f \in L_1(\mathbb{R}^d)$, its Fourier transform $\widehat{f}$ is defined as

$$\widehat{f}(\xi) := \int_{\mathbb{R}^d} f(x) \exp(-i\xi \cdot x) dx, \quad \xi \in \mathbb{R}^d.$$

  The definition of Fourier transform can be naturally extended to $L_2(\mathbb{R}^d)$ as well as tempered distributions. Particularly, for any $f \in L_2(\mathbb{R}^d)$, one has the following Parseval's identity:

$$\|f\|^2_{L_2(\mathbb{R}^d)} = \frac{1}{(2\pi)^d} \|\widehat{f}|^2_{L_2(\mathbb{R}^d)}.$$

  So $f \in L_2(\mathbb{R}^d)$ if and only if $\widehat{f} \in L_2(\mathbb{R}^d)$. Moreover, Fourier transform is invertible in $L_2(\mathbb{R}^d)$, and the inversion formula is formally given by

$$f(x) = \frac{1}{(2\pi)^d} \int_{\mathbb{R}^d} \widehat{f}(\xi) \exp(ix \cdot \xi) d\xi, \, x \in \mathbb{R}^d.$$

- Discrete Fourier transform. Given a d-dimensional signal u defined on the grid $\mathbf{N} := \mathbb{Z}_{N_1} \times \mathbb{Z}_{N_2} \times \cdots \times \mathbb{Z}_{N_d}$, the discrete Fourier transform of u is a discrete signal $\mathcal{F}(u)$ defined on the grid $\mathbf{K} := (2\pi\mathbb{Z}_{N_1}/N_1) \times (2\pi\mathbb{Z}_{N_2}/N_2) \times \cdots \times (2\pi\mathbb{Z}_{N_d}/N_d)$ such that

$$\mathcal{F}(u)[\mathbf{k}] = \frac{1}{\sqrt{|\mathbf{N}|}} \sum_{\mathbf{n}\in\mathbf{N}} u[\mathbf{n}] \exp(i\mathbf{k}\cdot\mathbf{n}),$$

where $|\mathbf{N}| = N_1 N_2 \cdots N_d$. Discrete Fourier transform is also invertible: for any v define on the grid $\mathbf{K}$, its inverse discrete Fourier transform is

$$\mathcal{F}^{-1}(v)[\mathbf{n}] = \frac{1}{\sqrt{|\mathbf{N}|}} \sum_{\mathbf{k}\in\mathbf{K}} v[\mathbf{k}] \exp(-i\mathbf{n}\cdot\mathbf{k}),\ \forall \mathbf{n} \in \mathbf{N}.$$

- Circular convolution. Given two finite signals $u, v \in \mathbb{R}^{N_1} \times \mathbb{R}^{N_2} \times \cdots \times \mathbb{R}^{N_d}$, $N_n \in \mathbb{Z}^+$, $n = 1, \ldots, d$, their circular convolution $u \circledast v$ is a finite signal of dimension $N_1 \times N_2 \times \cdots \times N_d$ such that, for any $[k_1, k_2, \ldots, k_d]$ with $0 \leqslant k_i < N_i$, $i = 1, 2, \ldots, d$,

$$\begin{aligned} &u \circledast v[k_1, k_2, \ldots, k_d] \\ &= \sum_{n_1=0}^{N_1-1} \cdots \sum_{n_d=0}^{N_d-1} u_p[k_1 - n_1, k_2 - n_2, \ldots, k_d - n_d] v_p[n_1, n_2, \ldots, n_d], \end{aligned}$$

where u_p and v_p are the $N_1 \times N_2 \times \cdots \times N_d$-periodic extension of u and v respectively, i.e.

$$u_p[n_1, \ldots, n_d] = u[n_1 \bmod N_1, \ldots, n_d \bmod N_d]$$

and

$$v_p[n_1, \ldots, n_d] = v[n_1 \bmod N_1, \ldots, n_d \bmod N_d]$$

for any $[n_1, \ldots, n_d] \in \mathbb{Z}^d$.

- Fourier series and Fourier coefficients. For any $c \in \ell_2(\mathbb{Z}^d)$, its Fourier series $\widehat{c}$ is a 2π-periodic function defined by

$$\widehat{c}(\xi) = \sum_{k \in \mathbb{Z}^d} c[k] \exp(-ik \cdot \xi).$$

  Conversely, for any 2π-periodic function g, Fourier coefficients of g are formed by a sequence $c := \{c[k],\, k \in \mathbb{Z}^d\}$ such that

$$c[k] = \frac{1}{(2\pi)^d} \int_{[-\pi,\pi)^d} g(\xi) \exp(ik \cdot \xi) d\xi,\ k \in \mathbb{Z}^d.$$

- Bracket product. For any $f \in L_2(\mathbb{R}^d)$ and any $g \in L_2(\mathbb{R}^d)$, their bracket product $[f, g]$ defined as

$$[f, g](\xi) = \sum_{k \in \mathbb{Z}^d} f(\xi + 2\pi k)\overline{g(\xi + 2\pi k)},\ \forall \xi \in \mathbb{R}^d.$$

  In particular,

$$[f, f] = \sum_{k \in \mathbb{Z}^d} |f(\xi + 2\pi k)|^2.$$

  It is easy to see by definition that $[f, g]$ is 2π-periodic and $[f, g] \in L_1(\mathbb{T}^d)$, where $\mathbb{T}^d := \mathbb{R}^d/(2\pi\mathbb{Z}^d)$.

Chapter 1

Introduction

Wavelets, which have been a fast growing research topic in the last few decades, are a versatile tool that possesses both rich mathematical content and great potential for applications. The versatility of wavelets is reflected in its various understanding from different groups of researchers. For instance, some people view wavelets as bases for certain function spaces, and some people view wavelets as a tool for spatial-frequency analysis. In general, wavelets are a special type of oscillatory functions with good spatial-frequency localization property. The oscillation nature of wavelets make them effective in capturing discontinuities or sharp spikes in data and functions, which induces a very powerful mathematical tool called *wavelet transform*. By applying (dyadic) dilations and translations, a set of wavelet prototype functions (usually referred as the set of *mother wavelets*) will generate a basis. This basis can provide a powerful tool for cutting up data and functions into different frequency bands and then analyzing each band with the desired scale or resolution.

Given a set of *mother wavelets* $\Psi \subset L_2(\mathbb{R}^d)$, we can apply dilations and translations to it and consequently obtain a basis as follows

$$X(\Psi) := \{\psi_{j,k} := 2^{jd/2}\psi(2^j \cdot -k),\ \psi \in \Psi, j \in \mathbb{Z}, k \in \mathbb{Z}^d\},$$

where the dilation factor 2^j controls the scale of wavelets and the translation factor k indicates the position. Then for any generic signal (or function) f with finite energy (i.e. $\int |f(t)|^2 dt < \infty$), we can analyze f over its wavelet coefficients computed as follows

$$c_{\psi,j,k} = \langle f, \psi_{j,k} \rangle,\ \psi \in \Psi, j \in \mathbb{Z}, k \in \mathbb{Z}^d.$$

In particular, when certain constraints (like high order vanishing moments) are imposed for those mother wavelets, the derived basis would define sparse representations of piecewise regular signals – namely, most wavelet coefficients are close to zero except those located at the neighbourhood of singular points. The sparse representation of given data and signal could be of help to certain post-processing techniques, like compression, denoising, etc.

Early development of wavelets is largely devoted to orthonormal cases. In 1909, A. Haar proposed the first example of orthonormal wavelet, which is currently known by the name of *Haar wavelet*. Theoretical study of wavelet and its rigorous formulation dated back to late 1970s and early 1980s. A major breakthrough for wavelet theory is the introduction of *multiresolution analysis* (MRA) by Mallat and Meyer [51, 56], whose emergence has greatly facilitated the construction of wavelets. Specially, a class of MRA-based compactly supported orthonormal wavelets was successfully constructed by Daubechies [26, 27], which is now widely recognized as the family of *Daubechies wavelets*. Daubechies wavelets are quite popular currently, and they have been adopted in many scientific research fields.

Along with the study of orthonormal wavelet basis, there had been a continuing research effort in the study of wavelet frames. In history, frames were introduced

by Duffin and Schaeffer in 1952 to study non-harmonic Fourier series [38]. The major difference between frames and orthonormal bases is that frames can be over-complete (or to say redundant). Univariate wavelet frames were early explored by Daubechies, Grossmann and Meyer in [29] in 1986. Similar as the case of orthonromal wavelet basis, the formulation of MRA [51, 56] is a major breakthrough for constructing wavelet frames as well. However, the original formulation of MRA is mainly designed for understanding and constructing orthonormal wavelet frame bases rather than redundant wavelet frame bases. In order to construct redundant wavelet frame bases, the originally MRA formulation was inevitably adapted and generalized. For example, J. Benedetto and S. Li proposed the notion of *frame multiresolution analysis* (FMRA) in [1], consequently several type of univariate FMRA based wavelet frames were constructed. Following a similar route, the construction of FMRA-based multivariate tensor-product wavelet frames was pushed forward in [2] in 2007. In contrast to Mallat and Meyer's original MRA and FMRA, a more general concept of MRA was formulated in [5], which has been a major motivation to the construction of wavelets and wavelet frames since its formulation. Yet, the MRA structure itself does not suggest the characterization of wavelet frames. A general characterization of multivariate wavelet frames was obtained by Ron and Shen in [62] in 1997. This characterization was also explicitly obtained by B. Han in [46]. However, this wavelet frame characterization is usually quite difficult to verify, which severely limits its practical use. Ron and Shen were able to combine the frame characterization with the MRA formulation raised in [6], and consequently proposed the renowned *unitary extension principle* and *oblique extension principle* for constructing wavelet tight frames [62]. Compared to other wavelet frame characterizations, the conditions indicated in the two extension principles are practically easy to check, which makes the construction of wavelet tight frames painless [62, 28].

This thesis is devoted to both the theory and the application of wavelets and wavelet frames, in which two major topics would be covered:

- low-dimensional band-limited wavelets and wavelet tight frames (framelets),
- wavelet tight frame based digital colour image restoration.

In this opening chapter, we first give a brief introduction on the above two topics to be studied in this thesis. After that, we will present the organization of this thesis.

1.1 Band-limited wavelets and wavelet frames

In the development of wavelet theory, the study of compactly supported wavelets and wavelets frames is the main stream. For instance, the renowned Harr wavelet, Daubechies wavelets [27] and spline wavelet frames [62] and pseudo-spline wavelet frames [28, 33] are all compactly supported. These wavelet constructions have been adopted and utilized in many different scientific research fields. However, there are certain cases in which the use of compactly supported wavelets would be inappropriate. For example, in certain applications the targeted signals would have their frequency components restricted to certain bands, the so-called *band-limited* case. As a compactly supported function can never be band-limited unless it is trivially zero, compactly supported wavelets and wavelet frames are unlikely to provide an efficient tool to analyze and process such band-limited signals. So in that case, the desired type of wavelets would be band-limited wavelets, i.e. the type of wavelets whose support in frequency domain is compact.

To date, well-known examples of band-limited wavelets include the orthonormal Shannon wavelets and the Meyer's wavelets [55]. Besides these two renowned examples, a systematic study of band-limited wavelet frames using FMRA was given

by Benedetto and Li in [1]. Recently, Chen and Goh gave a comprehensive study of univariate band-limited wavelets and wavelet frames derived using extension principles in [22]. However, most of these studies concentrate on the 1D case, while 2D and higher-dimensional cases are handled via the tensor product of 1D band-limited wavelets (see e.g. [52, 2]). 2D tensor-product band-limited wavelets have been used in various image processing tasks. For instance, the Meyer's wavelets are used in [35] for image deblurring and used in [66] for image compression. To the best of our knowledge, the systematic construction of non-separable multivariate band-limited wavelets had not been well studied in the past. Compared to tensor-product multivariate band-limited wavelets, non-separable band-limited wavelets have more degrees of freedom, which is likely to result in better designs such as smaller frequency support with fast rate of spatial decay.

In this thesis, we provide a systematic study on band-limited non-separable wavelets and wavelet tight frames in low-dimensional Euclidean spaces including $\mathbb{R}^2$ and $\mathbb{R}^3$. Our major contributions include:

- the introduction of a new class of non-separable band-limited refinable functions, and the construction of their associated band-limited non-separable wavelet tight frames.
- the introduction of a new class of non-separable stable band-limited refinable functions, and the construction of their associated band-limited Riesz wavelets as well as orthonormal wavelets.

Band-limited wavelets always vary smoothly in spatial domain. The oscillatory and smoothness nature make them effective in capturing smoothness variations in data sets and signals. Those smoothness variations are not rare to see in life. For example, when light is reflected on a surface of the same material with similar reflection property, the lightness intensities observed around the surface would

have smooth variations. However, such strong reflections are often associated with image degradation like over-exposure, a phenomenon that can be frequently seen in many digital colour photographs. In digital photography, over-exposure can often produce regions with pixel lightness values clipped at the maximum supporting limit, so those regions would be almost totally flat without any lightness variations.

In view of the above discussion, the constructed band-limited framelets in this thesis is likely to be a good tool for restoring the lightness variations within those clipped regions due to over-exposure. However, for restoring digital colour photographs, besides lightness degradation, the chromatic degradation needs to be considered as well. This leads us to the problem of digital colour image restoration.

1.2 Digital colour image restoration

Image restoration is a general topic, which includes sub-topics like image denoising, deblurring, inpainting, super-resolution, etc. The main difficulty for image restoration relies on the fact that those problems are commonly ill-posed. To resolve the ill-posedness of those problems, some regularization methods are needed. In recent years, wavelet frame based ℓ_1-regularization methods have been demonstrated to be very effective in image restoration (see, e.g. [17, 19, 16, 8, 15, 10, 13]).

Regular image restoration models are usually designed for $2D$ greyscale images. The complexity of colour perception and rendering in digital photography makes colour image restoration problem practically difficult. As we know, digital photography is about capturing photographs of scenes and objects using a camera equipped with electronic sensors. The captured photographs are then digitized and stored in computer file format for viewing or further post-processing. To shoot digital photographs with reasonable fair quality, there are several camera settings

to consider, including white balance, shutter speed, ISO, aperture, focal length, lens focus, etc. Among all those digital camera settings, the shutter speed, ISO and aperture are known to determine the *exposure* of the resulting digital photograph. In digital photography, *exposure* controls how much light can reach the digital sensors and the lightness of a photograph is determined by the amount of light shown. Inappropriate exposure may cause the loss of scene details in the final output. Besides that, there is a physical limitation on the *dynamic range* (ratio of maximum lightness and minimum lightness) that a camera can endure. An outdoor scene with strong or harsh lighting often has a much larger dynamic range than the bearing capacity of a regular image sensor, which then will lead to a loss of highlight/shadow details in the resulting photograph. For example, the dynamic range of a regular digital camera is about $10^3 : 1$ while the dynamic range of an outdoor scene on a sunny day ranges from $10^5 : 1$ to $10^9 : 1$. When recording such a high dynamic range (HDR) scene using a low dynamic range (LDR) camera, the out-coming digital photograph would often be degraded. Typically in that case, some bright parts of the scene would be recorded as "white", which is described as *over-exposure*; in the mean time, some dark areas would be indistinguishable from"black" in the image, which is described as *under-exposure*. In other words, the lightness values of those over-exposed pixels are clipped at the maximum value (e.g. 100) such that these pixels only show white colour, as the values of three colour channels (red, green, blue) at these pixels are also the maximum value. Similarly, the lightness values of under-exposed pixels are too small, close to the minimum value (e.g. 0), such that the image details can hardly be visually perceived. See Figure 1.1 for an illustration of photographs with over-exposed and under-exposed regions.

In summary, for restoring digital colour photographs with over/under-exposed regions, the following issues need to be handled:

(a) (b)

Figure 1.1: Two sample photographs with over/under-exposures. In the image shown in (a), the foreground leaves appear over-exposed and background behind looks under-exposed. In the image shown in (b) from [40], many regions of the church are over-exposed and many parts of the wall with plants are under-exposed.

(i) the clipped lightness values due to over/under-exposure,

(ii) the nearly invisible image details in under-exposed regions,

(iii) the missing chromatic information in the over-exposed regions.

Among all 3 issues listed as above, the 1st and 2nd one are about the lightness information of the photograph, while the 3rd one is about the chromatic information of the photograph. Typically, the lightness values and chromatic values have significantly different behaviour in digital photographs. For instance, in regions around clipped pixels due to over/under-exposure, lightness values tend to vary smoothly, which could possibly be fitted by smooth enough basis functions like band-limited framelets. However, around the same regions, the chromatic values possess more visible variations that are not smooth in appearance, which reflects the corresponding image details. In view of these facts, the strategy for recovering clipped lightness values and the one for restoring the missing chromatic information should be carefully designed so as to reveal these differences.

In this thesis, we proposed a wavelet tight frame based method for restoring

digital colour photographs with over/under-exposed regions. Our main contributions include:

(i) a band-limited framelet based regularization method for recovering clipped lightness values in over/under-exposed regions;

(ii) a new lightness attenuation function for simultaneously accommodating the recovered lightness and improving the contrast of under-exposed regions without amplifying image noise;

(iii) a tensor-product spline framelet based inpainting method for recovering the missing chromatic details of over-exposed regions.

1.3 Organization of this thesis

The rest of this thesis is organized as follows. Firstly in Chapter 2, we will give some preliminaries including multiresolution analysis (MRA), wavelets and wavelet frames, colour spaces and wavelet tight frame based image restoration models. Then in Chapter 3, we will introduce the construction of non-separable band-limited wavelet tight frames in low-dimensional Euclidean spaces including $\mathbb{R}^2$ and $\mathbb{R}^3$. Next in Chapter 4, we will focus on the construction of non-separable band-limited Riesz wavelets and orthonormal wavelets in $\mathbb{R}^2$ and $\mathbb{R}^3$. Finally in Chapter 5, we will turn to the application part, and present the details of our approach for digital colour image restoration using wavelet tight frames. Numerical results and discussions will be provided in this chapter as well.

Chapter 2

Preliminaries

In this chapter, we will present some preliminaries for the main objectives of this thesis. Firstly in section 1, we introduce the framework of *multiresolution analysis (MRA)*, together with some basic knowledge on Riesz wavelets, orthonormal wavelets and wavelet frames. In particular, we will introduce the renowned *unitary extension principle* (UEP) and *oblique extension principle* (OEP) for deriving MRA based wavelet tight frames. Next in section 2, we review some basic knowledge on band-limited functions for studying band-limited wavelets and wavelet frames. Then in section 3, we present some basic knowledge on digital colour images (photographs). Particularly, we will introduce a few *colour spaces* that are frequently used for representing, understanding or processing colours in digital photography. Finally in section 4, we review several wavelet tight frame based mathematical models for image restoration.

2.1 Multiresolution analysis, Riesz wavelets and wavelet frames

2.1.1 Multiresolution analysis

The original framework of **multiresolution analysis (MRA)** is given by Mallat and Meyer [51, 56], which provides a systematic way for understanding *orthonormal* wavelets. Examples of MRA-based orthonormal wavelets can be found in [55, 27]. In this thesis, we adopt a more generalized version of MRA proposed by de Boor, DeVore and Ron [6]. For any subspace $V \subseteq L_2(\mathbb{R}^d)$, we let $\mathrm{cls}\big(V\big)$ denote the L_2-closure of V (i.e. the smallest closed subspace of $L_2(\mathbb{R}^d)$ that contains V), then an MRA is a nested sequence $(V_j)_{j\in\mathbb{Z}}$ of closed subspaces of $L_2(\mathbb{R}^d)$ satisfying:

$$\text{(i)} \quad \cdots \subset V_{-2} \subset V_{-1} \subset V_0 \subset V_1 \subset V_2 \subset \cdots ; \tag{2.1}$$

$$\text{(ii)} \quad \mathrm{cls}\big(\bigcup_{j\in\mathbb{Z}} V_j\big) = L_2(\mathbb{R}^d); \tag{2.2}$$

$$\text{(iii)} \quad \bigcap_{j\in\mathbb{Z}} V_j = \{0\}. \tag{2.3}$$

To construct MRA, one usually starts with a function $\phi \in L_2(\mathbb{R}^d)$, and set

$$V_j := \mathrm{cls}\big(\mathrm{span}\{\phi(2^j \cdot -k) : k \in \mathbb{Z}^d\}\big),\ j \in \mathbb{Z}. \tag{2.4}$$

Then, it is implied by the following result that the MRA condition (2.3) is trivially satisfied for the sequence $\{V_j : j \in \mathbb{Z}\}$ defined in (2.4).

Theorem 2.1. *[6] Let $\phi \in L_2(\mathbb{R}^d)$, then the sequence $\{V_j : j \in \mathbb{Z}\}$ defined via* (2.4) *satisfies MRA condition* (2.3).

Now we turn to the MRA condition (2.1), then the following theorem is needed for characterizing each subspace V_j, $j \in \mathbb{Z}$, of $L_2(\mathbb{R}^d)$ defined as in (2.4).

Theorem 2.2. *[6] Let $\phi \in L_2(\mathbb{R}^d)$, then for the sequence $\{V_j : j \in \mathbb{Z}\}$ defined in (2.4), one has*

$V_j = \{f : \widehat{f}(\omega) = \tau(2^{-j}\omega)\widehat{\phi}(2^{-j}\omega) \in L_2(\mathbb{R}^d)$ *with τ being 2π-periodic and measurable.*$\}$.

Viewing from the above characterization, to ensure that the sequence defined in (2.4) satisfies MRA condition (2.1), we need to further assume that ϕ is *refinable*.

Definition 2.1. *A function $\phi \in L_2(\mathbb{R}^d)$ is said to be refinable if there exists a (measurable) 2π-periodic function $\widehat{a}(\omega)$ such that*

$$\widehat{\phi}(2\omega) = \widehat{a}(\omega)\widehat{\phi}(\omega). \tag{2.5}$$

In this case, $\widehat{a}(\omega)$ is called the refinement mask *of ϕ.*

Remark. For a refinable function ϕ, its refinement mask is not necessarily unique (in Lebesgue sense). In particular, the definition of $\widehat{a}(\omega)$ can be arbitrarily changed on the set $\{\omega : [\widehat{\phi}, \widehat{\phi}](\omega) = 0\}$. However, by appropriately setting the definition of refinement mask on $\{\omega : [\widehat{\phi}, \widehat{\phi}](\omega) = 0\}$, we can always assume without loss of generality that the refinement mask $\widehat{a}(\omega)$ of $\phi \in L_2(\mathbb{R}^d)$ is finite almost everywhere (a.e.).

Example 2.1. *[65] (Cardinal B-spline refinable functions) For any $m \in \mathbb{Z}^+$, let ϕ be the function of $L_2(\mathbb{R})$ defined by*

$$\widehat{\phi}(\omega) = e^{-i\mathcal{K}(m)\omega}\frac{\sin^m(\frac{\omega}{2})}{(\frac{\omega}{2})^m}, \ \forall \omega \in \mathbb{R}, \tag{2.6}$$

where

$$\mathcal{K}(m) = \begin{cases} 1, & m \text{ odd}, \\ 0, & m \text{ even}. \end{cases} \tag{2.7}$$

Then clearly one has

$$\widehat{\phi}(2\omega) = e^{-i\mathcal{K}(m)\omega/2}\cos^m(\frac{\omega}{2})\widehat{\phi}(\omega).$$

Note that $e^{-i\mathcal{K}(m)\omega/2}\cos^m(\frac{\omega}{2})$ *is* 2π*-periodic, thus* ϕ *is refinable with refinement mask* $e^{-i\mathcal{K}(m)\omega/2}\cos^m(\frac{\omega}{2})$.

Example 2.2. *[55, 52, 27] The Meyer's refinable function* Q_Ω *, with* $\frac{\pi}{2} < \Omega \leqslant \frac{2}{3}\pi$*, is defined by*

$$\widehat{Q_\Omega}(\omega) = \begin{cases} 1, & \text{if } |\omega| < 2\pi - 2\Omega, \\ h(\frac{|\omega|}{2}), & \text{if } 2\pi - 2\Omega \leq |\omega| \leq 2\Omega, \\ 0, & \text{otherwise.} \end{cases} \tag{2.8}$$

The transition function h *is chosen such that*

(1) $h(\pi - \Omega) = 1$, $h(\Omega) = 0$ *and* $0 < h(\cdot) < 1$ *on the interval* $(\pi - \Omega, \Omega)$.

(2) $\widehat{Q_\Omega}$ *satisfies*

$$[\widehat{Q_\Omega}, \widehat{Q_\Omega}](\omega) = 1, \forall \omega \in \mathbb{R}. \tag{2.9}$$

Then it is seen that Q_Ω *is refinable with refinement mask* τ_Ω*, which is a* 2π*-periodic function whose definition on* $[-\pi, \pi)$ *is*

$$\tau_\Omega(\omega) = \begin{cases} h(|\omega|), & \text{if } |\omega| \in [\pi - \Omega, \Omega], \\ 1, & \text{if } |\omega| < \pi - \Omega, \\ 0, & \text{otherwise,} \end{cases} \tag{2.10}$$

i.e. $\widehat{Q_\Omega}(2\omega) = \tau_\Omega(\omega)\widehat{Q_\Omega}(\omega)$*. Moreover, it is implied by* (2.9) *that* τ_Ω *satisfies the following* conjugate mirror filter (CQF) *condition*

$$|\tau_\Omega(\omega)|^2 + |\tau_\Omega(\omega + \pi)|^2 = 1.$$

See Figure 2.1 for brief sketch of $Q_{\frac{2}{3}\pi}$ *and* $\widehat{Q_{\frac{2}{3}\pi}}$.

By combining Theorem 2.2 and (2.5), we can conclude that:

Corollary 2.3. *If* $\phi \in L_2(\mathbb{R}^d)$ *is refinable, then the sequence defined in* (2.4) *satisfies MRA condition* (2.1).

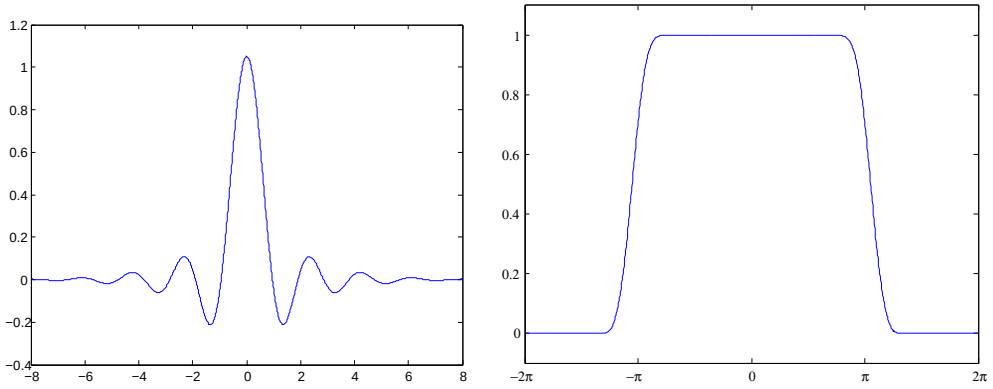

(a) $Q_{\frac{2}{3}\pi}$ (b) $\widehat{Q_{\frac{2}{3}\pi}}$

Figure 2.1: A sketch of the Meyer's refinable function $Q_{\frac{2}{3}\pi}$ in (a) spatial domain and (b) frequency domain.

Now we know from Theorem 2.1 and Corollary 2.3 that, if $\phi \in L_2(\mathbb{R}^d)$ is refinable, then the sequence $\{V_j : j \in \mathbb{Z}\}$ defined in (2.4) should satisfy MRA conditions (2.1) and (2.3). To further ensure that the sequence $\{V_j : j \in \mathbb{Z}\}$ defined in (2.4) satisfies MRA condition (2.2) as well, we need the following characterization.

Theorem 2.4. *[6] Let $\phi \in L_2(\mathbb{R}^d)$ be a refinable function, then the sequence $\{V_j, j \in \mathbb{Z}\}$ as in (2.4) satisfies the MRA condition (2.2) if and only if*

$$\bigcap_{j\in\mathbb{Z}}(2^j Z(\widehat{\phi})) \text{ is a set of measure zero,} \tag{2.11}$$

where $Z(\widehat{\phi})$ is the zero set of $\widehat{\phi}$.

The condition (2.11) is not difficult to fulfill. For example, when $\widehat{\phi}$ is non-zero over some region R around the origin, one has

$$\bigcap_{j\in\mathbb{Z}}(2^j Z(\widehat{\phi})) \subseteq \bigcap_{j\in\mathbb{Z}}(2^j(\mathbb{R}^d\backslash R))) = \mathbb{R}^d\backslash\bigcup_{j\in\mathbb{Z}}(2^j R) = \mathbb{R}^d\backslash\mathbb{R}^d = \emptyset.$$

Thus if $\widehat{\phi}$ is continuous at the origin with $\widehat{\phi}(\{0\}) \neq 0$, based on Theorem 2.4, the sequence in (2.4) would satisfy (2.2) automatically.

In summary, by combining Theorem 2.1, Corollary 2.3 and Theorem 2.4, the following corollary can be easily derived.

Corollary 2.5. *Let $\phi \in L_2(\mathbb{R}^d)$ be refinable. If $\widehat{\phi}$ is continuous at the origin with $\widehat{\phi}(\{0\}) \neq 0$, then ϕ is an MRA generator, i.e. the sequence $\{V_j : j \in \mathbb{Z}\}$ defined in* (2.4) *satisfies MRA conditions* (2.1), (2.2) *and* (2.3).

Specially, it is seen from the above corollary that the cardinal B-spline refinable functions in Example 2.1 and Meyer's refinable function in Example 2.2 are all MRA generators.

2.1.2 Riesz wavelets and wavelet frames

Definitions of Riesz basis and frame

Riesz basis and frame are two important concepts in functional analysis, particularly in the study of Hilbert spaces. Generally speaking, Riesz basis is a relaxation of the orthogonal (orthonormal) basis by allowing non-orthogonality, and frame is a further extension of Riesz basis by admitting linear dependency. Thus compared to orthonormal basis, Riesz basis and frame are more flexible to design, yet both of them have their corresponding stable decomposition and reconstruction algorithms, just like the regular orthogonal (orthonormal) basis does. Moreover, wavelet frames are potentially redundant and the redundancy may become crucial in some applications.

Now we explain the definitions of these two concepts in detail.

Definition 2.2. *In a Hilbert space $\mathcal{H}$, a sequence $\{x_i : i \in I\} \subset \mathcal{H}$ (where I is a countable index set) is called a* Riesz basis *of $\mathcal{H}$ if the linear span of $\{x_i : i \in I\}$ is dense in $\mathcal{H}$, and there exist some A, B with $0 < A \leqslant B < \infty$ such that*

$$A\|c\|_{\ell_2(I)}^2 \leqslant \|\sum_{i\in I} c_i x_i\|^2 \leqslant B\|c\|_{\ell_2(I)}^2, \ \forall c = (c_i)_{i\in I} \in \ell_2(I).$$

Furthermore, if $A = B = 1$ *in the above inequality, then the sequence* $\{x_i : i \in I\}$ *is said to be an* orthonormal basis *of* $\mathcal{H}$.

Definition 2.3. *In a Hilbert space* $\mathcal{H}$*, a sequence* $\{z_i : i \in I\} \subset \mathcal{H}$*, where* I *is a countable index set, is called a* frame *of* $\mathcal{H}$ *if there exist some* A', B' *with* $0 < A' \leqslant B' < \infty$*, such that*

$$A'\|z\|^2 \leqslant \sum_{i\in I} |\langle z, z_i\rangle|^2 \leqslant B'\|z\|^2, \forall z \in \mathcal{H}. \tag{2.12}$$

In this case, A' *is called the* lower frame bound *and* B' *is called the* upper frame bound. *Moreover, if* $A' = B' = 1$ *in* (2.12)*, then the sequence* $\{z_i : i \in I\}$ *is said to be a* tight frame *or a* Parseval frame *of* $\mathcal{H}$.

Introduction to affine wavelet system

At this stage, we introduce the kind of wavelet systems that we are mainly interested in – *affine wavelet system*.

Definition 2.4. *Given a collection of functions* $\Psi \subseteq L_2(\mathbb{R}^d)$*, the* affine system $X(\Psi)$ *generated by* Ψ *is*

$$X(\Psi) := \{2^{jd/2}\psi(2^j \cdot -k) : j \in \mathbb{Z}, k \in \mathbb{Z}^d, \psi \in \Psi\}. \tag{2.13}$$

In this case, Ψ *is referred as the set of* generators. *Specially,* $X(\Psi)$ *is called* finitely generated *if* Ψ *is a finite set;* $X(\Psi)$ *is called* MRA-based *if there exists an MRA sequence* $\{V_j : j \in \mathbb{Z}\}$ *such that* $\Psi \subset V_1$.

In principle, wavelet systems should provide 'good' bases – namely, orthonormal bases, Riesz bases, or frames for signal spaces of interest. In this thesis, we are only interested in the collection of functions Ψ such that (i) $X(\Psi)$ is MRA-based, and (ii) $X(\Psi)$ forms a *Riesz basis* or a *frame* of $L_2(\mathbb{R}^d)$.

Finding a set of functions Ψ such that $X(\Psi)$ is MRA-based is a relatively easy task. For example, suppose that we have an MRA $\{V_j : j \in \mathbb{Z}\}$ generated by a refinable function $\phi \in L_2(\mathbb{R}^d)$, whose refinement mask is $\tau_0(\omega)$. Then a set of generators $\Psi := \{\psi_1, \ldots, \psi_L\}$ can be obtained by setting

$$\widehat{\psi_\ell}(\omega) := \tau_\ell(\frac{\omega}{2})\widehat{\phi}(\frac{\omega}{2}),\ \ell = 1, \ldots, L, \tag{2.14}$$

where $\{\tau_\ell : \ell = 1, \ldots, L\}$ is a set of 2π-periodic measurable functions such that $\tau_\ell\widehat{\phi} \in L_2(\mathbb{R}^d)$, $\ell = 1, \ldots, L$. Thus $\Psi \subset L_2(\mathbb{R}^d)$. Using Theorem 2.2, we can conclude that $\Psi \subset V_1$, so the affine system $X(\Psi)$ is MRA-based. Under this setting, $\{\tau_\ell : \ell = 1, \ldots, L\}$ is referred as the set of *wavelet masks*. It is seen from (2.14) that, the key issue for deriving MRA-based affine wavelets and wavelet frames relies on 'finding' the appropriate set of *wavelet masks*.

If the affine system $X(\Psi)$ is a Riesz basis of $L_2(\mathbb{R}^d)$, then any generator $\psi \in \Psi$ is called a *Riesz wavelet*. Specially, if $X(\Psi)$ is an *orthonormal basis* of $L_2(\mathbb{R}^d)$, then any generator $\psi \in \Psi$ would be referred as an *orthonormal wavelet* or simply *wavelet*.

If the affine system $X(\Psi)$ forms a tight frame of $L_2(\mathbb{R}^d)$, then any generator $\psi \in \Psi$ is called a *framelet*.

Riesz basis and frame characterization in principle shift-invariant spaces

The study of *principle shift-invariant (PSI)* spaces is of particular importance for Riesz basis and frame characterization in affine systems. Recall that, a *principle shift-invariant (PSI)* space is a subspace of $L_2(\mathbb{R}^d)$ with the form

$$\mathcal{S}(\phi) = \mathrm{cls}\big(\mathrm{span}\{\phi(\cdot - k) : k \in \mathbb{Z}^d\}\big),\ \phi \in L_2(\mathbb{R}^d), \tag{2.15}$$

i.e. $\mathcal{S}(\phi)$ is the L_2-closure of the space spanned by $\{\phi(\cdot - k) : k \in \mathbb{Z}^d\}$. Then we have the following results.

Theorem 2.6. *[62] For any function $\phi \in L_2(\mathbb{R}^d)$, the sequence $\{\phi(\cdot - k) : k \in \mathbb{Z}^d\}$ forms a Riesz basis of $\mathcal{S}(\phi)$ defined in (2.15) if and only if there exist A, B with $0 < A \leqslant B < \infty$ such that*

$$A \leqslant [\widehat{\phi}, \widehat{\phi}] \leqslant B, \text{ a.e. on } \mathbb{R}^d. \tag{2.16}$$

The function ϕ is said to be *stable* if it satisfies (2.16). In particular, if $A = B = 1$ in (2.16), then ϕ is said to be *orthonormal*.

Theorem 2.7. *[62, 1] For any (non-zero) function $\phi \in L_2(\mathbb{R}^d)$, the sequence $\{\phi(\cdot - k) : k \in \mathbb{Z}^d\}$ forms a frame of $\mathcal{S}(\phi)$ defined in (2.15) if and only if there exist A', B' with $0 < A' \leqslant B' < \infty$ such that*

$$A' \leqslant [\widehat{\phi}, \widehat{\phi}] \leqslant B', \text{ a.e. on } \sigma(\mathcal{S}(\phi)), \tag{2.17}$$

where $\sigma(\mathcal{S}(\phi)) := \{\xi \in \mathbb{R}^d : [\widehat{\phi}, \widehat{\phi}](\xi) > 0\}$ is called the spectrum *of $\mathcal{S}(\phi)$. Specially, the sequence $\{\phi(\cdot - k) : k \in \mathbb{Z}^d\}$ forms a tight frame of $\mathcal{S}(\phi)$ if and only if $A' = B' = 1$ in (2.17).*

It is seen that, the set $\{\phi(\cdot - k) : k \in \mathbb{Z}^d\}$ forms a Riesz basis rather than a frame of $\mathcal{S}(\phi)$ only if the spectrum $\sigma(\mathcal{S}(\phi))$ is differed from $\mathbb{R}^d$ by a set of Lebesgue measure zero.

2.1.3 Extension principles for derving MRA-based wavelet tight frames

At this stage, we would like to introduce the two renowned *extension principles* for deriving MRA-based wavelet tight frames. However, deriving Riesz wavelets or wavelet frames from generic MRAs is always a challenging task. To facilitate the construction, usually some mild conditions need to be assumed for the choice of refinable function that generates the corresponding MRA. In this thesis, the

following condition is imposed for any refinable function $\phi \in L_2(\mathbb{R}^d)$ within the discussion of this section:

$$\widehat{\phi} \text{ is continuous at the origin with } \widehat{\phi}(\{0\}) = 1 \text{ and } [\widehat{\phi}, \widehat{\phi}] \text{ is (essentially) bounded.} \tag{2.18}$$

Specially, according to Corollary 2.5, the refinable function ϕ would be an MRA generator when condition (2.18) is assumed.

Unitary extension principle and oblique extension principle

For deriving MRA-based wavelet tight frames, we have the following renowned **Unitary Extension Principle (UEP)**:

Proposition 2.8. Unitary Extension Principle (UEP) *[62]. Let $\phi \in L_2(\mathbb{R}^d)$ be a refinable function with mask τ_0 and $\{\tau_\ell : \ell = 1, \ldots, L\}$ be a set of 2π-periodic functions. Assume that ϕ satisfies* (2.18) *and the masks $\{\tau_0, \tau_1, \ldots, \tau_L\}$ are essentially bounded and measurable. For a given $\Psi = \{\psi_\ell : \ell = 1, \ldots, L\}$ defined by* (2.14)*, the associated affine system $X(\Psi)$ forms a tight frame of $L_2(\mathbb{R}^d)$ provided that the masks $\{\tau_0, \tau_1, \ldots, \tau_L\}$ satisfy the following equalities:*

$$\sum_{\ell=0}^{L} \tau_\ell(\omega)\overline{\tau_\ell(\omega + \pi\nu)} = \delta_{\nu,\{0\}}, \quad \forall\, \nu \in \mathbb{Z}_2^d, \tag{2.19}$$

for almost all $\omega \in \{\gamma \in \mathbb{R}^d : [\widehat{\phi}, \widehat{\phi}](\gamma) > 0\}$.

If the affine system $X(\Psi)$ forms a tight frame of $L_2(\mathbb{R}^d)$, then it follows from the definition of tight frame that, for any $f \in L_2(\mathbb{R}^d)$,

$$\|f\|^2 = \sum_{j\in\mathbb{Z}} \sum_{\ell=1}^{L} \sum_{k\in\mathbb{Z}^d} |\langle f, \psi_{j,\ell,k}\rangle|^2, \tag{2.20}$$

where $\psi_{j,\ell,k} = 2^{jd/2}\psi_\ell(2^j \cdot -k)$. Note that (2.20) is equivalent to

$$f = \sum_{j\in\mathbb{Z}} \sum_{\ell=1}^{L} \sum_{k\in\mathbb{Z}^d} \langle f, \psi_{j,\ell,k}\rangle \psi_{j,\ell,k}, \tag{2.21}$$

which can be seen as an infinite level decomposition of f. However, in practice we seldom decompose a given function down to the level of negative infinity. The good thing is, when $\Psi = \{\psi_\ell : \ell = 1, \dots, L\}$ is derived from certain refinable function ϕ using UEP, we can decompose a function down to any given level J, and still obtain a tight frame system as follows:

$$\{2^{Jd/2}\phi(2^J \cdot -k), \psi_{j,\ell,k} : 1 \leqslant \ell \leqslant L, j \geqslant J, k \in \mathbb{Z}^d\}.$$

Theorem 2.9. *[62, 34] Let $\Psi := \{\psi_\ell : 1 \leqslant \ell \leqslant L\}$ be the set tight framelets constructed from the refinable function ϕ using UEP. Then for any $J \in \mathbb{Z}$, the system*

$$X(\phi, \Psi; J) := \{\phi_{J,k}, \psi_{j,\ell,k} : 1 \leqslant \ell \leqslant L, j \geqslant J, k \in \mathbb{Z}^d\},$$

where $\phi_{J,k} := 2^{Jd/2}\phi(2^J \cdot -k)$, forms a tight frame of $L_2(\mathbb{R}^d)$. In other words, for any $f \in L_2(\mathbb{R}^d)$,

$$f = \sum_{k\in\mathbb{Z}^d} \langle f, \phi_{J,k}\rangle \phi_{J,k} + \sum_{\ell=1}^{L} \sum_{j\geqslant J} \sum_{k\in\mathbb{Z}^d} \langle f, \psi_{j,\ell,k}\rangle \psi_{j,\ell,k}. \tag{2.22}$$

Construction 2.1. *[62] Let ϕ be the cardinal B-spline of order m as in (2.6), then ϕ is refinable with mask $\tau_0(\omega) = e^{-i\mathcal{K}(m)\frac{\omega}{2}} \cos^m(\frac{\omega}{2})$. Then we define*

$$\tau_k(\omega) := \sqrt{\binom{m}{k}} e^{-i\mathcal{K}(m)\omega/2} i^k \sin^k(\omega/2) \cos^{m-k}(\omega/2),\ 1 \leqslant k \leqslant m,$$

where $\mathcal{K}(m)$ is defined in (2.7). Then, the combined mask set $\{\tau_\ell\}_{\ell=0}^m$ satisfies

$$\sum_{\ell=0}^{m} \tau_\ell(\omega)\overline{\tau_\ell(\omega)} = \big(\sin^2(\omega/2) + \cos^2(\omega/2)\big)^m = 1,$$

and

$$\sum_{\ell=0}^{m} \tau_\ell(\omega)\overline{\tau_\ell(\omega+\pi)} = \big(\sin(\omega/2)\cos(\omega/2)\big)^m (1-1)^m = 0.$$

Thus according to UEP, for $\Psi := \{\psi_k : \widehat{\psi}(\cdot) = \tau_k(\cdot/2)\widehat{\phi}(\cdot/2),\ 1 \leqslant k \leqslant m\}$, the affine system $X(\Psi)$ forms a tight frame of $L_2(\mathbb{R})$.

Example 2.3. *(The piecewise linear spline framelet system) If $m = 2$ in (2.6), then the refinable function ϕ is simply the cardinal B-spline of order 2, i.e.*

$$\widehat{\phi}(\omega) = \frac{\sin^2(\omega/2)}{(\omega/2)^2}$$

with refinement mask

$$\tau_0(\omega) = \cos^2(\omega/2) = \frac{1}{2}(\cos(\omega) + 1) = \frac{1}{4}\big(\exp(i\omega) + 2 + \exp(-i\omega)\big).$$

Following Construction 2.1, we get two wavelet masks τ_1 and τ_2 such that

$$\tau_1(\omega) = \sqrt{2}i\cos(\omega/2)\sin(\omega/2) = \frac{\sqrt{2}}{2}i\sin(\omega) = \frac{\sqrt{2}}{4}\big(\exp(i\omega) - \exp(-i\omega)\big) \tag{2.23}$$

and

$$\tau_2(\omega) = -\sin^2(\omega/2) = \frac{1}{2}(\cos(\omega) - 1) = \frac{1}{4}\big(\exp(i\omega) - 2 + \exp(-i\omega)\big). \tag{2.24}$$

Using the masks τ_1 and τ_2 as defined in (2.23) and (2.24), one can obtain two corresponding wavelet tight framelets, which are denoted as ψ_1 and ψ_2 respectively. See Figure 2.2 for brief sketch of ϕ, ψ_1 and ψ_2.

It is seen that, the Fourier coefficients of the mask set $\{\tau_0, \tau_1, \tau_2\}$ are associated with the following discrete finite filters respectively:

$$h_0 = \frac{1}{4}[1 \quad 2 \quad 1],\ h_1 = \frac{\sqrt{2}}{4}[1 \quad 0 \quad -1],\ h_2 = \frac{1}{4}[1 \quad -2 \quad 1].$$

As an extension of UEP, the so-called **oblique extension principle** (OEP) is proposed.

Proposition 2.10. Oblique Extension Principle (OEP) [28]. *Let ϕ be a refinable function with mask τ_0 and $\{\tau_\ell : \ell = 1, \ldots, L\}$ be a set of 2π-periodic functions. Assume that ϕ satisfies (2.18) and the masks $\{\tau_0, \tau_1, \ldots, \tau_L\}$ are essentially bounded and measurable. For a given set $\Psi = \{\psi_\ell : \ell = 1, \ldots, L\}$ defined as*

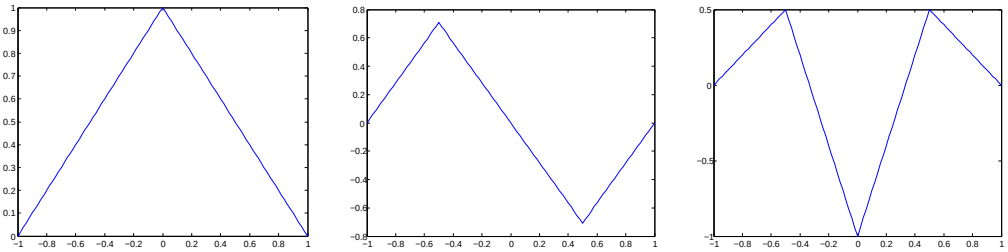

(a) ϕ (b) ψ_1 (c) ψ_2.

Figure 2.2: The piecewise linear spline framelet system.

(2.14), *if there exists a* 2π*-periodic function* Θ *which is non-negative, essentially bounded, continuous at the origin with* $\Theta(\{0\}) = 1$ *such that*

$$\tau_0(\omega)\overline{\tau_0(\omega+\nu\pi)}\Theta(2\omega) + \sum_{\ell=1}^{L} \tau_\ell(\omega)\overline{\tau_\ell(\omega+\nu\pi)} = \delta_{\nu,\{0\}}\Theta(\omega), \quad \forall\, \nu \in \mathbb{Z}_2^d, \qquad (2.25)$$

for almost all $\omega \in \{\gamma \in \mathbb{R}^d : [\widehat{\phi}, \widehat{\phi}](\gamma) > 0\}$*, then the resulting affine system* $X(\Psi)$ *forms a wavelet tight frame of* $L_2(\mathbb{R}^d)$.

It is seen that OEP coincides with UEP when $\Theta \equiv 1$, so the statement of OEP is more general. The flexibility of choosing Θ and the wavelet masks would greatly facilitate the search for new constructions in practice. Yet, it is a bit surprising that OEP can also be derived from UEP, thus the two are actually equivalent to each other. Interested readers may find the proof of this fact in [28, 34].

Quasi-affine systems and their associated algorithms

Shift-invariance is a desirable property in many applications (see, e.g. [23, 36]). However, it is easy to see that the affine system $X(\Psi)$ defined in (2.13) is not shift-invariant. Given an affine system $X(\Psi)$, Ron and Shen introduced the shift-invariant counterpart of it – the *quasi-affine system* [62] $X^q(\Psi)$, which is raised for studying the frame characterization of $X(\Psi)$.

Definition 2.5. *For any affine system $X(\Psi)$ with $\Psi \subset L_2(\mathbb{R}^d)$, its associated quasi-affine system $X^q(\Psi)$ is obtained by replacing each $\psi_{j,k} = 2^{jd/2}\psi(2^j \cdot -k)$, for $\psi \in \Psi, j < 0$ and $k \in \mathbb{Z}^d$, by a set of 2^{-jd} functions as follows*

$$2^{jd}\psi_{2^j(\cdot+\alpha)-k},\ \forall \alpha \in \mathbb{Z}^d_{2^{-j}}.$$

The frame characterization of $X(\Psi)$ and $X^q(\Psi)$ is closely related, as revealed by the following result.

Theorem 2.11. *[62] The affine system $X(\Psi)$ is a frame of $L_2(\mathbb{R}^d)$ if and only if its quasi-affine counterpart $X^q(\Psi)$ is a frame of $L_2(\mathbb{R}^d)$, and they share the same frame bounds. In particular, $X(\Psi)$ is a tight frame of $L_2(\mathbb{R}^d)$ if and only if $X^q(\Psi)$ is a tight frame of $L_2(\mathbb{R}^d)$.*

It follows that one can use UEP to derive MRA-based quasi-affine tight frame systems as well. Underlying a quasi-affine system, one has, for any $f \in L_2(\mathbb{R}^d)$, the multi-level decompositions similar as in (2.21) and (2.22).

In practice, signals are usually given in the form of finite (discrete) data. Finite signal processing by wavelets or wavelet frames is realized by using the set of masks (including the refinement mask and wavelet masks) of the MRA-based wavelet frame system as filters. In the following, we provide the framelet decomposition and reconstruction algorithm for MRA-based quasi-affine tight frame system derived from UEP.

Let $\phi \in L_2(\mathbb{R})$ be a refinable function with refinement mask τ_0, and $\{\tau_\ell\}_{\ell=1}^L$ be a set of 2π-periodic functions such that the condition (2.19) is satisfied. Then

---

Algorithm 2.1 Given any signal $v \in \mathbb{R}^{N_1} \times \cdots \times \mathbb{R}^{N_d}$ with $N_i \in \mathbb{Z}^+$, $i = 1, 2, \ldots, d$, setting $c_{0,0} = v$, and

(1) **Decomposition**: for $j = 1, 2, \ldots, J$

(a) obtaining the level-j approximation of v

$$c_{0,j} = \mathcal{F}^{-1}\big(\overline{\tau_0(2^{j-1}\cdot)}\mathcal{F}(c_{0,j-1})\big);$$

(b) obtaining the level-j framelet coefficients of v

$$c_{\ell,j} = \mathcal{F}^{-1}\big(\overline{\tau_\ell(2^{j-1}\cdot)}\mathcal{F}(c_{0,j-1})\big),\ \ell = 1, 2, \ldots, L.$$

(2) **Reconstruction**: For $j = J, J-1, \ldots, 1$, setting $\tilde{c}_{0,J} = c_{0,J}$, and

$$\tilde{c}_{0,j-1} = \mathcal{F}^{-1}\big(\tau_0(2^{j-1}\cdot)\mathcal{F}(\tilde{c}_{0,j})\big) + \sum_{\ell=1}^{L} \mathcal{F}^{-1}\big(\tau_\ell(2^{j-1}\cdot)\mathcal{F}(c_{\ell,j})\big).$$

Proposition 2.12. *[9, 34] The reconstruction of Algorithm* 2.1 *is perfect, i.e.* $\tilde{c}_{0,0} = c_{0,0} = v$.

For future reference, we use $W_j^h(f)$ to denote the set of wavelet coefficients of f up to level j, i.e.

$$W_j^h : f \mapsto [c_{1,1}^\top, c_{2,1}^\top, \cdots, c_{L,1}^\top, \cdots, c_{1,j}^\top, c_{2,j}^\top, \cdots, c_{L,j}^\top]^\top.$$

As revealed by the convolution theorem (see, e.g. [52]), frequency filtering is equivalent to spatial convolution. Particularly, when all masks are trigonometric polynomials with real (or complex) coefficients, the multi-level discrete framelet transform for MRA-based quasi-affine tight frame system can be interpreted as an iterated convolution scheme, where all Fourier coefficients of the mask set are utilized as discrete filters.

Let $\phi \in L_2(\mathbb{R})$ be a refinable function with refinement mask τ_0, and $\{\tau_\ell\}_{\ell=1}^L$ be a set of 2π-periodic functions such that the condition (2.19) is satisfied. If

$\tau_\ell(\omega) := \sum_{n\in\mathbb{Z}^d} h_\ell[k]\exp(-ik\cdot\xi)$, $\ell = 0,\dots,L$, are all trigonometric polynomials, we denote

$$h_{\ell,j}[k] = \begin{cases} h_\ell[k/2^j], & \text{if } k \in 2^j\mathbb{Z}^d, \\ 0, & \text{otherwise,} \end{cases}$$

and let

$$\widetilde{h}_{\ell,j} = \overline{h_{\ell,j}[-\cdot]}$$

for $0 \leqslant \ell \leqslant L$, $j \in \mathbb{Z}^*$. Then for any $j \in \mathbb{Z}^+$, the J-level framelet decomposition and reconstruction algorithm is implemented as

---

Algorithm 2.2 Given any signal $v \in \mathbb{R}^N$ with $N \in \mathbb{Z}^+$, let $c_{0,0} = v$, then

(1) **Decomposition**: for $j = 1, 2, \dots, J$

(a) obtaining the level-j approximation of v

$$c_{0,j} = \widetilde{h}_{0,j-1} \circledast c_{0,j-1};$$

(b) obtaining the level-j framelet coefficients of v

$$c_{\ell,j} = \widetilde{h}_{\ell,j-1} \circledast c_{0,j-1},\ \ell = 1, 2, \dots, L.$$

(2) **Reconstruction**: For $j = J, J-1, \dots, 1$,

$$c_{0,j-1} = \sum_{\ell=0}^{L} h_{\ell,j-1} \circledast c_{\ell,j}.$$

The above algorithm is essentially the same as a filter bank algorithm called *algorithme á trous* (see [47]), which was developed earlier for orthogonal and biorthogonal wavelet systems.

2.1.4 For the construction of Riesz wavelets and orthonormal wavelets in low dimensions

The constraint (2.18) is mild and easy to satisfy, which makes the searching of candidate refinable functions painless. Those candidate refinable functions, or those after minor modifications, could then be used to derive wavelet tight frames via UEP or OEP. However, when shifting to the construction of MRA-based Riesz wavelets, we have to consider the linear-independence nature of Riesz basis and put our discussions into a narrower setting. In order to construct Riesz wavelets from a candidate refinable function ϕ, we further impose the following constraint:

$$\phi \text{ is stable, and } \widehat{\phi} \text{ is real-valued.} \tag{2.26}$$

In particular, ϕ would be central skew-symmetric in spatial domain if $\widehat{\phi}$ is real-valued. It is widely recognized that symmetry is a crucial factor for wavelets and wavelet tight frames, and the utilization of refinable functions with symmetry would greatly facilitate the derivation of wavelets with symmetry.

If a refinable function $\phi \in L_2(\mathbb{R}^d)$, with $d = 2$ or 3, satisfying (2.18) and (2.26) is provided, we can then follow a scheme as in [60] to construct Riesz wavelets from ϕ. To be explicit, we first introduce the following mapping $\eta : \mathbb{Z}_2^d \mapsto \mathbb{Z}_2^d$ for $d = 2$ or 3, where

$$\begin{aligned}
&\text{for } d = 2, \text{ the map } \eta \text{ is}\\
&(0,0) \mapsto (0,0), (1,0) \mapsto (1,1), (0,1) \mapsto (0,1), (1,1) \mapsto (1,0);\\
&\text{for } d = 3, \text{ the map } \eta \text{ is}\\
&(0,0,0) \mapsto (0,0,0), \quad (1,0,0) \mapsto (1,1,0), \quad (0,1,0) \mapsto (0,1,1),\\
&(1,1,0) \mapsto (1,0,0), \quad (0,0,1) \mapsto (1,0,1), \quad (1,0,1) \mapsto (0,0,1),\\
&(0,1,1) \mapsto (0,1,0), \quad (1,1,1) \mapsto (1,1,1).
\end{aligned} \tag{2.27}$$

Next we can define a set of functions $\Psi^d = \{\psi_\kappa,\, \kappa \in \mathbb{Z}_2^d \backslash \{0\}\}$ by setting

$$\widehat{\psi_\kappa}(\xi) = \exp\big(i\eta(\kappa)\frac{\xi}{2}\big)\tau_0(\frac{\xi}{2}+\kappa\pi)[\widehat{\phi},\widehat{\phi}](\frac{\xi}{2}+\kappa\pi)\widehat{\phi}(\frac{\xi}{2}),\ \kappa \in \mathbb{Z}_2^d\backslash\{0\}, \tag{2.28}$$

Then we have the following result:

Theorem 2.13. *[60] Let $\phi \in L_2(\mathbb{R}^d)$, $d = 2$ or 3, be a refinable function satisfying* (2.18) *and* (2.26)*, and $\Psi^d = \{\psi_\kappa : \kappa \in \mathbb{Z}_2^d\backslash\{0\}\}$ be a set of functions determined by* (2.28)*. Then the affine system $X(\Psi^d)$ generated by Ψ^d as in* (2.13) *forms a Riesz basis of $L_2(\mathbb{R}^d)$. If in addition that the refinable function ϕ is orthonormal, then for the set $\Psi^d = \{\psi_\kappa : \kappa \in \mathbb{Z}_2^d\backslash\{0\}\}$ determined by* (2.28)*, the affine system $X(\Psi^d)$ forms an orthonormal basis of $L_2(\mathbb{R}^d)$.*

2.2 Band-limited functions

In this section, we introduce some basic facts on band-limited functions, which would be helpful to the theoretical study of *band-limited* wavelets and wavelet frames.

The definition of band-limited functions is directly linked to the notion *Fourier transform*, and a function is called *band-limited* if its Fourier transform is compactly supported. Fourier transform is naturally defined on $L_1(\mathbb{R}^d)$, and can be further extended to $L_2(\mathbb{R}^d)$ and tempered distributions. Moreover, we have the following renowned Plancherel's theorem

$$\|f\|^2_{L_2(\mathbb{R}^d)} = \frac{1}{(2\pi)^d}\|\widehat{f}\|^2_{L_2(\mathbb{R}^d)}$$

for any $f \in L_2(\mathbb{R}^d)$. Thus, Fourier transform induces an isometry (up to a positive scalar) in $L_2(\mathbb{R}^d)$. Hence an $L_2(\mathbb{R}^d)$ function can also be uniquely determined by its Fourier transform, which is also in $L_2(\mathbb{R}^d)$. In other words, we can always define an $L_2(\mathbb{R}^d)$ function in terms of its Fourier transform. Particularly, this rule

applies to all band-limited functions with bounded Fourier transforms. To avoid any ambiguity, in the following discussion we only consider square integrable band-limited functions whose Fourier transforms are integrable in Lebesgue sense. This constraint is to guarantee that the original functions can be pointwise evaluated by their Fourier transforms (via the inverse transform).

Renowned examples of band-limited functions in wavelet research and study include Shannon's refinable function, Meyer's refinable function and their derived wavelets. As we have already got a clear view of Meyer's refinable function in Example 2.2, in the following we give a brief introduction to Shannon's refinable function. Recall that, a Shannon refinable function ϕ is defined in the Fourier (frequency) domain as

$$\widehat{\phi}(\xi) = \mathbf{1}_{[-\pi,\pi)^d}(\xi),$$

which is exactly the characteristic function of the cube $[-\pi, \pi)^d$. Then by taking inverse Fourier transform, one can evaluate that

$$f(x) = \prod_{j=1}^{d} \mathrm{sinc}(x_j),\ x = (x_1, x_2, \ldots, x_d),$$

where the sinc function is the univariate function defined as

$$\mathrm{sinc}(t) = \begin{cases} \frac{sin(\pi t)}{\pi t}, & t \neq 0, \\ 1, & t = 0. \end{cases}$$

Then along the direction determined by any axis, the typical asymptotic rate of (spatial) decay for f is $O(\frac{1}{\|x\|_2})$, which is commonly considered to be slow. This typical slow asymptotic rate of decay is caused by the (essential) discontinuity of f in frequency domain.

It is well-known that for any univariate function, if it has higher order of smoothness in Fourier domain, then it would have fast asymptotic rate of decay in spatial domain (see, e.g. [30]). When moving to the multivariate functions,

the relation between spatial decay rate and frequency domain smoothness is a bit complicated, yet similar principle still follows. Note that, for a multivariate function, we only need to consider its decay rate over the real line when the single variable approaches infinity. However, for a univariate band-limited function, we must consider its decay rate with respect to different reference points and different orientations. Typically, if a reference point $\bar{x} \in \mathbb{R}^d$ and a specific orientation $\overrightarrow{n}$ are given, then for any band-limited function g, the decay rate of g along $\overrightarrow{n}$ with respect to $\bar{x}$ is revealed in the behavior of the univariate function $g(\bar{x} + \overrightarrow{n}t)$ as t approaches infinity. Note that $g(\bar{x} + \overrightarrow{n}t)$ can be evaluated from $\widehat{g}$ via

$$g(\bar{x} + \overrightarrow{n}t) = \frac{1}{(2\pi)^d} \int_{\mathbb{R}^d} \widehat{g}(\xi) \exp\left(i(\bar{x} + \overrightarrow{n}t) \cdot \xi\right) d\xi.$$

Let V be the space spanned by $\overrightarrow{n}$ in $\mathbb{R}^d$, and let $V^\perp$ be the orthogonal complement of V in $\mathbb{R}^d$, then if $\widehat{g}$ is band-limited and $\widehat{g}(\xi) \in C^m(\mathbb{R}^d)$, by Fubini's theorem one has

$$\begin{aligned} g(\bar{x} + \overrightarrow{n}t) &= \frac{1}{(2\pi)^d} \int_V \int_{V^\perp} \widehat{g}(\xi) \exp\left(i\bar{x} \cdot \xi\right) \exp\left(it\overrightarrow{n} \cdot \xi\right) d\xi_{V^\perp} d\xi_V \\ &= \frac{1}{(2\pi)^d} \int_{-\infty}^{\infty} \Big(\int_{V^\perp} \widehat{g}(s\overrightarrow{n} + \xi_{V^\perp}) \exp\left(i\bar{x} \cdot \xi\right) \exp\left(it\overrightarrow{n} \cdot (s\overrightarrow{n} + \xi_{V^\perp})\right) d\xi_{V^\perp} \Big)\, ds \\ &= \frac{1}{(2\pi)^d} \int_{-\infty}^{\infty} \exp\left(is(t + \bar{x} \cdot \overrightarrow{n})\right) \Big(\int_{V^\perp} \widehat{g}(s\overrightarrow{n} + \xi_{V^\perp}) \exp\left(i\bar{x} \cdot \xi_{V^\perp}\right) d\xi_{V^\perp} \Big)\, ds. \end{aligned}$$

We define $h(s) = \int_{V^\perp} \widehat{g}(s\overrightarrow{n} + \xi_{V^\perp}) \exp\left(i\bar{x} \cdot \xi_{V^\perp}\right) d\xi_{V^\perp}$, then $h(s)$ is band-limited. Moreover, by *Leibniz's integral rule* one has $h(s) \in C^m(\mathbb{R})$. Therefore, one can derive that

$$\begin{aligned} g(\bar{x} + \overrightarrow{n}t) &= \frac{1}{(2\pi)^d} \int_{-\infty}^{\infty} \exp\left(is(t + \bar{x} \cdot \overrightarrow{n})\right) h(s)\, ds \\ &= \frac{1}{(2\pi)^d} \frac{i^m}{(t + \bar{x} \cdot \overrightarrow{n})^m} \int_{-\infty}^{\infty} \exp\left(is(t + \bar{x} \cdot \overrightarrow{n})\right) h^{(m)}(s)\, ds. \end{aligned}$$

By Riemann-Lebesgue lemma, the term $\int_{-\infty}^{\infty} \exp\left(is(t + \bar{x} \cdot \overrightarrow{n})\right) h^{(m)}(s)\, ds$ goes to 0 as t goes to infinity. Thus the asymptotic rate of $g(\bar{x} + \overrightarrow{n}t)$ when t goes to

infinity is at $o(\frac{1}{|t|^m})$. This approximation of asymptotic rate of spatial decay is very coarse, yet it is enough to show the fact that: the smoother a band-limited function is in frequency domain, the faster asymptotic rate of decay it has in spatial domain. As in discussions of next two chapters, all constructed multivariate wavelets and framelets only have explicit definitions in frequency domain, their order of smoothness in frequency domain would become an important measurement for their asymptotic rate of decay in spatial domain.

2.3 Colour spaces

In this section, we present some fundamental knowledge on colour spaces. Colour spaces are recognized as specially designed systems for representing colours according to human vision and perception. Since the application part of this thesis is on colour image restoration, so the problem could be appropriately handled only if we comprehend colour in a correct way. However, the topic of colour is so broad that we are only able to do a very brief introduction to it. For more detailed knowledge on colours and colour spaces, the readers could refer to some standard textbooks (e.g. [64, 57, 42]).

Colour is a conception that is originated from human vision. As scientific research indicates, light sensors (cones) in human eye are sensitive to light in different wavelengths, typically *red, green* and *blue* (RGB). Thus by mixing those three *primary colours* with different percentage, one should be able to produce all colours that could be discerned by human eye. This fact also indicates that, to represent the set of colours that can be discerned by human eye, it is enough to use 3 parameters, e.g. *red, green, blue* colour values. Yet, colour representation is not restricted to the RGB setting. Different ways of representing and comprehending

colours (commonly using 3 colour values) lead to different *colour models*. Typical colour models including RGB colour model, CMY (cyan,magenta and yellow) colour model and HSI (hue, saturation and intensity) colour model, etc.

However, a colour model does not provide a comprehensive description of colours unless its colour values are associated with absolute colours that are physically determined. The association of colour models with absolute colours produces various complete colour descriptors called *colour spaces*. In the following, we introduce several typical colour spaces that are frequently used either in colour perception, colour specification or practical applications.

2.3.1 The CIEXYZ colour space

The CIEXYZ colour space is one of the first mathematically defined colour spaces in the study of colour perception. It was created by the *International Commission on Illumination (CIE)* in 1931. The derivation of the CIE colour space is based on the experimental work of W. D. Wright and J. Guild in the late 1920s. In this model, channel Y measures the *luminance* (or brightness), and X and Z channels are to measure the *chromaticity* (roughly, X stimulates human eye's response to red, and Z stimulates human eye's response to blue). More precisely, the CIE defined a set of three *colour matching functions* $\overline{x}(\lambda)$, $\overline{y}(\lambda)$ and $\overline{z}(\lambda)$, which can be considered as the spectral sensitivity curves of three types light receptors of a standard observer. Then, the tristimulus values (X,Y,Z) of a colour with spectral distribution $I(\lambda)$ can be evaluated by

$$X = \int_{380}^{740} I(\lambda)\overline{x}(\lambda)d\lambda,\ Y = \int_{380}^{740} I(\lambda)\overline{y}(\lambda)d\lambda,\ Z = \int_{380}^{740} I(\lambda)\overline{z}(\lambda)d\lambda,$$

where λ stands for the wavelength, and the interval $[380, 740]$ covers the spectral range (or spectrum) of visible light. It is noted that the mechanism for deriving the CIEXYZ colour space is quite similar to human eye's perception of colours,

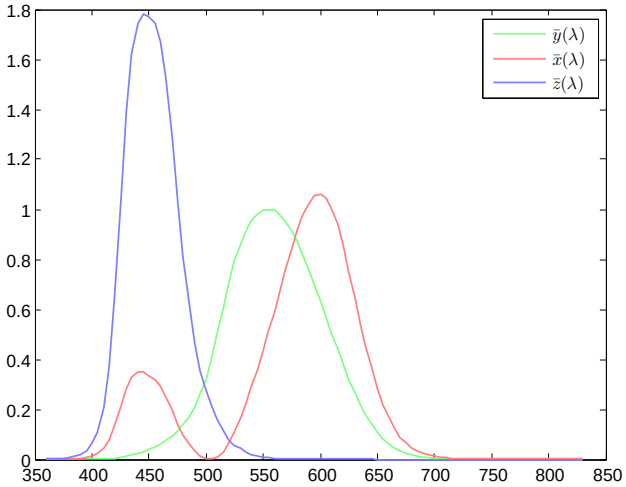

Figure 2.3: Three colour matching functions for the CIEXYZ colour space.

only with different sensitivity curves (colour matching functions versus human sensitivity curves with respect to red, green and blue).

2.3.2 The CIExyY colour space and the CIExy chromaticity diagram

Although the nature of human eye's perceptional mechanism indicates that a full description of visible colours should be done by using three parameters, the concept of colour can be merely divided into two parts: *brightness* and *chromaticity*. Particularly, in the CIEXYZ colour space the channel (or parameter) Y is specially designed to measure the brightness (luminance) only. As to the specification of chromaticity, one can use the following two normalized values x, y such that

$$x = \frac{X}{X+Y+Z}, \; y = \frac{Y}{X+Y+Z}.$$

The above definition of chromaticity specifiers induces the CIExyY colour space, which is widely used to specify colours in practice. It is seen that the conversion from CIExyY tristimulus values and CIEXYZ tristimulus values is fairly simple:

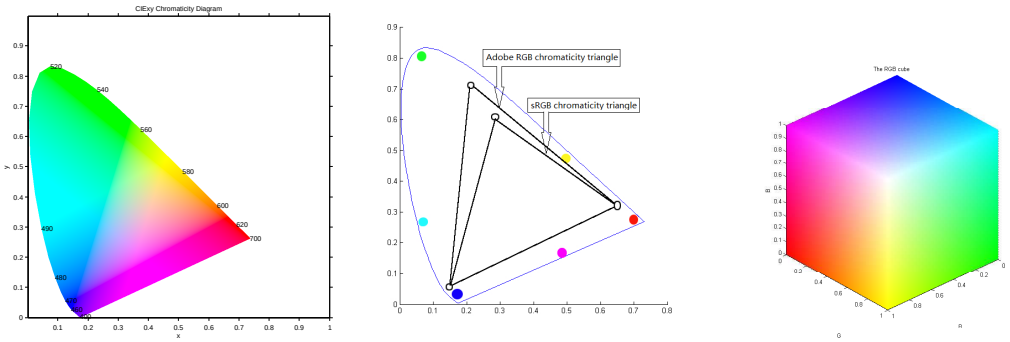

(a) (b) (c)

Figure 2.4: (a) the CIExy chromaticity diagram, (b) the sRGB triangle and Adobe RGB chromaticity triangle, (c) the RGB cube.

the Y values stay unchanged and

$$X = \frac{x}{y}Y,\ Z = \frac{1-x-y}{y}Y.$$

All chromaticities that can be discerned by human eye can be depicted in the CIExy plane, and this gives birth to a chromaticity representation known as the *CIExy chromaticity diagram* (see Figure 2.4 (a)).

2.3.3 RGB colour space

RGB colour model is no doubt the most commonly used one for representing colour images or producing colours in colour displaying devices. This is not surprising because its mechanism is consistent with human eye's perception of colours. Based on the RGB colour model, various RGB colour spaces can be derived, like the *standard RGB (sRBG) colour space*, *Adobe RGB colour space*, etc. Among them, sRGB colour space is most widely used, particularly in consumer digital cameras and monitors.

In an RGB colour space, the typical range for each primary colour value is $[0, 255]$, thus all colours that could be represented in an RGB colour space are

within the following cube:

$$\{(R, G, B) : 0 \leqslant R, G, B \leqslant 255\}.$$

The above cube in $\mathbb{R}^3$ is often referred as the *RGB-cube* (see Figure 2.4 (c)).

RGB colour spaces are *additive colour spaces*. So when the red, green and blue *additive primaries* are determined in the CIExy chromaticity diagram (gamut), any chromaticity within the triangle defined by the three primaries can be produced, see Figure 2.4 (b) for a brief illustration. To complete the description of a colour space, one also has to specify the illumination (brightness) and thus a *white point* is needed. CIE Standard Illuminant $D65$ (which corresponds to $X = 95.047$, $Y = 100.000$, $Z = 108.883$) is a frequently-used standard white point for many RGB colour spaces including sRGB, Adobe RGB, Apple RGB and so on.

The following table shows key parameters for the two most commonly used colour spaces – sRGB colour space and Adobe RGB colour space, where the three primaries are determined by their coordinates in the CIExy chromaticity diagram.

Colour Space	Red Primary	Green Primary	Blue Primary
sRGB	$(x, y) = (0.64, 0.33)$	$(x, y) = (0.30, 0.60)$	$(x, y) = (0.15, 0.06)$
Adobe RGB	$(x, y) = (0.64, 0.33)$	$(x, y) = (0.21, 0.71)$	$(x, y) = (0.15, 0.06)$

It is seen that the chromaticity triangle enclosed by the three Adobe RGB primaries is larger than that of the three sRGB primaries, so Adobe RGB colour space is able to display more colours, see Figure 2.4 (b) for a simple illustration. In other words, Adobe RGB colour space has larger *gamut* compared to sRGB colour space, which makes it popular among the circle of professional photographic artists.

2.3.4 HSV colour space

As we have mentioned previously, the perception of colour can be divided into two parts: brightness (luminance) and chromaticity. The chromaticity part can be further divided into two parts called *hue* and *saturation*. Although RGB is consistent with human eye's perception colours, representing colours in terms of *brightness, hue and saturation* is more natural to human brain's recognition of colour. Among those three colour descriptors, *Hue* is an essential colour attribute that describes a pure colour, while saturation measures the degree to which a pure colour is diluted by white light.

A typical way of representing colours in terms of *brightness, hue and saturation* is to use the *HSV* colour space, where H, S represent hue and saturation respectively, and V stands for *value*, which is simply an alternative way of saying brightness (luminance or intensity). HSV colour space is usually considered to be a deformation of RGB colour space. If we see RGB colour models as colour representations in regular Cartesian coordinates, then HSV is simply cylindrical-coordinate representations of those RGB points. In the cylindrical model, the angle around the central axis corresponds to the *hue* component, whereas the distance from the central axis stands for *saturation*, and the 'height' along the central axis corresponds to *value*, see Figure 2.5 (a) for a brief illustration. The definition of an HSV colour space would depend on its associated absolute (RGB) colour space (e.g. sRGB and Adobe RGB colour spaces both can be used to derive HSV colour spaces with the same conversion formula, however, their derived HSV colour spaces would be different).

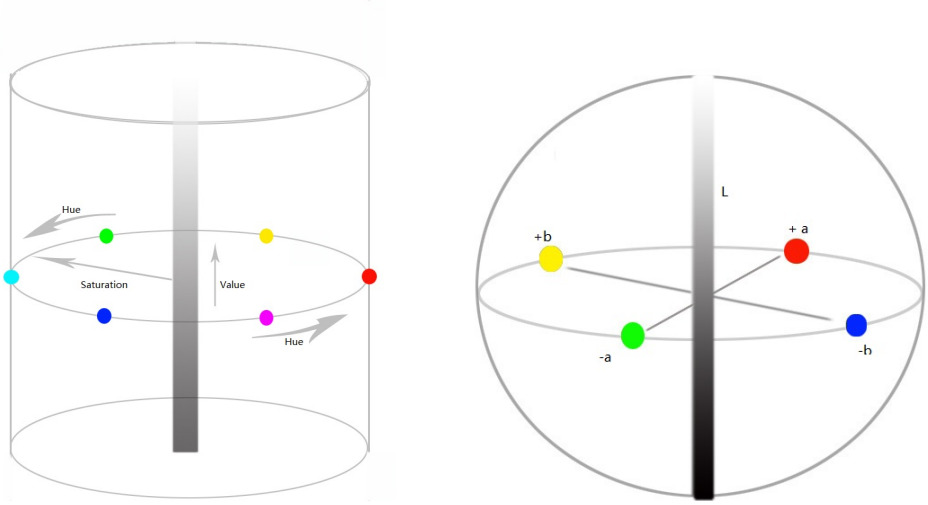

(a) (b)

Figure 2.5: Brief illustrations of the HSV and Lab colour models: (a) HSV colour model, (b) Lab colour model.

2.3.5 LAB colour space

Although RGB colour space is consistent with the colour perception of human eye, and HSV colour space is consistent with human interpretation of colours, these two colour spaces suffer from the same difficulty in computational photography. That is, the Euclidean metric defined on the two colour spaces is not perceptionally uniform. To overcome this difficulty, a new class of colour spaces are designed, and now they are commonly known as *Lab* colour spaces (here the term *Lab* does not stand for the word 'lab' but rather three separate alphabets with special meaning). In any Lab colour space, the L-coordinate represents the lightness of colour, the a-coordinate represents its position between red/magenta and green, and the b-coordinate represents its position between yellow and blue, see Figure 2.5 (b) for a brief illustration. One typical Lab colour space is the CIELAB colour space, which happens to be the most complete colour space specified by CIE as well.

In this thesis, the conversion between sRGB colour space and CIELAB colour

space is involved. So in the following, we provide the corresponding conversion formulas. To convert sRGB colour representation to CIELAB colour representation, we need to firstly set $r = R/255, g = G/255$, and $b = B/255$, and then obtain the (X', Y', Z') values via the following linear transform

$$\begin{pmatrix} X' \\ Y' \\ Z' \end{pmatrix} = \mathcal{A} \begin{pmatrix} r \\ g \\ b \end{pmatrix}$$

where

$$\mathcal{A} = \begin{pmatrix} 0.4124 & 0.3576 & 0.1805 \\ 0.2126 & 0.7152 & 0.0722 \\ 0.0193 & 0.1192 & 0.9505 \end{pmatrix}. \tag{2.29}$$

Next, by setting $X = 100X', Y = 100Y'$ and $Z = 100Z'$, the CIELAB colour values (L^*, a^*, b^*) can be obtained by

$$\begin{cases} L^* = 116g(Y/Y_w) - 16, \\ a^* = 500[g(X/X_w) - g(Y/Y_w)], \\ b^* = 200[g(Y/Y_w) - g(Z/Z_w)], \end{cases}$$

where (X_w, Y_w, Z_w) are the coordinates of the reference white point (e.g. $D65$) in CIEXYZ colour space, and

$$g(t) = \begin{cases} t^{\frac{1}{3}}, & \text{if } t > (\frac{6}{29})^3, \\ \frac{1}{3}(\frac{29}{6})^2 t + \frac{4}{29}, & \text{if } t \leqslant (\frac{6}{29})^3. \end{cases} \tag{2.30}$$

The conversion from CIELAB values (L^*, a^*, b^*) to sRGB values (R, G, B) is realized by simply reversing the prescribed procedure. That is, firstly we obtain the (X, Y, Z) values via

$$\begin{cases} Y = Y_w g^{-1}(\frac{1}{116}(L^* + 16)), \\ X = X_w g^{-1}(\frac{1}{116}(L^* + 16) + \frac{1}{500}a^*), \\ Z = Z_w g^{-1}(\frac{1}{116}(L^* + 16) - \frac{1}{200}b^*), \end{cases}$$

where g^{-1} is the inverse function of g in (2.30), and X_w, Y_w, Z_w are the coordinates of the reference white point (e.g. $D65$) in CIEXYZ colour space. Then, by setting $X' = X/100, Y' = Y/100$ and $Z' = Z/100$, we derive the normalized RGB values (r, g, b) from

$$\begin{pmatrix} r \\ g \\ b \end{pmatrix} = \mathcal{A}^{-1} \begin{pmatrix} X' \\ Y' \\ Z' \end{pmatrix},$$

where $\mathcal{A}^{-1}$ is the inverse of $\mathcal{A}$ defined in (2.29). Finally, we obtain the regular $sRGB$ values (R, G, B) by setting $R = 255r, G = 255g$ and $B = 255b$.

2.4 Wavelet tight frame based image restoration models

In this section, we review several mathematical models for $2D$ (greyscale/monochromatic) image restoration. This review would serve us as mathematical preparations for the colour image restoration problem, and it also introduces the numerical tools that are to be used in the application part of this thesis.

The classical image restoration problem is to estimate the underlying clean image from the corrupted (or degraded) observed image data. Typical image corruptions (or degradations) include blurring, missing of pixels, missing of colours or fine details, etc. Besides, almost all images suffer more or less from noise. If we view a $2D$ corrupted image as a vector (by concatenating its columns), then those corruption or degradation operators usually would have matrix representations. To be general, we let A be any kind of degradation operator, then the corruption process can be mathematically modeled as

$$g = Af + e, \tag{2.31}$$

where f is the original image vector, e is the additive noise component, and g is the observed/available image data. Following the image degradation model as in (2.31), the image restoration task is to recover the original image f from the degraded noisy observation g. However, with the present of noise and other degradation operators, exact recovery is rare. A more realistic thinking is to find a 'good' or 'reasonable' estimator of the original image f from the observed data g.

One common approach for estimating f from g is to solve the following *least square problem*

$$\min_h \|Ah - g\|_2^2. \tag{2.32}$$

It is easy to see that the first order optimality condition of the above *least square problem* is a linear equation system as follows

$$A^T Ah = A^T g, \tag{2.33}$$

where A^T is the transpose of A. Thus, if the matrix $A^T A$ is invertible, we can obtain the following kind of *least square solution*

$$h = (A^T A)^{-1} A^T g.$$

However, it can happen that the matrix $A^T A$ is not invertible (e.g., in the image inpainting problem, A is a diagonal matrix with 1s and 0s in its main diagonal, where the 0 entries represent the position of missing pixels, thus $A^T A = A$ is not invertible). And even when $A^T A$ is invertible, it is usually ill-conditioned. In this case, the noise component in the observed data g would inevitably be magnified by $(A^T A)^{-1}$, and the final outcome would be immersed by the magnified noise component.

To resolve the ill-posedness of the least square problem in (2.33), some *regularization techniques* need to be applied. In the literature, Tikhonov regularization

method was often applied for alleviating such ill-posedness:

$$\min_h \|Ah - g\|_2^2 + c\|h\|_2^2, \tag{2.34}$$

where $c > 0$ is a positive scalar. The model (2.34) is again a least square problem with first optimality condition

$$(A^T A + cI)h = A^T g, \tag{2.35}$$

where I is the identity map (matrix). Tikhonov regularization scheme in (2.34) had been very favored in many applications because of its easiness to incorporate prior information, and the existence of a closed form solution in (2.35). However, Tikhonov regularization scheme also suffers a few weaknesses. In particular, it tends to attenuate strong image edges and often makes the resulting image overly smoothed.

Tikhonov regularization method is essentially an ℓ_2-regularization method, whose solution can be obtained by solving a linear system as in (2.35). So ℓ_2-regularization models are often referred as *linear* models. For handling (ill-posed) image restoration problem, a major breakthrough is moving from linear models to *non-linear* models, like *total variation (TV)* based regularization models (see, e.g. [63, 41]) and wavelet tight frame based regularization models (see, e.g. [17, 19, 9, 14, 34]). Compared to the previous linear methods, non-linear models can often lead to results with better quality (see, e.g. [14]). Besides, although non-linear models do not have closed form solutions as those linear models do, they still can be solved by efficient iterative algorithms like *proximal forward backward splitting (PFBS)* [24, 17], *accelerated projected gradient (APG)* [68], *split Bregman* [41, 14], etc. In this thesis we mainly focus on wavelet tight frame (framelet) based image restoration models and their associated numerical solvers.

2.4.1 The general framelet based image restoration model

In this subsection, we introduce several wavelet tight frame (framelet) based mathematical models for $2D$ image restoration. For notional convenience, we let W be the framelet transform operator, A be some image degradation operator, and g be the observed image data. Then, the general image restoration model (see, e.g. [34, 67]) can be expressed as

$$\min_{\alpha} \frac{1}{2}\|AW^T\alpha - g\|_2^2 + \frac{\kappa}{2}\|(I - WW^T)\alpha\|_2^2 + \|\mathrm{diag}(\lambda)\cdot\alpha\|_1, \tag{2.36}$$

where I is the identity map, and $0 \leqslant \kappa \leqslant \infty$ is a nonnegative scalar. So to obtain the approximated image f, we first need to find an optimal solution α^* to (2.36), and synthesize the f from α^* by setting $f = W^T\alpha^*$.

The first term in (2.36) is an alternative way of writing the least square (2.32), which is usually referred as the *fidelity term*. The meaning of the second term in (2.36) is a bit complicated, yet it is easy to see that if $\alpha = Wh$ for some h, then this term would vanish. The third term in (2.36) is the ℓ_1-norm of the framelet coefficient vector α, which can be seen as a sparsity constraint for the framelet coefficients, and λ is the weight function of the coefficient set α.

2.4.2 Synthesis based model, analysis based model and balanced model

With a general image restoration model defined as in (2.36), different settings of the value κ therein would result in three different specific image restoration models that are described as follows:

- $\kappa = 0$, so
$$\min_{\alpha} \frac{1}{2}\|AW^T\alpha - g\|_2^2 + \|\mathrm{diag}(\lambda)\cdot\alpha\|_1,$$
and the above model is called the *synthesis based model*.

- $0 < \kappa < \infty$, so

$$\min_{\alpha} \frac{1}{2}\|AW^T\alpha - g\|_2^2 + \frac{\kappa}{2}\|(I - WW^T)\alpha\|_2^2 + \|\mathrm{diag}(\lambda)\cdot\alpha\|_1, \tag{2.37}$$

  which looks the same as (2.36), but one should keep in mind now that $0 < k < \infty$. In this case, (2.37) is called the *balanced model*.

- $\kappa = \infty$, in this case the term $\|(I - WW^T)\alpha\|_2^2$ has to vanish, so $\alpha - WW^T\alpha = 0$. By letting $u = W^T\alpha$, one has $\alpha = Wu$, so (2.36) can be rewritten as

$$\min_{u} \frac{1}{2}\|Au - g\|_2^2 + \|\mathrm{diag}(\lambda)Wu\|_1, \tag{2.38}$$

  which is called the *analysis based model*.

It is noted that when the rows of W constitute an orthonormal basis, then we have $WW^T = I$ and hence the three models are exactly the same. However, when the rows of W form a redundant tight frame, then $WW^T \neq I$ and hence the three models are mutually different and cannot be derived from each other. It is also observed that the ℓ_1-minimization models in compressed sensing closely resemble the synthesis model, while the TV-norm regularization model [63] is analysis based model in nature.

The effectiveness of the three image restoration models largely depends on the given data sets and applications. For the analysis based model, the framelet coefficients Wu is often linked to the smoothness of u. Thus for image restoration tasks, the framelet based analysis model tends to generate smoother images than synthesis based model, as shown in many experimental works (e.g. [14]). On the contrary, the synthesis model explores the sparse representation of the underlying solution in the redundant frame system, which usually enhances edges while bringing in artifacts as well (see, e.g. [9]). In comparison, the balanced model balances the smoothness of the underlying image as well as the sparsity of coefficients of

the image in the redundant frame system (see, e.g. [8, 9, 10, 18, 19]), thus it serves us as a bridge between the analysis based model and synthesis based model.

2.4.3 Numerical solvers of image restoration models

Although different in form, algorithms and convergence analysis of synthesis based model and balanced model are quite the same, so in the following context we put the two together as a whole and call it the *general balanced model* [34].

For simplicity, we view the coefficient set α as a vector of dimension m (i.e. $\alpha \in \mathbb{R}^m$), and then the *proximal forward-backward splitting (PFBS) algorithm* (see, e.g. [9, 10, 15, 16, 17, 24]) can be applied to solve the general balanced model.

For notation convenience, we write the *general balanced model* as

$$\min_{\alpha} F_1(\alpha) + F_2(\alpha) \tag{2.39}$$

with $F_1(\alpha) := \|\mathrm{diag}(\lambda)\alpha\|$ and

$$F_2(\alpha) := \frac{1}{2}\|AW^T\alpha - g\|_2^2 + \frac{\kappa}{2}\|(I - WW^T)\alpha\|_2^2,\ 0 \leqslant \kappa < \infty.$$

It is obvious that F_2 is $L - Lipschitz$ continuous for some $L \leqslant \rho_{max}(A^TA) + \kappa$. Then, PFBS algorithm for solving the general balanced model is implemented as follows:

Algorithm 2.3: Proximal Forward-backward Splitting (PFBS) Method

---

Given $\lambda \in \mathbb{R}_+^m$, we set up the initial guess α_0. Then for $k = 0, 1, 2, \ldots$, we generate α_{k+1} from α_k based on the following iterations until the pre-defined stopping criterion is fulfilled:

(i) set $\beta_k = \alpha_k - \nabla F_2(\alpha_k)/L$;

(ii) set $\alpha_{k+1} = \mathcal{T}_{\lambda/L}(\beta_k)$, where

$$\mathcal{T}_{\lambda/L}(\beta_k) = [t_{\lambda_1/L}(\beta_{k,1}), \cdots, t_{\lambda_n/L}(\beta_{k,n})]$$

is the soft-thresholding operator with threshold vector λ/L

$$t_{\lambda_i/L}(\beta_{k,i}) = \text{sign}(\beta_{k,i}) \cdot \max(|\beta_{k,i}| - \lambda_i/L, 0),\ 1 \leqslant i \leqslant n.$$

As a final step for image restoration, the approximated image is then obtained by setting $f = W^T\alpha_{k+1}$.

Step (i) and step (ii) in the above PFBS algorithm can be combined as a single step as follows:

$$\alpha_{k+1} = \text{prox}_{F_1/L}(\alpha_k - \nabla F_2(\alpha_k)/L),$$

where the proximal operator prox_F with respect to function F is defined as

$$\text{prox}_F(\alpha) = \arg\min_{\gamma} F(\gamma) + \frac{1}{2}\|\gamma - \alpha\|_2^2.$$

The convergence analysis of the PFBS algorithm is seen in the following theorem.

Theorem 2.14. *[34] Consider a minimization problem with the form of* (2.39)*, where* $F_1(\alpha) = \|\text{diag}(\lambda)\alpha\|_1$ *and* $F_2(\alpha) : \mathbb{R}^m \mapsto \mathbb{R}$ *is continuous, differentiable with L-Lipschitz continuous gradient. Let* $F := F_1 + F_2$ *and* α^* *be any solution of* (2.39)*. Then the sequence* $\{\alpha_k : k = 0, 1, \ldots\}$ *generated by Algorithm 2.3 satisfies*

$$F(\alpha_k) - F(\alpha^*) \leqslant L\frac{\|\alpha^* - \alpha_0\|_2^2}{2k}.$$

Consequently, given any $\epsilon > 0$*, we have*

$$F(\alpha_k) - F(\alpha^*) \leqslant \epsilon,\ \textit{whenever}\ k \geqslant L\frac{\|\alpha^* - \alpha_0\|_2^2}{2\epsilon}.$$

Moreover, when the solution to (2.39) *is unique, we have*

$$\lim_{k\to\infty} \|\alpha_k - \alpha^*\|_2 = 0.$$

It is seen from the above analysis that the PFBS algorithm generates an ϵ-optimal solution of (2.39) in $O(L/\epsilon)$ iterations. Although the speed is reasonably fast, there are even faster algorithms available. A typical example is the *accelerated proximal gradient (APG) algorithm* [68], which is obtained by adjusting step $\beta_k = \alpha_k - \nabla F_2/L$ and can be explicitly described as follows:

Algorithm 2.4: Accelerated Proximal Gradient (APG) Method

Given $\lambda \in \mathbb{R}^n_+$, set up $\alpha_0 = \alpha_{-1} \in \mathbb{R}^n$, $t_0 = 1$ and $t_{-1} = 0$. Then for $k = 0, 1, 2, \ldots$, we generate α_{k+1} from α_k based on the following iteration until the pre-defined stopping criterion is satisfied:

(i) set $\beta_k = \alpha_k + \frac{t_{k-1}-1}{t_k}(\alpha_k - \alpha_{k-1})$;

(ii) set $\gamma_k = \beta_k - \nabla F_2(\beta_k)/L$;

(iii) set $\alpha_{k+1} = \mathcal{T}_{\lambda/L}(\gamma_k)$;

(vi) compute $t_{k+1} = \frac{1+\sqrt{1+4t_k^2}}{2}$.

The following theorem shows that, to obtain an ϵ-optimal solution, we only need to apply approximately $O(\sqrt{L/\epsilon})$ iterations of APG. The speed of convergence of the APG algorithm is thus considerably faster compared to that of the PFBS algorithm.

Theorem 2.15. *[34] Let $\{\alpha_k : k = 0, 1, \ldots\}$, $\{\beta_k : k = 0, 1, \ldots\}$ and $\{t_k : k = 0, 1, \ldots\}$ be the sequences generated in Algorithm 2.4. Then for any $k \geqslant 1$ and any optimal solution α^* to the general balanced model in the form of (2.36), we have*

$$F(\alpha_k) - F(\alpha^*) \leqslant 2L\frac{\|\alpha^* - \alpha_0\|_2^2}{(k+1)^2},$$

where F is the objective function of (2.36) *with* $0 \leqslant \kappa < \infty$. *Consequently, given any* $\epsilon > 0$, *we have*

$$F(\alpha_k) - F(\alpha^*) \leqslant \epsilon, \text{ whenever } k \geqslant \sqrt{\frac{2L}{\epsilon}}\|\alpha^* - \alpha_0\|_2 - 1.$$

Moreover, if the solution to the general balanced model is unique, then

$$\lim_{k\to\infty} \|\alpha_k - \alpha^*\|_2 = 0.$$

As to the *analysis based model* defined in (2.38), for notation convenience we write $H(u) = \frac{1}{2}\|Au - g\|_2^2$, then the analysis based model becomes

$$\min_u H(u) + \|\mathrm{diag}(\lambda)Wu\|_1. \tag{2.40}$$

The main difficulty for solving the analysis based model (2.40) lies in the fact that the term $\|Wu\|_1$ is both non-smooth and non-separable, as compared to the *general balanced model*. The main idea for overcoming this difficulty is to transfer (2.40) into the a problem with separable non-smooth terms only. A typical approach for doing this is to replace the term Wu in (2.40) by a new variable d, and then add a new hard constraint $d = Wu$ therein. Then (2.40) becomes

$$\min_{u,d} H(u) + \|\mathrm{diag}(\lambda)d\|_1 \text{ subject to } d = Wu. \tag{2.41}$$

The model (2.41) can be solved by an alternating algorithm based on the Bregman distance with an inexact solver. This algorithm is currently well-known by the name of *split Bregman algorithm* [41, 14], whose detailed implementation is given as follows:

Algorithm 2.5: Split Bregman Method

(i) Set up initial guess d_0 and b_0, and choose some $\delta \in (0, 1]$ and $\mu > 0$.

(ii) For $k = 0, 1, \ldots$ do the following iterations until the pre-defined convergence criterion is satisfied

$$\begin{cases} u_{k+1} = (A^T A + \mu I)^{-1}\big(A^T g + \mu W^T (d_k - b_k)\big), \\ d_{k+1} = \mathcal{T}_{\lambda/\mu}(W u_{k+1} + b_k), \\ b_{k+1} = b_k + \delta(W u_{k+1} - d_{k+1}). \end{cases}$$

Convergence of the split Bregman algorithm is illustrated in the following theorem

Theorem 2.16. *[14, 34] Assume that there exists at least one solution u^* of* (2.40)*. Assume that $0 \leqslant \delta \leqslant 1$ and $\mu > 0$. Then, the following properties hold for the unconstraint split Bregman algorithm:*

$$\lim_{k \to +\infty} \|\mathrm{diag}(\lambda) W u_k\|_1 + H(u_k) = \|\mathrm{diag}(\lambda) W u^*\|_1 + H(u^*).$$

Furthermore, $\lim_{k \to +\infty} \|u_k - u^*\|_2 = 0$ *whenever the solution to* (2.40) *is unique.*

The split Bregman algorithm can handle additional linear equality constraints as well, which leads to the so-called *constraint split Bregman algorithm* (see, e.g. [14]). More precisely, given the *constraint analysis based model* defined as follows:

$$\|\mathrm{diag}(\lambda) W u\|_1 \text{ subject to } Au = g,$$

where A is a linear operator, we can solve it using the following iterative scheme:

Algorithm 2.6: Constraint Split Bregman Method

(i) Set up initial guess d_0 and b_0 and c_0, and choose $\delta_i \in (0, 1]$, $i = 1, 2$, $\mu > 0$ and $\rho > 0$.

(ii) For $k = 0, 1, \ldots$ do the following iterations until the pre-defined convergence criterion is satisfied

$$\begin{cases} u_{k+1} = (\rho A^T A + \mu I)^{-1}\big(\rho A^T(g - c_k) + \mu W^T(d_k - b_k)\big), \\ d_{k+1} = \mathcal{T}_{\lambda/\mu}(W u_{k+1} + b_k), \\ b_{k+1} = b_k + \delta_1(W u_{k+1} - d_{k+1}), \\ c_{k+1} = c_k + \delta_2 \kappa(A u_{k+1} - g). \end{cases}$$

Convergence of the above algorithm is guaranteed, similar to the non-constraint case (see, e.g. [14]).

Chapter 3

Band-limited Tight Frames in Low Dimensions

As mentioned in Chapter 2, this thesis only involves MRA-based constructions of wavelets and wavelet tight frames. So, to construct non-separable band-limited wavelet frames, we first provide the construction of their corresponding non-separable band-limited refinable functions.

3.1 On the construction of non-separable band-limited refinable functions

The main idea for our construction of non-separable band-limited refinable function originates from the construction of *box splines* [7, 59], i.e. multiplying univariate Meyer's refinable function along multiple orientations given by the standard box-spline direction matrices. More explicitly, suppose $\varphi \in L_2(\mathbb{R})$ is a univariate refinable function such that $\widehat{\varphi}$ is (essentially) bounded. Let τ be its refinement mask and Ξ be a $d \times n$ full rank direction matrix with integer entries and $n \geqslant d$,

then we can define a refinable function $\phi_\Xi \in L_2(\mathbb{R}^d)$ as follows:

$$\widehat{\phi_\Xi}(\xi) = \prod_{r\in \mathrm{col}(\Xi)} \widehat{\varphi}(r\cdot\xi), \quad \xi = (\xi_1, \dots, \xi_d)^T \in \mathbb{R}^d, \tag{3.1}$$

where col(Ξ) enumerates all column vectors of the direction matrix Ξ.

The function ϕ_Ξ in (3.1) may also be defined by tempered distribution. In fact, when $\varphi \in L_1(\mathbb{R}) \cap L_2(\mathbb{R})$, we can set an n-variate separable function $f(u) := \prod_{j=1}^n \varphi(u_j)$, $u = (u_1, \cdots, u_n)^T$. Then we can define the *multivariate F-truncated powers* associated with f and Ξ (see [71]), which is a tempered distribution such that

$$T_f(\cdot \mid \Xi)(h) = \int_{\mathbb{R}^n} f(u)h(\Xi u)du$$

for any rapidly decreasing function h in $\mathbb{R}^d$. From the above definition of $T_f(\cdot \mid \Xi)$, one can derive that

$$\begin{aligned}
\widehat{T_f(\cdot \mid \Xi)}(h) &= T_f(\cdot \mid \Xi)(\widehat{h}) \\
&= \int_{\mathbb{R}^n} f(u)\widehat{h}(\Xi u)du \\
&= \int_{\mathbb{R}^n} f(u) \int_{\mathbb{R}^d} h(\xi)\exp(-i\Xi u\cdot\xi)d\xi du.
\end{aligned}$$

By Fubini's theorem, one can change the order of integration of the last integral, thus

$$\begin{aligned}
\widehat{T_f(\cdot \mid \Xi)}(h) &= \int_{\mathbb{R}^d} h(\xi) \int_{\mathbb{R}^n} f(u)\exp(-i\Xi u\cdot\xi)du\ d\xi \\
&= \int_{\mathbb{R}^d} h(\xi) \int_{\mathbb{R}^n} f(u)\exp(-iu\cdot\Xi^\top\xi)du\ d\xi \\
&= \int_{\mathbb{R}^d} h(\xi) \int_{\mathbb{R}^n} \prod_{j=1}^n \varphi(u_j)\exp(-iu\cdot\Xi^\top\xi)du\ d\xi \\
&= \int_{\mathbb{R}^d} \prod_{r\in\mathrm{col}(\Xi)} \widehat{\varphi}(r\cdot\xi)h(\xi)d\xi,
\end{aligned}$$

which implies $\widehat{T_f(\cdot \mid \Xi)} = \prod_{r\in\mathrm{col}(\Xi)} \widehat{\varphi}(r\cdot\xi)$, so

$$T_f(\cdot \mid \Xi) = \phi_\Xi.$$

This equivalence between $T_f(\cdot \mid \Xi)$ and ϕ_Ξ is established in [71]. Moreover, it is also shown in Proposition 3.1 of [71] that

$$\phi_\Xi(x) = \frac{1}{\sqrt{\det(\Xi\Xi^{\mathrm{T}})}} \int_{u\in\Xi^{-1}x, u\in\mathbb{R}^n} f(u)d\mu, \forall x \in \mathbb{R}^d,$$

where Ξ^{-1} is the inverse map of Ξ, and μ is the $n-d$ dimensional Lebesgue measure of the hyper plane $\Xi^{-1}x$.

Clearly, the function ϕ_Ξ defined in (3.1) is still refinable as

$$\widehat{\phi_\Xi}(2\xi) = \prod_{r\in\mathrm{col}(\Xi)} \widehat{\varphi}(2r\cdot\xi) = \prod_{r\in\mathrm{col}(\Xi)} \tau(r\cdot\xi)\widehat{\varphi}(r\cdot\xi) = \tau_\Xi(\xi)\widehat{\phi_\Xi}(\xi), \quad \xi\in\mathbb{R}^d,$$

and $\tau_\Xi(\xi) = \prod_{r\in\mathrm{col}(\Xi)} \tau(r\cdot\xi)$ is a 2π-periodic function of $\mathbb{R}^d$, since all elements of r are integers and τ is a 2π-periodic function.

Prior to the derivation any tight frames from the above class of band-limited refinable functions, we present a few results as theoretical preparations.

3.2 Auxiliary lemmas, theorems and corollaries

We first introduce a lemma concerning the map η as defined in (2.27), which is taken from the proof of Theorem 2.12 in [60].

Lemma 3.1. *Let τ be a real-valued measurable 2π-periodic function defined on $\mathbb{R}^d$, $d = 2$ or 3, and*

$$\tau_\nu(\xi) = \exp\left(i\eta(\nu)\cdot\xi\right)\tau(\xi+\nu\pi),\ \nu\in\mathbb{Z}_2^d.$$

Then for any $\kappa\in\mathbb{Z}_2^d\backslash\{0\}$, one has

$$\sum_{\nu\in\mathbb{Z}_2^d} \tau_\nu(\xi)\overline{\tau_\nu(\xi+\kappa\pi)} = 0.$$

Proof. It can be verified by direct calculation that, for either $d = 2$ or 3, the map η defined in (2.27) satisfies the following property:

for any ν_1, $\nu_2 \in \mathbb{Z}_2^d$, if $\nu_1 \neq \nu_2$, then $(\eta(\nu_1) - \eta(\nu_2))(\nu_1 - \nu_2)$ is an odd number.

Let $\kappa \in \mathbb{Z}_2^d \backslash \{0\}$ be fixed. We view $\mathbb{Z}_2^d$ as an additive group modulo 2, so for any $\nu \in \mathbb{Z}_2^d$, there exists a unique $\tilde{\nu} \in \mathbb{Z}_2^d$ different from ν such that $\tilde{\nu} = \nu + \kappa$ in $\mathbb{Z}_2^d$. Conversely one has $\nu + \kappa = \tilde{\nu}$ in $\mathbb{Z}_2^d$ as well. Since τ is 2π-periodic, one has $\tau(\xi + \nu\pi + \kappa\pi) = \tau(\xi + \tilde{\nu}\pi)$ and $\tau(\xi + \tilde{\nu}\pi + \kappa\pi) = \tau(\xi + \nu\pi)$. Then

$$
\begin{aligned}
&\tau_\nu(\xi)\overline{\tau_\nu(\xi + \kappa\pi)} + \tau_{\tilde{\nu}}(\xi)\overline{\tau_{\tilde{\nu}}(\xi + \kappa\pi)} \\
&= \tau(\xi + \nu\pi)\tau(\xi + \tilde{\nu}\pi)\Big(\exp(i\eta(\nu) \cdot \xi) \exp(-i\eta(\nu) \cdot (\xi + \kappa\pi)) \\
&\qquad + \exp(i\eta(\tilde{\nu}) \cdot \xi) \exp(-i\eta(\tilde{\nu}) \cdot (\xi + \kappa\pi)) \Big) \\
&= \tau(\xi + \nu\pi)\tau(\xi + \tilde{\nu}\pi)\Big(\exp(-i\eta(\nu) \cdot \kappa\pi) + \exp(-i\eta(\tilde{\nu}) \cdot \kappa\pi) \Big) \\
&= \tau(\xi + \nu\pi)\tau(\xi + \tilde{\nu}\pi) \exp(-i\eta(\nu) \cdot \kappa\pi) \Big(1 + \exp(-i(\eta(\tilde{\nu}) - \eta(\nu)) \cdot \kappa\pi) \Big) \\
&= \tau(\xi + \nu\pi)\tau(\xi + \tilde{\nu}\pi) \exp(-i\eta(\nu) \cdot \kappa\pi) \Big(1 + \exp(-i(\eta(\tilde{\nu}) - \eta(\nu)) \cdot (\tilde{\nu} - \nu)\pi) \Big) \\
&= \tau(\xi + \nu\pi)\tau(\xi + \tilde{\nu}\pi) \exp(-i\eta(\nu) \cdot \kappa\pi)(1 + (-1)) \\
&= 0.
\end{aligned}
$$

Thus

$$
\sum_{\nu \in \mathbb{Z}_2^d} \Big(\tau_\nu(\xi)\overline{\tau_\nu(\xi + \kappa\pi)} + \tau_{\tilde{\nu}}(\xi)\overline{\tau_{\tilde{\nu}}(\xi + \kappa\pi)} \quad \Big) = 0. \tag{3.2}
$$

Note that when ν enumerates all $\mathbb{Z}_2^d$, $\tilde{\nu}$ would enumerate all $\mathbb{Z}_2^d$ as well, hence (3.2) is

$$
2 \sum_{\nu \in \mathbb{Z}_2^d} \tau_\nu(\xi)\overline{\tau_\nu(\xi + \kappa\pi)} = 0,
$$

so $\sum_{\nu \in \mathbb{Z}_2} \tau_\nu(\xi)\overline{\tau_\nu(\xi + \kappa\pi)} = 0$ is shown and the proof is complete. □

To facilitate the derivation of MRA-based wavelet tight frames using extension principles as well as the above lemma, we assume in this chapter that any refinable function ϕ in discussion satisfies the following condition:

$$\begin{aligned} &\widehat{\phi} \text{ is real-valued, continuous at the origin with } \widehat{\phi}(\{0\}) = 1, \\ &\text{and } [\widehat{\phi}, \widehat{\phi}] \text{ is essentially bounded.} \end{aligned} \tag{3.3}$$

Now, let ϕ be a refinable function with mask τ satisfying (3.3). Suppose there exists a set of real-valued measurable 2π-periodic functions, denoted by $\{p(\xi),\, a_s(\xi) :\, s = 1, \ldots, N\}$, satisfying the following condition:

$$\sum_{\kappa \in \mathbb{Z}_2^d} |\tau(\xi + \kappa\pi)|^2 + \sum_{s=1}^{N} \sum_{\mu \in \mathbb{Z}_2^d} |a_s(\xi + \mu\pi)|^2 + |p(\xi)|^2 = 1, \tag{3.4}$$

then we may define a set of 2π-periodic functions

$$\{\tau_\kappa,\, a_{s,\mu} :\, \kappa \in \mathbb{Z}_2^d \backslash \{0\},\, \mu \in \mathbb{Z}_2^d,\, s = 1, \ldots, N\}$$

as follows:

$$\begin{cases} \tau_\kappa(\xi) = \exp(i\eta(\kappa) \cdot \xi)\tau(\xi + \kappa\pi), & \kappa \in \mathbb{Z}_2^d \backslash \{0\}; \\ a_{s,\mu}(\xi) = \exp(i\eta(\mu) \cdot \xi) a_s(\xi + \mu\pi), & \mu \in \mathbb{Z}_2^d,\, s = 1, \ldots, N. \end{cases} \tag{3.5}$$

The following theorem shows that the above set of 2π-periodic functions defines the generators of a wavelet tight frame of $L_2(\mathbb{R}^d), d = 2, 3$.

Theorem 3.2. *Let $\phi \in L_2(\mathbb{R}^d)$ be a band-limited refinable function with mask τ satisfying* (3.3)*. Suppose that $\{p(\xi),\, a_s(\xi) :\, s = 1, \ldots, N\}$ is a set of real-valued measurable 2π-periodic functions satisfying* (3.4) *and let $\{\tau_\kappa,\, a_{s,\mu} :\, \kappa \in \mathbb{Z}_2^d \backslash \{0\},\, \mu \in \mathbb{Z}_2^d,\, s = 1, \ldots, N\}$ be given as* (3.5)*. Define a set of functions Ψ as follows:*

$$\Psi = \{\psi_\kappa :\, \kappa \in \mathbb{Z}_2^d \backslash \{0\}\} \cup \{\psi_{s,\mu} :\, \mu \in \mathbb{Z}_2^d,\, s = 1, \ldots, N\} \cup \{\psi_p\} \tag{3.6}$$

where

$$\begin{cases} \widehat{\psi_\kappa}(\xi) = \tau_\kappa(\frac{\xi}{2})\widehat{\phi}(\frac{\xi}{2}), & \kappa \in \mathbb{Z}_2^d\backslash\{0\}; \\ \widehat{\psi_{s,\mu}}(\xi) = a_{s,\mu}(\frac{\xi}{2})\widehat{\phi}(\frac{\xi}{2}), & \mu \in \mathbb{Z}_2^d,\ s = 1, \dots, N; \\ \widehat{\psi_p}(\xi) = p(\xi)\tau(\frac{\xi}{2})\widehat{\phi}(\frac{\xi}{2}) = p(\xi)\widehat{\phi}(\xi). \end{cases} \tag{3.7}$$

Then the affine system $X(\Psi)$ generated by Ψ as in (2.13) *forms a tight frame of* $L_2(\mathbb{R}^d)$.

Proof. Define

$$P(\xi) = 1 - \sum_{s=1}^{N} \sum_{\mu\in\mathbb{Z}_2^d} |a_s(\xi + \mu\pi)|^2 - \sum_{\kappa\in\mathbb{Z}_2^d} |\tau(\xi + \kappa\pi)|^2,$$

and let $B(\xi) = p(2\xi)\tau(\xi), \Theta(\xi) = 1 - P(\xi)$. Then we have $|p(\xi)|^2 = P(\xi)$ and

$$\begin{aligned} & \Theta(2\xi)\tau(\xi)\overline{\tau(\xi)} + \sum_{\kappa\in\mathbb{Z}_2^d\backslash\{0\}} \tau_\kappa(\xi)\overline{\tau_\kappa(\xi)} + \sum_{s=1}^{N}\sum_{\mu\in\mathbb{Z}_2^d} a_{s,\mu}(\xi)\overline{a_{s,\mu}(\xi)} + B(\xi)\overline{B(\xi)} \\ = \ & -P(2\xi)\tau(\xi)\overline{\tau(\xi)} + 1 - P(\xi) + |p(2\xi)|^2\tau(\xi)\overline{\tau(\xi)} \\ = \ & -P(2\xi)\tau(\xi)\overline{\tau(\xi)} + 1 - P(\xi) + P(2\xi)\tau(\xi)\overline{\tau(\xi)} \\ = \ & 1 - P(\xi) = \Theta(\xi), \end{aligned}$$

i.e.

$$\Theta(2\xi)\tau(\xi)\overline{\tau(\xi)} + \sum_{\kappa\in\mathbb{Z}_2^d\backslash\{0\}} \tau_\kappa(\xi)\overline{\tau_\kappa(\xi)} + \sum_{s=1}^{N}\sum_{\mu\in\mathbb{Z}_2^d} a_{s,\mu}(\xi)\overline{a_{s,\mu}(\xi)} + B(\xi)\overline{B(\xi)} = \Theta(\xi). \tag{3.8}$$

Let $\tau_{\{0\}} = \tau$. By Lemma 3.1, we have for all $\nu \in \mathbb{Z}_2^d\backslash\{0\}$

$$\sum_{\kappa\in\mathbb{Z}_2^d} \tau_\kappa(\xi)\overline{\tau_\kappa(\xi + \nu\pi)} = 0, \text{ and } \sum_{\mu\in\mathbb{Z}_2^d} a_{s,\mu}(\xi)\overline{a_{s,\mu}(\xi + \nu\pi)} = 0, \ s = 1, \dots, N.$$

Thus for any $\nu \in \mathbb{Z}_2^d \backslash \{0\}$,

$$\begin{aligned}
&\Theta(2\xi)\tau(\xi)\overline{\tau(\xi+\nu\pi)} + \sum_{\kappa\in\mathbb{Z}_2^d\backslash\{0\}} \tau_\kappa(\xi)\overline{\tau_\kappa(\xi+\nu\pi)} + \sum_{s=1}^{N}\sum_{\mu\in\mathbb{Z}_2^d} a_{s,\mu}(\xi)\overline{a_{s,\mu}(\xi+\nu\pi)} \\
&\quad + B(\xi)\overline{B(\xi+\nu\pi)} \\
&= -P(2\xi)\tau(\xi)\overline{\tau(\xi+\nu\pi)} + |p(2\xi)|^2\tau(\xi)\overline{\tau(\xi+\nu\pi)} \\
&= -P(2\xi)\tau(\xi)\overline{\tau(\xi+\nu\pi)} + P(2\xi)\tau(\xi)\overline{\tau(\xi+\nu\pi)} \\
&= 0.
\end{aligned} \tag{3.9}$$

The equalities in (3.8) and (3.9) imply that the set of combined masks

$$\{\tau_\kappa(\xi),\, a_{s,\mu}(\xi),\, B(\xi) :\, \kappa \in \mathbb{Z}_2^d,\, \mu \in \mathbb{Z}_2^d,\, s = 1, \ldots, N;\}$$

satisfies (2.25) in OEP. Together with condition (3.3) on ϕ, one can conclude via OEP that the system $X(\Psi)$ as (2.13), with Ψ given as (3.6), forms a tight frame of $L_2(\mathbb{R}^d)$. □

In the case that the function $p(\xi)$ vanishes in (3.4), the corresponding wavelet ψ_p defined in (3.7) also vanishes and we have the following corollary.

Corollary 3.3. *Suppose that $\phi \in L_2(\mathbb{R}^d)$ is a band-limited refinable function satisfying* (3.3)*. Let its mask τ and $\{a_s : 1 \leqslant s \leqslant N\}$ be a set of real-valued measurable 2π-periodic functions satisfying*

$$\sum_{s=1}^{N}\sum_{\mu\in\mathbb{Z}_2^d} |a_s(\xi+\mu\pi)|^2 + \sum_{\kappa\in\mathbb{Z}_2^d} |\tau(\xi+\kappa\pi)|^2 = 1. \tag{3.10}$$

Define

$$\Psi' = \{\psi_\kappa :\, \kappa \in \mathbb{Z}_2^d\backslash\{0\}\} \cup \{\psi_{s,\mu} :\, \mu \in \mathbb{Z}_2^d,\, s = 1, \ldots, N\}, \tag{3.11}$$

where ψ_κ and $\psi_{s,\mu}$ are given as (3.7)*. Then the affine system $X(\Psi')$ generated by Ψ' as in* (2.13) *forms a tight frame of $L_2(\mathbb{R}^d)$.*

Remark. The above corollary can also be proved straightforwardly using UEP.

Theorem 3.2 and Corollary 3.3 provide explicit construction schemes to construct wavelet tight frames of $L_2(\mathbb{R}^d), d = 2, 3$. The requirement for applying Theorem 3.2 and Corollary 3.3 is that there exists a refinable function ϕ that satisfies (3.3) and a set of 2π-periodic functions $\{p(\xi),\, a_s(\xi) : s = 1, \ldots, N\}$ that satisfies (3.4) or (3.10). It is noted that (3.3) imposed on refinable functions is very mild. In contrast, some other types of wavelet tight frames were constructed by (e.g. [1, 2]) by requiring that the refinable function ϕ not only generates an MRA but also satisfies

$$\{\phi(\cdot - k) : k \in \mathbb{Z}^d\} \text{ is a tight frame of } V_0 := \mathcal{S}(\phi), \tag{3.12}$$

which, according to Theorem 2.7, is equivalent to

$$[\widehat{\phi}, \widehat{\phi}](\xi) = 1 \text{ a.e. on } \sigma(\mathcal{S}(\phi)).$$

Thus, if $\{\phi(\cdot - k) : k \in \mathbb{Z}^d\}$ forms a tight frame but not an orthonormal basis of $\mathcal{S}(\phi)$, then the spectrum set $\sigma(\mathcal{S}(\phi)) := \{\gamma : [\widehat{\phi}, \widehat{\phi}](\gamma) > 0\}$ differs from $\mathbb{R}^d$ by a set of non-zero measure (see [61, 1]). In this case, the term $[\widehat{\phi}, \widehat{\phi}]$ cannot be continuous. So in summary, if ϕ is a band-limited refinable function satisfying (3.12), then $\widehat{\phi}$ will not be continuous unless it is degenerated to the orthonormal case. Such a refinable function with discontinuities in frequency domain decays very slowly in spatial domain. On the contrary, the refinable function ϕ needed in Theorem 3.2 or Corollary 3.3 can be arbitrarily smooth in frequency domain, as long as it satisfies (3.3). Such refinable functions can have very rapid decay in spatial domain. In summary, the UEP/OEP based Theorem 3.2 or Corollary 3.3 provides a very convenient way to construct wavelet tight frames with fast decay in spatial domain.

3.3 Constructions of band-limited wavelet tight frames

To apply Theorem 3.2 or Corollary 3.3, we need to construct refinable functions that satisfy condition (3.3), and sets of 2π-periodic functions $\{p(\xi), a_s : s = 1, \ldots, N\}$ that satisfy (3.4) or (3.10). Based on the univariate Meyer's refinable function Q_Ω, we first construct a class of non-separable band-limited refinable functions that satisfies (3.3) using the representative box-spline direction matrices Ξ. For instance, in $\mathbb{R}^2$,

$$\Xi = \begin{bmatrix} \overbrace{1 \cdots 1}^{m_1} & \overbrace{0 \cdots 0}^{m_2} & \overbrace{1 \cdots 1}^{m_3} \\ 0 \cdots 0 & 1 \cdots 1 & 1 \cdots 1 \end{bmatrix}, \tag{3.13}$$

and in $\mathbb{R}^3$,

$$\Xi = \begin{bmatrix} \overbrace{1 \cdots 1}^{m_1} & \overbrace{0 \cdots 0}^{m_2} & \overbrace{0 \cdots 0}^{m_3} & \overbrace{1 \cdots 1}^{m_4} \\ 0 \cdots 0 & 1 \cdots 1 & 0 \cdots 0 & 1 \cdots 1 \\ 0 \cdots 0 & 0 \cdots 0 & 1 \cdots 1 & 1 \cdots 1 \end{bmatrix}. \tag{3.14}$$

Plugging any above direction matrix into (3.1), we have a refinable function $\phi^\Omega_{d,m} \in L_2(\mathbb{R}^d)$ defined by

$$\widehat{\phi^\Omega_{d,m}}(\xi) = \prod_{r \in \mathrm{col}(\Xi)} \widehat{Q_\Omega}(r \cdot \xi) = \widehat{Q_\Omega}^{m_{d+1}}(\sum_{j=1}^{d} \xi_j) \prod_{j=1}^{d} \widehat{Q_\Omega}^{m_j}(\xi_j) \tag{3.15}$$

for any $\xi = (\xi_1, \ldots, \xi_d)^T \in \mathbb{R}^d$, where Q_Ω is the Meyer's refinable function as in (2.8), $\frac{\pi}{2} < \Omega \leqslant \frac{2\pi}{3}$, and $m = (m_1, \ldots, m_{d+1}) \in (\mathbb{Z}^+)^{d+1}$ for $d = 2$ or 3. The associated refinement mask of $\phi^\Omega_{d,m}$ is

$$\tau_{d,m}(\xi) = \tau_\Omega^{m_{d+1}}(\sum_{j=1}^{d} \xi_j) \prod_{j=1}^{d} \tau_\Omega^{m_j}(\xi_j),\ \xi = (\xi_1, \ldots, \xi_d)^T \in \mathbb{R}^d, \tag{3.16}$$

where τ_Ω is the refinement mask of the univariate function Q_Ω defined by (2.10). The refinable function defined by (3.15) indeed satisfies (3.3), as we will show later in the proof of Theorem 3.4. The remaining is then about constructing a set of measurable 2π-periodic functions $\{p(\xi), a_s(\xi) : s = 1, \dots, N\}$ such that (3.4) or (3.10) holds. The solution to (3.4) is certainly not unique. One trivial solution is setting $a_s = 0, s = 1, \dots, N$ and $p(\xi) = (1 - \sum_{\kappa\in\mathbb{Z}_2^d} |\tau(\xi + \kappa\pi)|^2)^{1/2}$. However, the resulting wavelet $\widehat{\psi_p}$ may not be continuously differentiable, even though $\widehat{\phi}$ is sufficiently smooth. In the next theorem, we propose a solution to (3.4) whose resulting wavelets have sufficient smoothness in frequency domain. More specifically, suppose that the univariate Meyer's refinable function Q_Ω satisfies $\widehat{Q_\Omega} \in C^n(\mathbb{R})$ for some nonnegative integer n. We are seeking for the wavelet set Ψ defined in (3.6) (or Ψ' defined in (3.11)) such that $\widehat{\psi} \in C^n(\mathbb{R}^d)$, for any $\psi \in \Psi$ (or Ψ').

Theorem 3.4. *Let $\phi^\Omega_{d,m}$ be a refinable function defined as* (3.15) *with its mask $\tau_{d,m}$ given by* (3.16) *and $\frac{\pi}{2} < \Omega \leqslant \frac{2\pi}{3}$, $m \in (\mathbb{Z}^+)^{d+1}$ for $d = 2$ or 3. Define a set of 2π-periodic functions $\{h_j, j = 1, \dots, d+1\}$ as follows:*

$$\begin{cases} h_j(\xi) = \sqrt{1 - \tau_\Omega^{2(m_j-1)}(\xi_j)}\, \prod_{s=1}^{j} \tau_\Omega(\xi_s) \prod_{t=j+1}^{d} \tau_\Omega^{m_t}(\xi_t), \ j = 1, \dots, d; \\ h_{d+1}(\xi) = \tau_\Omega(\sum_{j=1}^d \xi_j + \pi) \sqrt{1 + \sum_{s=1}^{m_{d+1}-1} \tau_\Omega^{2s}(\sum_{j=1}^d \xi_j)}\, \prod_{j=1}^d \tau_\Omega^{m_j}(\xi_j), \end{cases} \tag{3.17}$$

where τ_Ω is the refinement mask of Q_Ω given by (2.10)*. Then we have $\phi_{d,m}$ satisfies* (3.3)*, and*

$$\sum_{j=1}^{d+1} \sum_{\nu\in\mathbb{Z}_2^d} |h_j(\xi + \nu\pi)|^2 + \sum_{\nu\in\mathbb{Z}_2^d} |\tau_{d,m}(\xi + \nu\pi)|^2 = 1. \tag{3.18}$$

Proof. We first verify that the function $\phi^\Omega_{d,m}$ in (3.15) satisfies (3.3) Since the function $\widehat{\phi^\Omega_{d,m}}$ is finitely supported, $[\widehat{\phi^\Omega_{d,m}}, \widehat{\phi^\Omega_{d,m}}]$ is a finite summation of the sequence $\{|\widehat{\phi^\Omega_{d,m}}|^2(\cdot + 2\pi k), k \in \mathbb{Z}^d\}$ in any finite interval. Thus, $[\widehat{\phi^\Omega_{d,m}}, \widehat{\phi^\Omega_{d,m}}]$ is continuous as long as $|\widehat{\phi^\Omega_{d,m}}|^2$ is continuous. The facts that $\widehat{\phi^\Omega_{d,m}}(0) = 1$ and $\widehat{\phi^\Omega_{d,m}}(2\pi k) = 0$ for all $k \in \mathbb{Z}^d \backslash \{0\}$ lead to $[\widehat{\phi^\Omega_{d,m}}, \widehat{\phi^\Omega_{d,m}}](0) = 1$. The verification of (3.3) on $\phi^\Omega_{d,m}$ is done.

Secondly, it is seen that h_j given by (3.17) is real for $j = 1, \ldots, d, d+1$. Moreover,

$$\begin{cases} |h_j(\xi)|^2 = \big(1 - \tau_\Omega^{2(m_j-1)}(\xi_j)\big) \prod_{s=1}^{j} \tau_\Omega^2(\xi_s) \prod_{t=j+1}^{d} \tau_\Omega^{2m_t}(\xi_t),\ j = 1, \ldots, d; \\ |h_{d+1}(\xi)|^2 = \big(1 - \tau_\Omega^{2m_{d+1}}(\sum_{j=1}^{d} \xi_j)\big) \prod_{j=1}^{d} \tau_\Omega^{2m_j}(\xi_j). \end{cases}$$

Thus, we have

$$\begin{aligned} |\tau_{d,m}(\xi)|^2 + |h_{d+1}(\xi)|^2 &= \tau_\Omega^{2m_{d+1}}(\sum_{j=1}^{d} \xi_j) \prod_{j=1}^{d} \tau_\Omega^{2m_j}(\xi_j) + \big(1 - \tau_\Omega^{2m_{d+1}}(\sum_{j=1}^{d} \xi_j)\big) \prod_{j=1}^{d} \tau_\Omega^{2m_j}(\xi_j) \\ &= \prod_{j=1}^{d} \tau_\Omega^{2m_j}(\xi_j), \end{aligned}$$

By induction, we have

$$|\tau_{d,m}(\xi)|^2 + |h_{d+1}(\xi)|^2 + \sum_{j=1}^{s} |h_j(\xi)|^2 = \prod_{j=1}^{s} \tau_\Omega^2(\xi_j) \prod_{j=s+1}^{d} \tau_\Omega^{2m_j}(\xi_j), \tag{3.19}$$

holds for any s, $s = 1, \ldots, d$. Plugging $s = d$ into (3.19), we have

$$|\tau_{d,m}(\xi)|^2 + \sum_{j=1}^{d+1} |h_j(\xi)|^2 = |\tau(\xi)|^2 + |h_{d+1}(\xi)|^2 + \sum_{j=1}^{d} |h_j(\xi)|^2 = \prod_{j=1}^{d} \tau_\Omega^2(\xi_j).$$

By the fact that $\tau_\Omega^2(\cdot) + \tau_\Omega^2(\cdot + \pi) = 1$,

$$\begin{aligned} &\sum_{\nu \in \mathbb{Z}_2^d} \big(|\tau_{d,m}(\xi + \nu\pi)|^2 + \sum_{j=1}^{d+1} |h_j(\xi + \nu\pi)|^2\big) = \sum_{\nu \in \mathbb{Z}_2^d} \prod_{j=1}^{d} \tau_\Omega^2(\xi_j + \nu_j\pi) \\ &= \prod_{j=1}^{d} \big(\tau_\Omega^2(\xi_j) + \tau_\Omega^2(\xi_j + \pi)\big) = 1. \end{aligned}$$

Therefore

$$\sum_{\nu \in \mathbb{Z}_2^d} \big(|\tau_{d,m}(\xi + \nu\pi)|^2 + \sum_{j=1}^{d+1} |h_j(\xi + \nu\pi)|^2\big) = 1,$$

which is (3.18). The proof is done. □

Theorem 3.4 provides a solution to (3.10). Together with Theorem 3.2, we have

Corollary 3.5. *Let $\phi^{\Omega}_{d,m}$ be a refinable function defined as* (3.15) *with its mask $\tau_{d,m}$ given by* (3.16) *and $\frac{\pi}{2} < \Omega \leqslant \frac{2\pi}{3}$, $m \in (\mathbb{Z}^+)^{d+1}$ for $d = 2$ or 3. Define*

$$\begin{cases} \tau_\kappa(\xi) = \exp(i\eta(\kappa)\cdot\xi)\tau_{d,m}(\xi+\kappa\pi), & \kappa \in \mathbb{Z}_2^d\backslash\{0\}; \\ h_j^\mu(\xi) = \exp\big(i\eta(\mu)\cdot\xi\big)h_j(\xi+\mu\pi), & \mu \in \mathbb{Z}_2^d,\ j = 1,\dots,d+1, \end{cases} \tag{3.20}$$

where $\{h_j,\ j = 1,\dots,d+1\}$ is given by (3.17). *Let*

$$\Psi = \{\psi_\kappa :\ \kappa \in \mathbb{Z}_2^d\backslash\{0\}\} \cup \{\psi_j^\mu :\ \mu \in \mathbb{Z}_2^d, j = 1,\dots,d+1\},$$

where

$$\begin{cases} \widehat{\psi_\kappa}(\xi) = \tau_\kappa(\frac{\xi}{2})\widehat{\phi}(\frac{\xi}{2}), & \kappa \in \mathbb{Z}_2^d\backslash\{0\}; \\ \widehat{\psi_j^\mu}(\xi) = h_j^\mu(\frac{\xi}{2})\widehat{\phi}(\frac{\xi}{2}), & \mu \in \mathbb{Z}_2^d,\ j = 1,\dots,d+1. \end{cases} \tag{3.21}$$

Then the dyadic affine system $X(\Psi)$ generated by Ψ as (2.13) *forms a tight frame of $L_2(\mathbb{R}^d)$. Moreover, if $\widehat{Q_\Omega} \in C^n(\mathbb{R})$ for some $n \in \mathbb{Z}^*$, then $\widehat{\psi} \in C^n(\mathbb{R}^d)$ for any $\psi \in \Psi$.*

Proof. Firstly, by Theorem 3.4 and Corollary 3.3, the affine system $X(\Psi)$ of the form (2.13) is a tight frame of $L_2(\mathbb{R}^d)$ for the set Ψ defined by (3.21). Secondly, suppose that $\widehat{Q_\Omega} \in C^n(\mathbb{R})$ for some $n \in \mathbb{Z}^*$, then for the function $\phi^{\Omega}_{d,m}$ defined by (3.15), we have $\widehat{\phi^{\Omega}_{d,m}} \in C^n(\mathbb{R}^d)$ and $\tau_\Omega \in C^n(\mathbb{R})$. Then for h_{d+1} in (3.17), $\sqrt{1+\sum_{s=1}^{m_d-1}\tau_\Omega^{2s}(\sum_{j=1}^d \xi_j)} \in C^n(\mathbb{R}^d)$ since $\sum_{s=1}^{m_d-1}\tau_\Omega^{2s}(\sum_{j=1}^d \xi_j) \in C^n(\mathbb{R}^d)$ is non-negative. Thus, we observe that

$$\sqrt{1-\tau_\Omega^{2(m_j-1)}(\xi_j)} = \begin{cases} 0 \in C^n(\mathbb{R}^d), & \text{if } m_j = 1; \\ \tau_\Omega(\xi_j+\pi)\sqrt{1+\sum_{\ell=1}^{m_j-2}\tau_\Omega^{2\ell}(\xi_j)} \in C^n(\mathbb{R}), & \text{if } m_j \geqslant 2. \end{cases}$$

Hence $\sqrt{1-\tau_\Omega^{2(m_j-1)}(\xi_j)} \in C^n(\mathbb{R})$, which leads to $h_j \in C^n(\mathbb{R}^d)$, $j = 1,2,\dots,d$. Since the exponential function $\exp\big(i\eta(\nu)\cdot\xi\big)$ is C^∞ for all $\nu \in \mathbb{Z}_2^d$, the set of wavelet masks defined in (3.20) satisfies

$$\{\tau_\kappa,\ h_j^\mu :\ \kappa \in \mathbb{Z}_2^d\backslash\{0\}, \mu \in \mathbb{Z}_2^d, j = 1,\dots,d+1\} \subset C^n(\mathbb{R}^d).$$

By the definition (3.21) of the framelets Ψ and the fact that $\widehat{\phi^{\Omega}_{d,m}} \in C^n(\mathbb{R}^d)$, we have $\widehat{\psi} \in C^n(\mathbb{R}^d)$ for any $\psi \in \Psi$. The proof is done. □

3.4 Examples

In this section, we will apply the results developed in previous sections to construct some examples of non-separable band-limited framelets. The construction of these framelets starts with the univariate Meyer's refinable function. Same as [27], the term h in the mask τ_Ω of the form (2.10) corresponding to the Meyer's refinable function is given as follows:

$$h(\xi) = \cos\Big(\frac{\pi}{2} \cdot \beta\big(\frac{1}{2}\big(\frac{|2\xi| - \pi}{2\Omega - \pi} + 1\big)\big)\Big), \tag{3.22}$$

where $\beta(x) = (\int_0^1 t^n(1-t)^n dt)^{-1} \int_0^x t^n(1-t)^n dt$ for some nonnegative integer n. The smoothness of the associated Meyer's refinable function in frequency domain is closely related to the value of n. More specifically, let Q_Ω denote the Meyer's refinable function determined by (3.22) and (2.10). Then $\widehat{Q_\Omega}$ will be differentiable up to order n, i.e., $\widehat{Q_\Omega} \in C^n(\mathbb{R})$ (see [52] for more details). Through all examples constructed in this thesis, we always set $n = 3$ such that

$$\beta(x) = x^4(35 - 84x + 80x^2 - 20x^3),$$

and start with the Meyer's refinable function defined by (2.10) and (3.22) with $\Omega = \frac{2}{3}\pi$, denoted by $Q_{\frac{2}{3}\pi}$.

Example 3.1. *In this example, we use the direction matrix of the form* (3.13) *with* $m = (1, 1, 1)$*, to generate the non-separable refinable function* $\phi \in L_2(\mathbb{R}^2)$ *as follows:*

$$\widehat{\phi}(\xi_1, \xi_2) = \widehat{Q_{\frac{2}{3}\pi}}(\xi_1)\widehat{Q_{\frac{2}{3}\pi}}(\xi_2)\widehat{Q_{\frac{2}{3}\pi}}(\xi_1 + \xi_2).$$

Then the refinable mask of ϕ is given by (3.16),

$$\tau_{2,m}(\xi_1,\xi_2)=\tau_{\frac{2}{3}\pi}(\xi_1)\tau_{\frac{2}{3}\pi}(\xi_2)\tau_{\frac{2}{3}\pi}(\xi_1+\xi_2),$$

where $\tau_{\frac{2}{3}\pi}$ is the mask of the Meyer's refinable function given by (2.10). *Following* (3.17), *we define*

$$\begin{cases} h_1(\xi_1,\xi_2)=\sqrt{1-\tau^{2\times 0}_{\frac{2}{3}\pi}(\xi_1)}\tau_{\frac{2}{3}\pi}(\xi_1)\tau_{\frac{2}{3}\pi}(\xi_2)\tau_{\frac{2}{3}\pi}(\xi_1+\xi_2)=0,\\ h_2(\xi_1,\xi_2)=\sqrt{1-\tau^{2\times 0}_{\frac{2}{3}\pi}(\xi_2)}\tau_{\frac{2}{3}\pi}(\xi_2)\tau_{\frac{2}{3}\pi}(\xi_1)\tau_{\frac{2}{3}\pi}(\xi_1+\xi_2)=0,\\ h_3(\xi_1,\xi_2)=\tau_{\frac{2}{3}\pi}(\xi_1+\xi_2+\pi)\tau_{\frac{2}{3}\pi}(\xi_1)\tau_{\frac{2}{3}\pi}(\xi_2). \end{cases}$$

By Corollary 3.5, we have a framelet system for $L_2(\mathbb{R}^2)$ whose associated masks are given as follows:

$$\begin{cases} \tau_\kappa=\exp\big(i\eta(\kappa)\cdot\xi\big)\tau(\xi+\kappa\pi), & \kappa\in\mathbb{Z}_2^2\backslash\{0\};\\ h_3^\mu=\exp\big(i\eta(\mu)\cdot\xi\big)h_3(\xi+\mu\pi), & \mu\in\mathbb{Z}_2^2, \end{cases} \tag{3.23}$$

where $\xi=(\xi_1,\xi_2)^T$. See Figure 3.1 for the plots of the refinable function ϕ and the seven framelets derived from (3.23) *in spatial domain.*

Example 3.2. *In this example, the power vector $m=(2,1,1)$ is used to generate the following non-separable refinable function $\phi\in L_2(\mathbb{R}^2)$:*

$$\widehat{\phi}(\xi_1,\xi_2)=\widehat{Q_{\frac{2}{3}\pi}}^{\,2}(\xi_1)\widehat{Q_{\frac{2}{3}\pi}}(\xi_2)\widehat{Q_{\frac{2}{3}\pi}}(\xi_1+\xi_2).$$

Then by (3.16), *the refinable mask of ϕ is given as*

$$\tau_{2,m}(\xi)=\tau^2_{\frac{2}{3}\pi}(\xi_1)\tau_{\frac{2}{3}\pi}(\xi_2)\tau_{\frac{2}{3}\pi}(\xi_1+\xi_2).$$

If we apply Corollary 3.5 to the refinable function ϕ defined as above, then one can easily check that there would be a total of 11 *framelets introduced. However, by directly using Theorem 3.2, we can construct from ϕ a tight frame system of*

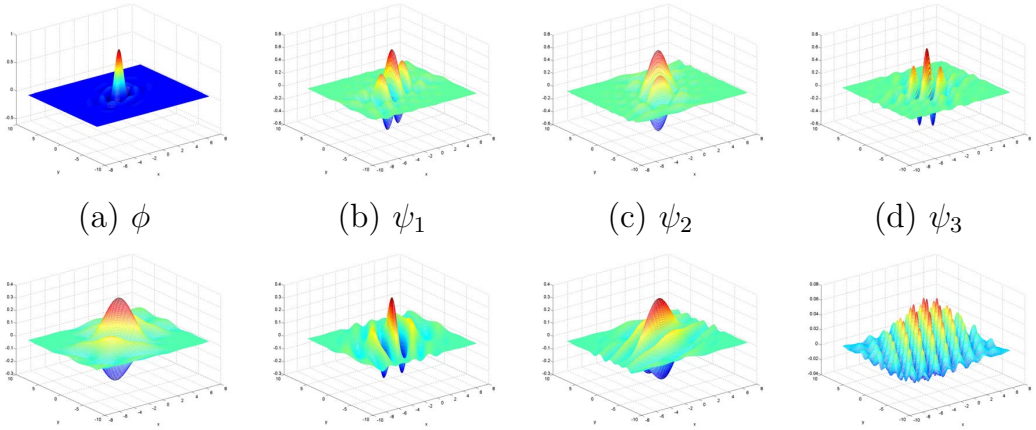

(a) ϕ (b) ψ_1 (c) ψ_2 (d) ψ_3

(e) ψ_4 (f) ψ_5 (g) ψ_6 (h) ψ_7

Figure 3.1: Graphs of the refinable function and its associated framelets as introduced in Example 3.1. (a) Refinable function; and (b)–(h) the associated framelets.

$L_2(\mathbb{R}^2)$ with fewer number framelets, and all framelets would still retain the same order of smoothness as that of ϕ in Fourier domain. More explicitly, we define

$$a_1(\xi) = \tau^2_{\frac{2}{3}\pi}(\xi_1)\tau_{\frac{2}{3}\pi}(\xi_2)\tau_{\frac{2}{3}\pi}(\xi_1+\xi_2+\pi)$$

and

$$p(\xi) = \sqrt{2}\tau_{\frac{2}{3}\pi}(\xi_1)\tau_{\frac{2}{3}\pi}(\xi_1+\pi).$$

Then the set of 2π-periodic functions $\{p(\xi), \tau(\xi), a_1(\xi)\}$ satisfies (3.4):

$$|p(\xi)|^2 + \sum_{\kappa\in\mathbb{Z}_2^2} |\tau(\xi+\kappa\pi)|^2 + \sum_{\mu\in\mathbb{Z}_2^2} |a_1(\xi+\mu\pi)|^2 = 1.$$

By Theorem 3.2, we have a framelet system with eight *tight framelets for $L_2(\mathbb{R}^2)$, whose associated masks are given as follows:*

$$\begin{cases} \exp\big(i\eta(\kappa)\cdot\xi\big)\tau(\xi+\kappa\pi), & \kappa\in\mathbb{Z}_2^2\backslash\{0\};\\ \exp\big(i\eta(\mu)\cdot\xi\big)a_1(\xi+\mu\pi), & \mu\in\mathbb{Z}_2^2;\\ p(2\xi)\tau(\xi)\,. \end{cases} \tag{3.24}$$

In our example, $\tau_{\frac{2}{3}\pi}$ is given by (3.22) such that $\tau_{\frac{2}{3}\pi}\in C^3(\mathbb{R})$, and thus all masks defined by (3.24) are also in $C^3(\mathbb{R}^2)$. As a result, the Fourier transforms of the

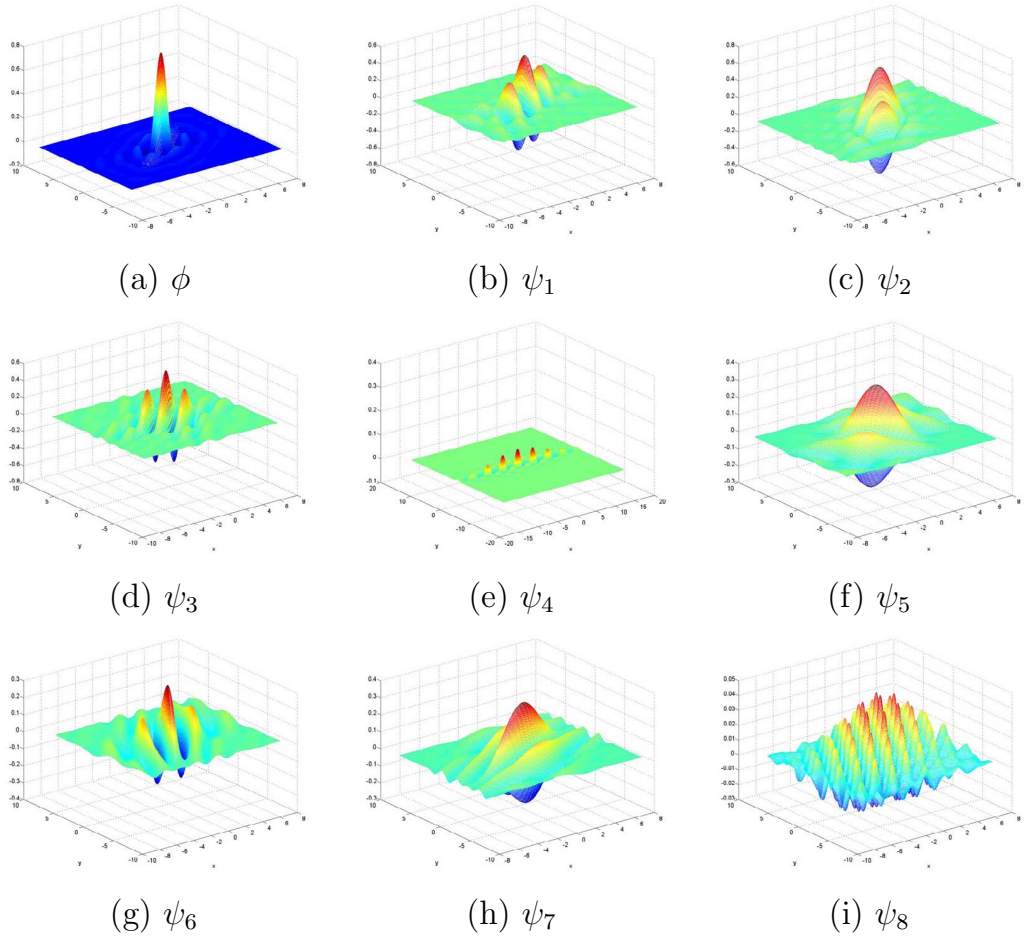

(a) ϕ (b) ψ_1 (c) ψ_2

(d) ψ_3 (e) ψ_4 (f) ψ_5

(g) ψ_6 (h) ψ_7 (i) ψ_8

Figure 3.2: Graphs of the refinable function and its associated framelets as introduced in Example 3.2. (a) Refinable function; and (b)–(i) the associated framelets.

associated framelets are in $C^3(\mathbb{R}^2)$ too. See Figure 3.2 for the graphs of the refinable function and its associated eight framelets in spatial domain.

Chapter 4

Non-separable Band-limited Stable Refinable Functions, Riesz Wavelets and Orthonormal Wavelets in Low Dimensions

In the previous chapter, we have introduced a class of non-separable band-limited refinable functions for deriving band-limited framelets. However, a major technical difficulty is encountered when we change topic to the construction of Riesz wavelets and orthonormal wavelets. We note that, in order to use Theorem 2.13 to construct MRA-based Riesz wavelets (and orthonormal wavelets) in low dimensions, one needs to require that the corresponding refinable function is stable. Unfortunately, any refinable function constructed via (3.15) in the previous chapter simply fails to be stable.

Proposition 4.1. *Let $\phi^{\Omega}_{d,m}$, $d = 2$ or 3, be a refinable function defined as* (3.15)*, where Q_Ω is the univariate Meyer's refinable function with $\frac{\pi}{2} < \Omega \leqslant \frac{2\pi}{3}$, then $\phi^{\Omega}_{d,m}$*

is not stable.

Proof. This is a corollary of Theorem 4.5 with $\frac{\pi}{2} < \Omega \leqslant \frac{2\pi}{3}$. □

Thus, in order to construct Riesz wavelets and orthonormal wavelets in low dimensions using Theorem 2.13, we need to construct a new class of band-limited stable refinable functions satisfying (2.18). Before going deep into the details of this issue, we first introduce two results on the refinable and stable properties of band-limited functions, which would become useful in later sections of this chapter.

4.1 Two results on band-limited refinable functions

The following result implies that it is fairly 'easy' to construct band-limited refinable functions.

Lemma 4.2. *For any $\phi \in L_2(\mathbb{R}^d)$, suppose that the set $S_1 = \operatorname{supp}(\widehat{\phi})$ is a subset of $[-\frac{4}{3}\pi, \frac{4}{3}\pi]^d$ and the set $S_2 = \{\xi : \widehat{\phi}(2\xi) \neq 0\} \cap \{\xi : \widehat{\phi}(\xi) = 0\}$ is of measure zero. Then there exists a 2π-periodic measurable function τ (not necessarily unique) such that*

$$\widehat{\phi}(2\xi) = \tau(\xi)\widehat{\phi}(\xi) \text{ a.e. on } \mathbb{R}^d,$$

i.e. ϕ is refinable with mask τ.

Proof. Firstly, we define a compactly supported function $b(\xi)$, such that

$$b(\xi) = \begin{cases} \frac{\widehat{\phi}(2\xi)}{\widehat{\phi}(\xi)}, & \text{if } \widehat{\phi}(\xi) \neq 0; \\ 0, & \text{otherwise.} \end{cases}$$

By the definition of $b(\xi)$, we have

$$\widehat{\phi}(2\xi) = b(\xi)\widehat{\phi}(\xi),\ \forall \xi \in \{\gamma : \widehat{\phi}(\gamma) \neq 0\} \cup \{\gamma : \widehat{\phi}(\gamma) = 0, \widehat{\phi}(2\gamma) = 0\}.$$

Since the complement of $\{\gamma : \widehat{\phi}(\gamma) \neq 0\} \cup \{\gamma : \widehat{\phi}(\gamma) = 0, \widehat{\phi}(2\gamma) = 0\}$ is the set $\{\gamma : \widehat{\phi}(2\gamma) \neq 0\} \cap \{\gamma : \widehat{\phi}(\gamma) = 0\}$, which is of Lebesgue measure zero, we have then

$$\widehat{\phi}(2\xi) = b(\xi)\widehat{\phi}(\xi) \text{ a.e. on } \mathbb{R}^d.$$

Secondly, since $\mathrm{supp}(\widehat{\phi}) \subseteq [-\frac{4\pi}{3}, \frac{4\pi}{3}]^d$, then

$$\mathrm{supp}\big(b(\xi)\big) \subseteq [-\frac{2\pi}{3}, \frac{2\pi}{3}]^d \subset (-\pi, \pi)^d.$$

by its definition. Let τ be a 2π-periodic extension of b such that

$$\tau(\xi) = b(\xi), \, \forall \, \xi \in [-\pi, \pi)^d,$$

or equivalently

$$\tau(\xi) = \sum_{k \in \mathbb{Z}^d} b(\xi + 2\pi k), \, \xi \in \mathbb{R}^d.$$

Then we have

$$\tau(\xi)\widehat{\phi}(\xi) = b(\xi)\widehat{\phi}(\xi) = \widehat{\phi}(2\xi) \text{ a.e. on } [-\pi, \pi)^d. \tag{4.1}$$

For those $\xi \in \mathbb{R}^d \backslash [-\pi, \pi)^d$, $\tau(\xi)\widehat{\phi}(\xi) \neq 0$ only if $\xi \in \mathrm{supp}(\tau) \cap \mathrm{supp}(\widehat{\phi})$. Note that $\mathrm{supp}(\tau)$ is a subset of $\bigcup\limits_{k \in \mathbb{Z}^d} \Big([-\frac{2\pi}{3}, \frac{2\pi}{3}]^d + 2\pi k\Big)$, and $\mathrm{supp}(\widehat{\phi})$ is a subset of $[-\frac{4}{3}\pi, \frac{4}{3}\pi]^d$, thus $\big(\mathbb{R}^d \backslash [-\pi, \pi)^d\big) \cap \mathrm{supp}(\tau) \cap \mathrm{supp}(\widehat{\phi})$ is a subset of

$$\big(\mathbb{R}^d \backslash [-\pi, \pi)^d\big) \cap \Big(\bigcup_{k \in \mathbb{Z}^d} \big([-\frac{2\pi}{3}, \frac{2\pi}{3}]^d + 2\pi k\big)\Big) \cap [-\frac{4}{3}\pi, \frac{4}{3}\pi]^d, \tag{4.2}$$

It is seen that the set defined in (4.2) is contained within $\partial([-\frac{4}{3}\pi, \frac{4}{3}\pi]^d)$ (the set of all boundary points of the cube $[-\frac{4}{3}\pi, \frac{4}{3}\pi]^d$), which is of Lebesgue measure zero in $\mathbb{R}^d$. Thus, the set $\big(\mathbb{R}^d \backslash [-\pi, \pi)^d\big) \cap \mathrm{supp}(\tau) \cap \mathrm{supp}(\widehat{\phi})$ is of Lebesgue measure zero in $\mathbb{R}^d$. In other words,

$$\tau(\xi)\widehat{\phi}(\xi) = 0 = \widehat{\phi}(2\xi), \text{ a.e. on } \mathbb{R}^d \backslash [-\pi, \pi)^d. \tag{4.3}$$

By both (4.1) and (4.3), we have

$$\widehat{\phi}(2\xi) = \tau(\xi)\widehat{\phi}(\xi) \text{ a.e. on } \mathbb{R}^d.$$

The proof is complete. □

In order to construct MRA-based band-limited Riesz wavelets with good time-frequency localization property, we shall require the corresponding refinable function to be well time-frequency localized. In particular, the candidate refinable functions at least should be continuous in frequency domain. Then, the following lemma serves as an easy-to-use tool for checking their stableness.

Lemma 4.3. *Let ϕ be a band-limited refinable function on $\mathbb{R}^d$. If $\widehat{\phi}$ is continuous, then ϕ is stable if and only if $[\widehat{\phi}, \widehat{\phi}](\xi) > 0$ for all $\xi \in [-\pi, \pi]^d$.*

Proof. Since $\widehat{\phi}$ is continuous and compactly supported, $[\widehat{\phi}, \widehat{\phi}]$ is also continuous by its definition. If ϕ is stable, then by definition there exists some constant $c > 0$ such that $[\widehat{\phi}, \widehat{\phi}] \geqslant c$ a.e. on $\mathbb{R}^d$. Since $[\widehat{\phi}, \widehat{\phi}]$ is continuous, we have $[\widehat{\phi}, \widehat{\phi}](\xi) \geqslant c$ for all $\xi \in \mathbb{R}^d$, which implies that $[\widehat{\phi}, \widehat{\phi}](\xi) > 0$ for all $\xi \in \mathbb{R}^d$, and the same inequality holds for all $\xi \in [-\pi, \pi]^d$.

If $[\widehat{\phi}, \widehat{\phi}](\xi) > 0$ for all $\xi \in [-\pi, \pi]^d$, then since $[\widehat{\phi}, \widehat{\phi}]$ is continuous and $[-\pi, \pi]^d$ is compact, the infimum of $[\widehat{\phi}, \widehat{\phi}]$ can be achieved and it is greater than 0, i.e., there exists a positive constant c_1 such that $[\widehat{\phi}, \widehat{\phi}] \geqslant c_1$ on $[-\pi, \pi]^d$. Also since $[\widehat{\phi}, \widehat{\phi}]$ is continuous, the supremum of $[\widehat{\phi}, \widehat{\phi}]$ on the compact set $[-\pi, \pi]^d$ is less than infinity, i.e., there exists a positive constant c_2 such that $[\widehat{\phi}, \widehat{\phi}] \leqslant c_2$ on $[-\pi, \pi]^d$. Then since $[\widehat{\phi}, \widehat{\phi}]$ is 2π-periodic, we conclude $0 < c_1 \leqslant [\widehat{\phi}, \widehat{\phi}] \leqslant c_2 < \infty$ on $\mathbb{R}^d$, which implies that ϕ is stable. The proof is complete. □

4.2 The construction of band-limited stable refinable functions and wavelets

4.2.1 The construction of non-separable band-limited stable refinable functions

To gain stableness for the type of refinable functions defined as in (3.1), the basic idea is to use a class of specially designed direction matrices Ξ. Motivated by the direction matrices of the form (3.13) and (3.14), we propose the following direction matrices for the construction of stable refinable functions in $\mathbb{R}^2$ and $\mathbb{R}^3$:
in $\mathbb{R}^2$,

$$\Xi = \begin{bmatrix} \overbrace{1 \cdots 1}^{m_1} & \overbrace{0 \cdots 0}^{m_2} & \overbrace{\rho^{-1} \cdots \rho^{-1}}^{m_3} \\ 0 \cdots 0 & 1 \cdots 1 & \rho^{-1} \cdots \rho^{-1} \end{bmatrix}, \tag{4.4}$$

and in $\mathbb{R}^3$,

$$\Xi = \begin{bmatrix} \overbrace{1 \cdots 1}^{m_1} & \overbrace{0 \cdots 0}^{m_2} & \overbrace{0 \cdots 0}^{m_3} & \overbrace{\rho^{-1} \cdots \rho^{-1}}^{m_4} \\ 0 \cdots 0 & 1 \cdots 1 & 0 \cdots 0 & \rho^{-1} \cdots \rho^{-1} \\ 0 \cdots 0 & 0 \cdots 0 & 1 \cdots 1 & \rho^{-1} \cdots \rho^{-1} \end{bmatrix},$$

where ρ is a positive scalar and $m_i, i = 1, \ldots, 4$ are positive integers. By adopting direction matrices as mentioned above, we define the following band-limited functions in $L_2(\mathbb{R}^d)$ for $d = 2, 3$:

$$\widehat{\phi^{\rho,\Omega}_{d,m}}(\xi) = \widehat{Q_\Omega}^{m_{d+1}}\big(\rho^{-1}(\sum_{j=1}^{d} \xi_j)\big) \prod_{j=1}^{d} \widehat{Q_\Omega}^{m_j}\big(\xi_j\big) \tag{4.5}$$

for any $\xi = (\xi_1, \ldots, \xi_d) \in \mathbb{R}^d$, where Q_Ω is the Meyer's refinable function of the form (2.8), $\frac{\pi}{2} < \Omega \leqslant \frac{2}{3}\pi$, and $m = (m_1, \ldots, m_{d+1}) \in (\mathbb{Z}^+)^{d+1}$ for $d = 2$ or 3. For the support of $\widehat{\phi^{\rho,\Omega}_{d,m}}$ in (4.5), we have the following observation

Proposition 4.4. *Let $\phi_{d,m}^{\rho,\Omega}$ be a band-limited refinable function defined by* (4.5)*, then $\widehat{\phi_{d,m}^{\rho,\Omega}}(\xi) > 0$ if and only if $\xi = (\xi_1, \ldots, \xi_d)$ satisfies the following two conditions:*

(i) $\xi \in (-2\Omega, 2\Omega)^d$*;*

(ii) $-2\rho\Omega < \sum_{j=1}^{d} \xi_j < 2\rho\Omega$*.*

Proof. The necessity and sufficiency of the two conditions can be easily justified by the definition (4.5) and the fact that $\widehat{Q}_\Omega(\gamma) > 0$ if and only if $\gamma \in (-2\Omega, 2\Omega)$. □

Then, we can have the following result for characterizing the refinability and stableness of band-limited functions defined via (4.5).

Theorem 4.5. *The function $\phi_{d,m}^{\rho,\Omega}$ defined in* (4.5)*, with $d = 2$ or 3 and $\frac{\pi}{2} < \Omega \leqslant \frac{2}{3}\pi$, is refinable whenever $\rho > 0$. Moreover, the function $\phi_{d,m}^{\rho,\Omega}$ is stable if and only if*

$$\rho > \frac{d(\pi - \Omega)}{\Omega}. \tag{4.6}$$

We would temporarily give a proof of Theorem 4.5 for $d = 3$ only, as later we will prove a more general result concerning the case of $d = 2$, and the proof of Theorem 4.5 for $d = 2$ would be automatically covered there.

Proof of Theorem 4.5 for $d = 3$: The entire proof is divided into two separate parts.

Part I, the refinability of $\phi_{d,m}^{\rho,\Omega}$.

Given a band-limited function $\phi_{3,m}^{\rho,\Omega}$ defined in (4.5), we have $\phi_{3,m}^{\rho,\Omega} \in L_2(\mathbb{R}^3)$. Moreover, one can verify that for any $\rho > 0$,

(i) $\mathrm{supp}\big(\widehat{\phi_{3,\mathrm{m}}^{\rho,\Omega}}\big) \subseteq [-2\Omega, 2\Omega]^3 \subseteq [-\frac{4\pi}{3}, \frac{4\pi}{3}]^3$, since $\Omega \leqslant \frac{2}{3}\pi$,

(ii) $\{\xi : \widehat{\phi_{3,m}^{\rho,\Omega}}(2\xi) \neq 0\}$ is a subset of $\{\xi : \widehat{\phi_{3,m}^{\rho,\Omega}}(\xi) \neq 0\}$, which implies the set $\{\xi : \widehat{\phi_{3,m}^{\rho,\Omega}}(2\xi) \neq 0\} \cap \{\xi : \widehat{\phi_{3,m}^{\rho,\Omega}}(\xi) = 0\}$ is empty.

Therefore by Lemma 4.2, any band-limited function $\phi_{3,m}^{\rho,\Omega}$ as in (4.5) is refinable.

Part II, the stableness of $\phi_{d,m}^{\rho,\Omega}$.

Sufficiency of (4.6). By Lemma 4.3, to verify $\phi_{3,m}^{\rho,\Omega}$ is stable, we only need to verify that

$$[\widehat{\phi_{3,m}^{\rho,\Omega}}, \widehat{\phi_{3,m}^{\rho,\Omega}}](\xi) > 0, \forall\, \xi \in [-\pi, \pi]^3. \tag{4.7}$$

We prove (4.7) on two disjoint subsets of $[-\pi, \pi]^3 = S_1 \cup S_2$, where

$$S_1 = \{\xi : \xi = (\xi_1, \xi_2, \xi_3) \in [-\pi, \pi]^3, |\sum_{j=1}^{3} \xi_j| < 2\rho\Omega\},$$

and

$$S_2 = \{\xi : \xi = (\xi_1, \xi_2, \xi_3) \in [-\pi, \pi]^3, |\sum_{j=1}^{3} \xi_j| \geqslant 2\rho\Omega\}.$$

If $\xi \in S_1$, then by the definition of $\phi_{3,m}^{\rho,\Omega}$, one has $\widehat{\phi_{3,m}^{\rho,\Omega}}(\xi) > 0$, which implies $[\widehat{\phi_{3,m}^{\rho,\Omega}}, \widehat{\phi_{3,m}^{\rho,\Omega}}](\xi) > 0$. The next is to verify the inequality (4.7) holds for all $\xi \in S_2$. Suppose $\xi = (\xi_1, \xi_2, \xi_3) \in S_2$. Without loss of generality, we may assume $\sum_{j=1}^{3} \xi_j \geqslant 2\rho\Omega$ and $\xi_1 = \max\{\xi_1, \xi_2, \xi_3\}$, then

$$3\xi_1 \geqslant \sum_{j=1}^{3} \xi_j \geqslant 2\rho\Omega. \tag{4.8}$$

By substituting (4.6), i.e. $\rho > \frac{3(\pi-\Omega)}{\Omega}$ into (4.8), we get

$$3\xi_1 > 2\frac{3(\pi - \Omega)}{\Omega}\Omega = 6(\pi - \Omega),$$

or equivalently

$$\xi_1 - 2\pi > -2\Omega.$$

Meanwhile, since $\xi_1 \leqslant \pi$, we have

$$\xi_1 - 2\pi \leqslant \pi - 2\pi = -\pi < 0 < 2\Omega.$$

Together with the fact that $\xi_j \in [-\pi, \pi] \subset (-2\Omega, 2\Omega)$, $j = 1, 2, 3$, we can conclude that the point $(\xi_1 - 2\pi, \xi_2, \xi_3)$ satisfies Condition (i) of Proposition 4.4. Moreover, we have

$$(\xi_1 - 2\pi) + \xi_2 + \xi_3 \leqslant 3\pi - 2\pi = \pi < 6(\pi - \Omega) < 2\rho\Omega$$

and

$$\xi_1 - 2\pi + \xi_2 + \xi_3 \geqslant 2\rho\Omega - 2\pi > 6(\pi - \Omega) - 2\pi = 4\pi - 6\Omega \geqslant 0 > -2\rho\Omega.$$

Thus, the point $(\xi_1 - 2\pi, \xi_2, \xi_3)$ satisfies Condition (ii) of Proposition 4.4. By Proposition 4.4, we have $\widehat{\phi^{\rho,\Omega}_{3,m}}(\xi_1 - 2\pi, \xi_2, \xi_3) > 0$. This implies, via the definition of the bracket product $[\cdot, \cdot]$, that

$$[\widehat{\phi^{\rho,\Omega}_{3,m}}, \widehat{\phi^{\rho,\Omega}_{3,m}}](\xi) > 0,\ \xi = (\xi_1, \xi_2, \xi_3).$$

The proof for the sufficiency of (4.6) is complete.

Necessity of (4.6). We show it by contrapositive. Let us assume that (4.6) fails, i.e. $\rho \leqslant \frac{3(\pi-\Omega)}{\Omega}$ holds, then we consider the point $\tilde{\xi} = (\xi_1, \xi_2, \xi_3) \in [-\pi, \pi]^3$, with $\xi_1 = \xi_2 = \xi_3 = 2(\pi - \Omega)$. Since $\sum_{j=1}^{3} \xi_j = 6(\pi - \Omega) \geqslant 2\rho\Omega$, one can conclude that $\tilde{\xi}$ fails to fulfill item (ii) of Proposition 4.4, which leads to $\widehat{\phi^{\rho,\Omega}_{3,m}}(\tilde{\xi}) = 0$. Next observing that $2(\pi - \Omega) - 2\pi = -2\Omega$, one has $\tilde{\xi} - 2k\pi \notin (-2\Omega, 2\Omega)^3$ for any $k \in \mathbb{Z}_2^3 \backslash \{0\}^3$. Consequently, for the point $\tilde{\xi} - 2k\pi$ with any $k \in \mathbb{Z}_2^3 \backslash \{0\}^3$, item (ii) of Proposition 4.4 also fails. As for those $k \in \mathbb{Z}^3 \backslash \mathbb{Z}_2^3$, clearly one has $\tilde{\xi} - 2k\pi$ lies beyond the cube $(-2\Omega, 2\Omega)^3$, thus $\widehat{\phi}(\tilde{\xi} - 2k\pi) = 0$ for all $k \in \mathbb{Z}^3 \backslash \mathbb{Z}_2^3$. To sum up, the previous arguments show that if $\rho \leqslant \frac{3(\pi-\Omega)}{\Omega}$, then for $\tilde{\xi} = \big(2(\pi - \Omega), 2(\pi - \Omega), 2(\pi - \Omega)\big) \in [-\pi, \pi]^3$, one has $\widehat{\phi^{\rho,\Omega}_{3,m}}(\tilde{\xi} - 2k\pi) = 0$ for all $k \in \mathbb{Z}^3$, which implies

$$[\widehat{\phi^{\rho,\Omega}_{3,m}}, \widehat{\phi^{\rho,\Omega}_{3,m}}](\tilde{\xi}) = 0.$$

Thus by Lemma 4.3, $\phi^{\rho,\Omega}_{3,m}$ must be unstable, whence the necessity part is shown, and the entire proof is complete. □

By Theorem 4.5, the refinable function defined by (4.5) with $\Omega = \frac{2}{3}\pi$ is stable if and only if $\rho > 1$ for $\mathbb{R}^2$, and $\rho > \frac{3}{2}$ for $\mathbb{R}^3$. Moreover, a direct calculation shows that the area of the support of the stable refinable function in $\mathbb{R}^2$ in frequency domain satisfies

$$\inf_{\rho>1} \text{area of supp}(\widehat{\phi^{\rho,\frac{2}{3}\pi}_{2,m}}) = \frac{48}{9}\pi^2.$$

In the next result, we show that, by using some other type of directional matrices, it is possible to construct stable refinable functions in $\mathbb{R}^2$ with smaller support in frequency domain. The direction matrix for $\mathbb{R}^2$ we discussed is defined as follows:

$$\Xi = \begin{bmatrix} \overbrace{1 \ \cdots \ 1}^{m_1} & \overbrace{0 \ \cdots \ 0}^{m_2} & \overbrace{\sigma^{-1}\cos\theta \ \cdots \ \sigma^{-1}\cos\theta}^{m_3} \\ 0 \ \cdots \ 0 & 1 \ \cdots \ 1 & \sigma^{-1}\sin\theta \ \cdots \ \sigma^{-1}\sin\theta \end{bmatrix}. \tag{4.9}$$

The above choice of direction matrix leads to the following class of band-limited functions in $L_2(\mathbb{R}^2)$:

$$\widehat{\phi^{\sigma,\theta}_{m,\Omega}}(\xi) = \widehat{Q_\Omega}^{m_1}(\xi_1)\widehat{Q_\Omega}^{m_2}(\xi_2)\widehat{Q_\Omega}^{m_3}\big(\sigma^{-1}(\xi_1\cos\theta + \xi_2\sin\theta)\big) \tag{4.10}$$

for any $\xi = (\xi_1, \ldots, \xi_d) \in \mathbb{R}^d$, where Q_Ω is the Meyer's refinable function of the form (2.8), $\frac{\pi}{2} < \Omega \leqslant \frac{2}{3}\pi$, $m = (m_1, m_2, m_3) \in (\mathbb{Z}^+)^3$, $\sigma > 0$, and $0 \leqslant \theta \leqslant \frac{\pi}{2}$. We have the following observation for the support of $\widehat{\phi^{\sigma,\theta}_{m,\Omega}}$ defined as in (4.10)

Proposition 4.6. *Let $\phi^{\sigma,\theta}_{m,\Omega}$ be a band-limited refinable function defined by* (4.10)*, then $\widehat{\phi^{\sigma,\theta}_{m,\Omega}}(\xi) > 0$ if and only if $\xi = (\xi_1, \xi_2)$ satisfies the following two conditions:*

(i) $\xi \in (-2\Omega, 2\Omega)^2$*;*

(ii) $-2\sigma\Omega < \xi_1\cos\theta + \xi_2\sin\theta < 2\sigma\Omega$*.*

Proof. The necessity and sufficiency of the two conditions can be easily justified by the definition (4.10) and the fact that $\widehat{Q}_\Omega(\gamma) > 0$ if and only if $\gamma \in (-2\Omega, 2\Omega)$. □

It is easy to see that the direction matrix defined by (4.4) is indeed a special case of the matrix defined by (4.9) with $\theta = \frac{\pi}{4}$ and $\sigma = \frac{\sqrt{2}}{2}\rho$. Then, we have the following characterization for the type of refinable functions defined in (4.10).

Theorem 4.7. *The function $\phi^{\sigma,\theta}_{m,\Omega}$ defined in* (4.10)*, with $\frac{\pi}{2} < \Omega \leqslant \frac{2\pi}{3}$ and $\sigma > 0$, is refinable. Moreover, for any $\theta \in [0, \frac{\pi}{2}]$, $\phi^{\sigma,\theta}_{m,\Omega}$ is stable if and only if $\sigma > \sigma_0(\theta, \Omega)$, where $\sigma_0(\theta, \Omega)$ is defined by*

$$\sigma_0(\theta,\Omega) = \begin{cases} \frac{\pi\cos\theta}{2\Omega}, & 0 \leqslant \theta \leqslant \arctan\frac{2\Omega-\pi}{2(\pi-\Omega)}; \\ \frac{(\pi-\Omega)(\cos\theta+\sin\theta)}{\Omega}, & \arctan\frac{2\Omega-\pi}{2(\pi-\Omega)} < \theta < \frac{\pi}{2} - \arctan\frac{2\Omega-\pi}{2(\pi-\Omega)}; \\ \frac{\pi\sin\theta}{2\Omega}, & \frac{\pi}{2} - \arctan\frac{2\Omega-\pi}{2(\pi-\Omega)} \leqslant \theta \leqslant \frac{\pi}{2}. \end{cases} \tag{4.11}$$

Proof. Similar as in Theorem 4.5, the entire proof is divided into two parts.

Part I, the refinability of $\phi^{\sigma,\theta}_{m,\Omega}$.

Firstly, for any band-limited function $\phi^{\sigma,\theta}_{m,\Omega}$ in (4.10), one can verify that

(i) $\mathrm{supp}(\widehat{\phi^{\sigma,\theta}_{m,\Omega}}) \in [-2\Omega, 2\Omega]^2 \subseteq [-\frac{4}{3}\pi, \frac{4}{3}\pi]^2$, since $\Omega \leqslant \frac{2\pi}{3}$,

(ii) the set $\{\xi : \widehat{\phi^{\sigma,\theta}_{m,\Omega}}(2\xi) \neq 0\}$ is a subset of $\{\xi : \widehat{\phi^{\sigma,\theta}_{m,\Omega}}(\xi) \neq 0\}$, which implies that the set $\{\xi : \widehat{\phi^{\sigma,\theta}_{m,\Omega}}(2\xi) \neq 0\} \cap \{\xi : \widehat{\phi^{\sigma,\theta}_{m,\Omega}}(\xi) = 0\}$ is empty.

Then by Lemma 4.6, any band-limited function $\phi^{\sigma,\theta}_{m,\Omega}$ as in (4.10) is refinable.

Part II, the stableness of $\phi^{\sigma,\theta}_{m,\Omega}$. By the definition of $\phi^{\sigma,\theta}_{m,\Omega}$ in (4.10), we have $\widehat{\phi^{\sigma,\theta}_{m,\Omega}}(\xi_1, \xi_2) = \widehat{\phi^{\sigma,\frac{\pi}{2}-\theta}_{m,\Omega}}(\xi_2, \xi_1)$ for any $\theta \in [0, \frac{\pi}{2}]$. Thus, we only need to prove the result for $\theta \in [0, \frac{\pi}{4}]$.

Sufficiency. We first prove that if $\sigma > \sigma_0(\theta, \Omega)$, then $\phi^{\sigma,\theta}_{m,\Omega}$ is stable. By Lemma 4.3, the stability of $\phi^{\sigma,\theta}_{m,\Omega}$ is guaranteed as long as

$$[\widehat{\phi^{\sigma,\theta}_{m,\Omega}}, \widehat{\phi^{\sigma,\theta}_{m,\Omega}}](\xi) > 0, \forall\, \xi \in [-\pi, \pi]^2 \tag{4.12}$$

for any $\sigma > \sigma_0(\theta, \Omega)$. We prove the above inequality (4.12) on two separate subsets of $[-\pi, \pi]^2 = S_1 \cup S_2$, where

$$S_1 = \{(\xi_1, \xi_2) : (\xi_1, \xi_2) \in [-\pi, \pi]^2, |\xi_1 \cos\theta + \xi_2 \sin\theta| < 2\sigma\Omega\},$$

and

$$S_2 = \{(\xi_1, \xi_2) : (\xi_1, \xi_2) \in [-\pi, \pi]^2, |\xi_1 \cos\theta + \xi_2 \sin\theta| \geqslant 2\sigma\Omega\}.$$

The inequality (4.12) on S_1 is obvious. The fact that $\widehat{\phi^{\sigma,\theta}_{m,\Omega}}(\xi) > 0$ for any $\xi \in S_1$ implies

$$[\widehat{\phi^{\sigma,\theta}_{m,\Omega}}, \widehat{\phi^{\sigma,\theta}_{m,\Omega}}](\xi) > 0, \ \forall \xi \in S_1.$$

The next step is to prove (4.12) for any $\xi \in S_2$. By the symmetry of S_2, it is sufficient to prove that (4.12) holds on the subset $S_3 \subset S_2$ given by

$$S_3 = \{(\xi_1, \xi_2) : (\xi_1, \xi_2) \in [-\pi, \pi]^2, \xi_1 \cos\theta + \xi_2 \sin\theta \geqslant 2\sigma\Omega\}.$$

Furthermore, by the definition of $[\cdot, \cdot]$, the inequality (4.12) holds for all $\xi \in S_3$ as long as the following statement holds: $\forall\, \xi = (\xi_1, \xi_2) \in S_3$,

$$\begin{cases} \widehat{\phi^{\sigma,\theta}_{m,\Omega}}(\xi_1 - 2\pi, \xi_2) > 0, & \text{if } \xi_1 \geqslant \xi_2; \\ \widehat{\phi^{\sigma,\theta}_{m,\Omega}}(\xi_1, \xi_2 - 2\pi) > 0, & \text{otherwise.} \end{cases} \tag{4.13}$$

The proof of the two inequalities in (4.13) is based on Proposition 4.6. We will only give a detailed proof of the first inequality and the proof of the second inequality in (4.13) is essentially the same as that of the first. Assume that $\xi_1 \geqslant \xi_2$:

The case of $0 \leqslant \theta \leqslant \arctan \frac{2\Omega - \pi}{2(\pi - \Omega)}$. Since $\xi_1 \geqslant \xi_2$, $(\xi_1, \xi_2) \in S_3$, we have

$$\xi_1(\cos\theta + \sin\theta) \geqslant \xi_1 \cos\theta + \xi_2 \sin\theta \geqslant 2\sigma\Omega.$$

Since $\sigma > \sigma_0(\theta, \Omega) = \frac{\pi \cos\theta}{2\Omega}$ and $0 \leqslant \tan\theta \leqslant \frac{2\Omega - \pi}{2(\pi - \Omega)}$, we have then

$$\xi_1 \geqslant \frac{2\sigma\Omega}{\cos\theta + \sin\theta} > \frac{2\Omega \frac{\pi\cos\theta}{2\Omega}}{\cos\theta + \sin\theta} = \frac{\pi}{1 + \tan\theta} \geqslant \frac{\pi}{1 + \frac{2\Omega - \pi}{2(\pi - \Omega)}} = 2(\pi - \Omega),$$

which implies

$$\xi_1 - 2\pi > -2\Omega.$$

Together with the fact that $\xi_1 - 2\pi \leqslant -\pi < 0$ as $\xi_1 \leqslant \pi$, we have

$$(\xi_1 - 2\pi, \xi_2) \in (-2\Omega, 2\Omega)^2.$$

Hence $(\xi_1 - 2\pi, \xi_2)$ satisfies Condition (i) of Proposition 4.6. Next, the inequality $\xi_1 \cos\theta + \xi_2 \sin\theta \geqslant 2\sigma\Omega$ implies that for $\sigma > \frac{\pi \cos\theta}{2\Omega}$,

$$(\xi_1 - 2\pi)\cos\theta + \xi_2 \sin\theta \geqslant 2\sigma\Omega - 2\pi\cos\theta > \pi\cos\theta - 2\pi\cos\theta = -\pi\cos\theta > -2\sigma\Omega.$$

Meanwhile since $\xi_1 \leqslant \pi$, $\xi_2 \leqslant \pi$, and $0 \leqslant \theta \leqslant \frac{\pi}{4}$,

$$(\xi_1 - 2\pi)\cos\theta + \xi_2 \sin\theta \leqslant (\pi - 2\pi)\cos\theta + \pi\sin\theta = \pi(\sin\theta - \cos\theta) \leqslant 0.$$

The above two inequalities imply that Condition (ii) of Proposition 4.6 also holds for $\sigma > \frac{\pi\cos\theta}{2\Omega}$ since

$$-2\sigma\Omega < (\xi_1 - 2\pi)\cos\theta + \xi_2\sin\theta \leqslant 0 < 2\sigma\Omega.$$

The first inequality in (4.13) is then proved by Proposition 4.6.

The case of $\arctan\frac{\mathbf{2\Omega}-\pi}{\mathbf{2}(\pi-\mathbf{\Omega})} < \theta \leqslant \frac{\pi}{\mathbf{4}}$. Since $\xi_1\cos\theta + \xi_2\sin\theta \geqslant 2\sigma\Omega$ and $\xi_1 \geqslant \xi_2$, we have

$$\xi_1(\cos\theta + \sin\theta) \geqslant \xi_1\cos\theta + \xi_2\sin\theta \geqslant 2\sigma\Omega.$$

Since $\sigma > \sigma_0(\theta, \Omega) = \frac{(\pi-\Omega)(\cos\theta+\sin\theta)}{\Omega}$, we have then

$$\xi_1 \geqslant \frac{2\sigma\Omega}{\cos\theta + \sin\theta} > \frac{2\sigma_0(\theta,\Omega)\Omega}{\cos\theta+\sin\theta} = 2(\pi - \Omega),$$

which leads to

$$\xi_1 - 2\pi > 2(\pi - \Omega) - 2\pi = -2\Omega.$$

Together with

$$\xi_1 - 2\pi \leqslant \pi - 2\pi = -\pi < 2\Omega, \quad -2\Omega < -\pi \leqslant \xi_2 \leqslant \pi < 2\Omega,$$

we have $(\xi_1 - 2\pi, \xi_2) \in (-2\Omega, 2\Omega)^2$. Thus $(\xi_1 - 2\pi, \xi_2)$ satisfies Condition (i) of Proposition 4.6. Next, by the fact that $\xi_1 \cos\theta + \xi_2 \sin\theta \geqslant 2\sigma\Omega$ and $\sigma > \sigma_0(\theta, \Omega) = \frac{(\pi-\Omega)(\cos\theta+\sin\theta)}{\Omega}$, we have

$$(\xi_1 - 2\pi)\cos\theta + \xi_2 \sin\theta + 2\sigma\Omega \geqslant 4\sigma\Omega - 2\pi\cos\theta > \cos\theta\big(4(\pi-\Omega)(1+\tan\theta) - 2\pi\big).$$

Notice that $\tan\theta > \frac{2\Omega-\pi}{2(\pi-\Omega)}$, we have then

$$(\xi_1 - 2\pi)\cos\theta + \xi_2 \sin\theta + 2\sigma\Omega > \cos\theta \cdot \big(4(\pi-\Omega)(1 + \frac{2\Omega-\pi}{2(\pi-\Omega)}) - 2\pi\big) = 0.$$

Thus

$$(\xi_1 - 2\pi)\cos\theta + \xi_2 \sin\theta > -2\sigma\Omega. \tag{4.14}$$

Meanwhile, we have

$$(\xi_1 - 2\pi)\cos\theta + \xi_2 \sin\theta \leqslant (\pi - 2\pi)\cos\theta + \pi\sin\theta = \pi(\sin\theta - \cos\theta) \leqslant 0 < 2\sigma\Omega,$$

since $(\xi_1, \xi_2) \in [-\pi, \pi]^2$ and $0 \leqslant \theta \leqslant \frac{\pi}{4}$. Together with (4.14), we have

$$-2\sigma\Omega < (\xi_1 - 2\pi)\cos\theta + \xi_2 \sin\theta < 2\sigma\Omega.$$

Thus $(\xi_1 - 2\pi, \xi_2)$ satisfies Condition (ii) of Proposition 4.6 and the first inequality is justified.

Necessity. In this part, we prove the necessity by contrapositive, that is, if $0 < \sigma \leqslant \sigma_0(\theta, \Omega)$, then $\phi^{\sigma,\theta}_{m,\Omega}$ in (4.10) is not stable. Suppose that $0 < \sigma \leqslant \sigma_0(\theta, \Omega)$ as defined by (4.11), i.e.

$$\begin{cases} 0 < \sigma \leqslant \frac{\pi\cos\theta}{2\Omega}, & 0 \leqslant \theta \leqslant \arctan\frac{2\Omega-\pi}{2(\pi-\Omega)}; \\ 0 < \sigma \leqslant \frac{(\pi-\Omega)(\cos\theta+\sin\theta)}{\Omega}, & \arctan\frac{2\Omega-\pi}{2(\pi-\Omega)} < \theta \leqslant \frac{\pi}{4}. \end{cases} \tag{4.15}$$

The case when $\theta \in [\mathbf{0}, \arctan\frac{\mathbf{2\Omega}-\pi}{\mathbf{2}(\pi-\mathbf{\Omega})}]$. Consider the point $\tilde{\xi} = (\pi, 0) \in [-\pi, \pi]^2$. It is seen via (4.15) that $\pi\cos\theta + 0\sin\theta = \pi\cos\theta \geqslant 2\sigma\Omega$, which contradicts Condition (ii) of Proposition 4.6. Thus, $\widehat{\phi^{\sigma,\theta}_{m,\Omega}}(\tilde{\xi}) = 0$. Next, for the point

$(-\pi, 0) = \tilde{\xi} - 2\pi(1,0)$. Similarly we have $-\pi \cdot \cos\theta + 0 \cdot \sin\theta \leqslant -2\sigma\Omega$, which also contradicts Condition (ii) of Proposition 4.6. Thus, $\widehat{\phi^{\sigma,\theta}_{m,\Omega}}(\tilde{\xi} - 2\pi(1,0)) = 0$. For the point $(\pi, -2\pi) = \tilde{\xi} - 2\pi(0,1)$, we have $(\pi, -2\pi) \notin (-2\Omega, 2\Omega)^2$, which contradicts Condition (i) of Proposition 4.6, thus $\widehat{\phi^{\sigma,\theta}_{m,\Omega}}(\tilde{\xi} - 2\pi(0,1)) = 0$. So far, we have verified that for $\tilde{\xi} = (\pi, 0)$, one has $\widehat{\phi^{\sigma,\theta}_{m,\Omega}}(\tilde{\xi} - 2\pi k) = 0$, for $k = (0,0), (1,0)$ and $(0,1)$. For any other $k \in \mathbb{Z}^2$, clearly $\widehat{\phi^{\sigma,\theta}_{m,\Omega}}(\tilde{\xi} - 2\pi k) = 0$ as $\tilde{\xi} - 2\pi k$ lies outside of the support of $\widehat{\phi^{\sigma,\theta}_{m,\Omega}}$. In summary, $[\widehat{\phi^{\sigma,\theta}_{m,\Omega}}, \widehat{\phi^{\sigma,\theta}_{m,\Omega}}](\tilde{\xi}) = 0$, for $\tilde{\xi} = (\pi, 0)$. By Lemma 4.3, $\phi^{\sigma,\theta}_{m,\Omega}$ is not stable.

The case when $\arctan\frac{\mathbf{2\Omega}-\pi}{\mathbf{2}(\pi-\mathbf{\Omega})} < \theta \leqslant \frac{\pi}{\mathbf{4}}$. Consider the point $\tilde{\xi} = \big(2(\pi - \Omega), 2(\pi - \Omega)\big) \in [-\pi, \pi]^2$. By (4.15), we have

$$2(\pi - \Omega)\cos\theta + 2(\pi - \Omega)\sin\theta = 2(\pi - \Omega)(\cos\theta + \sin\theta) \geqslant 2\sigma\Omega,$$

which implies $\widehat{\phi^{\sigma,\theta}_{m,\Omega}}(\tilde{\xi}) = 0$. Also, since $2(\pi - \Omega) - 2\pi = -2\Omega$, we have $\tilde{\xi} - 2\pi k \notin (-2\Omega, 2\Omega)^2$ for $k = (1,0)$, $(0,1)$ and $(1,1)$. Thus, $\widehat{\phi^{\sigma,\theta}_{m,\Omega}}(\tilde{\xi} - 2\pi k) = 0$, for all $k \in \mathbb{Z}^2_2$. For any other $k \in \mathbb{Z}^2$, $\widehat{\phi^{\sigma,\theta}_{m,\Omega}}(\tilde{\xi} - 2\pi k) = 0$ as $\tilde{\xi} - 2\pi k$ is outside of the support of $\widehat{\phi^{\sigma,\theta}_{m,\Omega}}$. All together, we have $\widehat{\phi^{\sigma,\theta}_{m,\Omega}}(\tilde{\xi} - 2\pi k) = 0$ for all $k \in \mathbb{Z}^2$, which implies

$$[\widehat{\phi^{\sigma,\theta}_{m,\Omega}}, \widehat{\phi^{\sigma,\theta}_{m,\Omega}}](\tilde{\xi}) = 0, \text{ for } \tilde{\xi} = \big(2(\pi - \Omega), 2(\pi - \Omega)\big).$$

By Lemma 4.3, $\phi^{\sigma,\theta}_{m,\Omega}$ is not stable. The proof is complete. □

For a given Ω, the area of the support of $\widehat{\phi^{\sigma,\theta}_{m,\Omega}}$ defined by (4.10) with $\sigma = \sigma_0(\theta, \Omega)$ will achieve its minimum at $\theta = \arctan\frac{2\Omega-\pi}{2\pi-2\Omega}$. For the Meyer's refinable function Q_Ω with $\Omega = \frac{2}{3}\pi$ (the value of Ω commonly used), the value of θ should be set as $\theta = \arctan\frac{1}{2}$ to minimize the support of the resulting stable refinable function in frequency domain. A direction calculation leads to

$$\inf_{\sigma > \sigma_0(\arctan\frac{1}{2}, \frac{2}{3}\pi)} \text{area of supp}(\widehat{\phi^{\sigma,\arctan\frac{1}{2}}_{m,\frac{2}{3}\pi}}) = \frac{46}{9}\pi^2.$$

4.2.2 Construction of band-limited Riesz wavelets and orthonormal wavelets

Once a stable refinable function ϕ is constructed via (4.5) or (4.10), a set of Riesz wavelets Ψ^d of $L_2(\mathbb{R}^d)$ can be immediately constructed using Theorem 2.13, with

$$\Psi^d = \left\{ \psi_\mu : \widehat{\psi_\mu}(\xi) = \exp\left(i\eta(\mu)\cdot\frac{\xi}{2}\right)[\widehat{\phi},\widehat{\phi}](\frac{\xi}{2}+\mu\pi)\tau(\frac{\xi}{2}+\mu\pi)\widehat{\phi}(\frac{\xi}{2}), \mu\in\mathbb{Z}_2^d\backslash\{0\} \right\},$$

where τ is the refinement mask of ϕ. Suppose that $\widehat{Q_\Omega} \in C^n(\mathbb{R})$ for some $n \in \mathbb{Z}^*$, then $\widehat{\phi} \in C^n(\mathbb{R}^d)$ by its definition.

Moreover, any band-limited stable refinable function ϕ given by (4.5) or (4.10) can also be used to construct orthonormal band-limited wavelets using the classical orthonormalization technique. That is, given any band-limited stable refinable function, we can define a new band-limited function $\widetilde{\phi}$ by setting

$$\widehat{\widetilde{\phi}} := \frac{\widehat{\phi}}{\sqrt{[\widehat{\phi},\widehat{\phi}]}}. \tag{4.16}$$

Then we have $[\widehat{\widetilde{\phi}},\widehat{\widetilde{\phi}}] \equiv 1$, i.e., $\widetilde{\phi}$ is orthonormal. Moreover,

$$\widehat{\widetilde{\phi}}(2\xi) = \frac{\widehat{\phi}(2\xi)}{\sqrt{[\widehat{\phi},\widehat{\phi}](2\xi)}} = \frac{\sqrt{[\widehat{\phi},\widehat{\phi}](\xi)}}{\sqrt{[\widehat{\phi},\widehat{\phi}](2\xi)}}\tau(\xi)\widehat{\widetilde{\phi}}(\xi),$$

where τ is the mask of ϕ. Thus, the refinement mask $\widetilde{\tau}$ of $\widetilde{\phi}$ is

$$\widetilde{\tau}(\xi) = \frac{\sqrt{[\widehat{\phi},\widehat{\phi}](\xi)}}{\sqrt{[\widehat{\phi},\widehat{\phi}](2\xi)}}\tau(\xi). \tag{4.17}$$

Again using (2.13), we can immediately obtain a set of non-separable band-limited orthonormal wavelets $\widetilde{\Psi}^d$ of $L_2(\mathbb{R}^d)$:

$$\widetilde{\Psi}^d = \left\{ \widetilde{\psi}_\mu : \widehat{\widetilde{\psi}_\mu}(\xi) = \exp\left(i\eta(\mu)\cdot\frac{\xi}{2}\right)\widetilde{\tau}(\frac{\xi}{2}+\mu\pi)\widehat{\widetilde{\phi}}(\frac{\xi}{2}), \mu\in\mathbb{Z}_2^d\backslash\{0\} \right\}, \tag{4.18}$$

where $\widetilde{\tau}$ is the mask of $\widetilde{\phi}$.

It is seen that, once we have a band-limited stable refinable function in hand, the construction of band-limited orthonormal wavelets is very easy by the simple normalization technique (4.16). In contrast, the construction of orthonormal compactly supported wavelets is much more difficult. One reason is that a compactly supported function in spatial domain will extend the support of the resulting function to infinity after applying (4.16), while a band-limited function is still band-limited after applying (4.16). Thus, the normalization (4.16) can be used for constructing orthonormal wavelets with compact support in frequency domain, but cannot be used for constructing orthonormal wavelets with compact support in spatial domain. In the end, we summarize the spatial decay property of the orthonormal wavelets defined by (4.18) in terms of their smoothness in frequency domain in the following proposition.

Proposition 4.8. *Let ϕ be a stable band-limited refinable function defined by* (4.5) *or* (4.10)*, and let $\widetilde{\phi}$ be defined by* (4.16)*. Suppose that $\widehat{Q_\Omega} \in C^n(\mathbb{R})$ for some $n \in \mathbb{Z}^*$. Then $\widehat{\widetilde{\phi}} \in C^n(\mathbb{R}^d)$ and for the set of orthonormal wavelets $\widetilde{\Psi}^d$ defined by* (4.18)*, we have $\widehat{\widetilde{\psi}} \in C^n(\mathbb{R}^d), \forall\, \widetilde{\psi} \in \widetilde{\Psi}^d$.*

Proof. Firstly, notice that $\widehat{\phi}$ is nonnegative as $\widehat{Q_\Omega}$ is nonnegative. Together with the fact that $\widehat{\phi} \in C^n(\mathbb{R}^d)$, $|\widehat{\phi}|^2 = \widehat{\phi}^2 \in C^n(\mathbb{R}^d)$. Moreover, $\widehat{\phi}$ is compactly supported implies that $[\widehat{\phi}, \widehat{\phi}](\cdot) = \sum_{k\in\mathbb{Z}^d} |\widehat{\phi}|^2(\cdot + 2\pi k)$ is a finite summation of the sequence $\{|\widehat{\phi}|^2(\cdot + 2\pi k),\, k \in \mathbb{Z}^d\}$ in any finite interval. Thus, $[\widehat{\phi}, \widehat{\phi}] \in C^n(\mathbb{R}^d)$. Since ϕ is stable, there exists some $c > 0$ such that $[\widehat{\phi}, \widehat{\phi}] > c$. Then we have $\frac{1}{\sqrt{[\widehat{\phi}, \widehat{\phi}]}} \in C^n(\mathbb{R}^d)$ and thus $\widehat{\widetilde{\phi}} \in C^n(\mathbb{R}^d)$.

Secondly, given any $\widetilde{\psi} \in \widetilde{\Psi}$, to prove that $\widetilde{\psi} \in C^n(\mathbb{R}^d)$, it is sufficient to show

$\widetilde{\tau} \in C^n(\mathbb{R}^d)$. Recall that the refinement mask τ of ϕ is defined as

$$\tau(\xi) = \sum_{k\in\mathbb{Z}^d} b(\xi + 2\pi k),\ \xi \in \mathbb{R}^d,$$

where $b(\xi) = \frac{\widehat{\phi}(2\xi)}{\widehat{\phi}(\xi)}$ if $\phi(\xi) > 0$ and 0 otherwise, as shown in the proof of Lemma 4.2. Indeed, we have that $b(\cdot) = \widehat{\phi}(2\cdot) \in C^n(\mathbb{R}^d)$ which can be proved as follows. By the definition (4.5) or (4.10) of ϕ, it is easy to see that $\widehat{\phi}(\xi) = 1$ if $\phi(2\xi) > 0$, which implies $b(\xi) = \widehat{\phi}(2\xi)$ if $\phi(2\xi) > 0$. If $\phi(2\xi) = 0$, $b(\xi) = 0$. Thus, $b(\cdot) = \widehat{\phi}(2\cdot)$. Notice that the support of $b(\xi)$ is strictly within $(-\pi, \pi)^d$, we have $\tau(\xi) \in C^n(\mathbb{R}^d)$. Since ϕ is stable, there exists a constant $c > 0$ such that $[\widehat{\phi}, \widehat{\phi}] > c$, together with $[\widehat{\phi}, \widehat{\phi}] \in C^n(\mathbb{R}^d)$, we have $\frac{\sqrt{[\widehat{\phi},\widehat{\phi}](\xi)}}{\sqrt{[\widehat{\phi},\widehat{\phi}](2\xi)}} \in C^n(\mathbb{R}^d)$. Putting all together, we have then $\widetilde{\tau} \in C^n(\mathbb{R}^d)$ by its definition (4.17). The proof is complete. □

4.3 Examples

Example 4.1. *In this example, we use the direction matrix of the form* (4.4)*, with* $m = (1, 1, 1)$ *and* $\rho = \frac{5}{4}$*, to generate the band-limited function* $\phi \in L_2(\mathbb{R}^2)$ *defined as follows:*

$$\widehat{\phi}(\xi_1, \xi_2) = \widehat{Q_{\frac{2}{3}\pi}}(\xi_1)\widehat{Q_{\frac{2}{3}\pi}}(\xi_2)\widehat{Q_{\frac{2}{3}\pi}}\big(\frac{4}{5}(\xi_1 + \xi_2)\big).$$

By Theorem 4.5, ϕ *is refinable and stable. After obtaining a stable refinable function, we can then use the construction scheme proposed in* (2.28) *to construct a Riesz wavelet system of three wavelets, whose associated masks are given as follows:*

$$\exp(i\eta(\kappa)\cdot\xi)[\widehat{\phi}, \widehat{\phi}](\xi + \kappa\pi)\tau(\xi + \kappa\pi),\ \kappa \in \mathbb{Z}_2^2\backslash\{0\},$$

where τ *is the refinable mask of* ϕ*. See Figure 4.1 for the graphs of the refinable function and its associated three Riesz wavelets in spatial domain.*

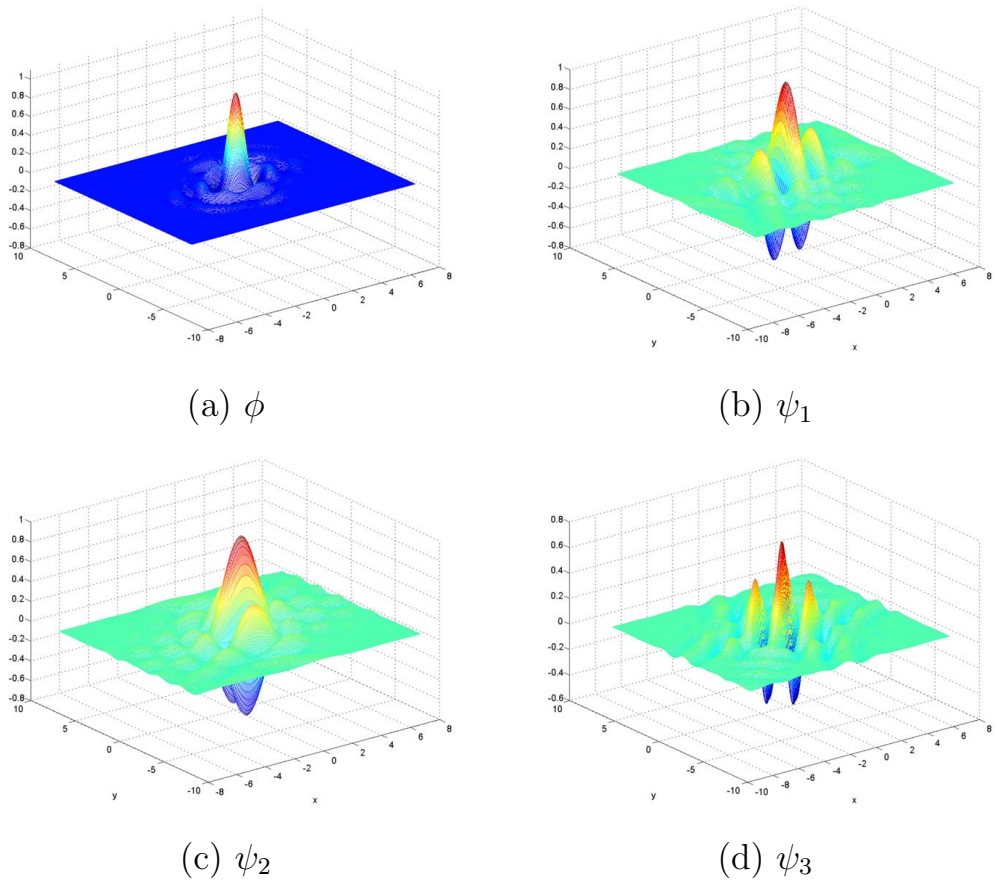

(a) ϕ (b) ψ_1

(c) ψ_2 (d) ψ_3

Figure 4.1: Graphs of the refinable function and its associated three Riesz wavelets as introduced in Example 4.1. (a) Refinable function, and (b)–(d) the associated Riesz wavelets.

Example 4.2. *In this example, we use the direction matrix of the form* (4.9)*, with* $m = (1, 1, 1)$*,* $\sigma = \frac{\sqrt{5}}{2}$ *and* $\theta = \arctan \frac{1}{2}$*, to generate the band-limited function* $\phi \in L_2(\mathbb{R}^2)$ *defined as follows:*

$$\widehat{\phi}(\xi_1, \xi_2) = \widehat{Q_{\frac{2\pi}{3}}}(\xi_1)\widehat{Q_{\frac{2\pi}{3}}}(\xi_2)\widehat{Q_{\frac{2\pi}{3}}}\big(\xi_1 + \frac{1}{2}\xi_2\big). \tag{4.19}$$

By Theorem 4.7, ϕ *is refinable and stable. Then, by using the standard orthonormalization technique, we have an orthonormal refinable function* $\widetilde{\phi}$ *defined by*

$$\widehat{\widetilde{\phi}} = \frac{\widehat{\phi}}{\sqrt{[\widehat{\phi}, \widehat{\phi}]}},$$

and the refinable mask $\tilde{\tau}$ *of* $\tilde{\phi}$ *is* $\widetilde{\tau}(\xi) = \frac{\sqrt{[\widehat{\phi},\widehat{\phi}](\xi)}}{\sqrt{[\widehat{\phi},\widehat{\phi}](2\xi)}}\tau(\xi)$*, where* τ *is the refinable mask of* ϕ *in* (4.19)*. Again, using the scheme of* (2.28)*, we can construct a wavelet system of three orthonormal wavelets from* $\tilde{\phi}$*, whose masks are given as follows:*

$$\exp(i\eta(\kappa) \cdot \xi)\widetilde{\tau}(\xi + \kappa\pi),\ \kappa \in \mathbb{Z}_2^2 \backslash \{0\}.$$

See Figure 4.2 for the graphs of the refinable function and its associated three orthonormal wavelets in spatial domain.

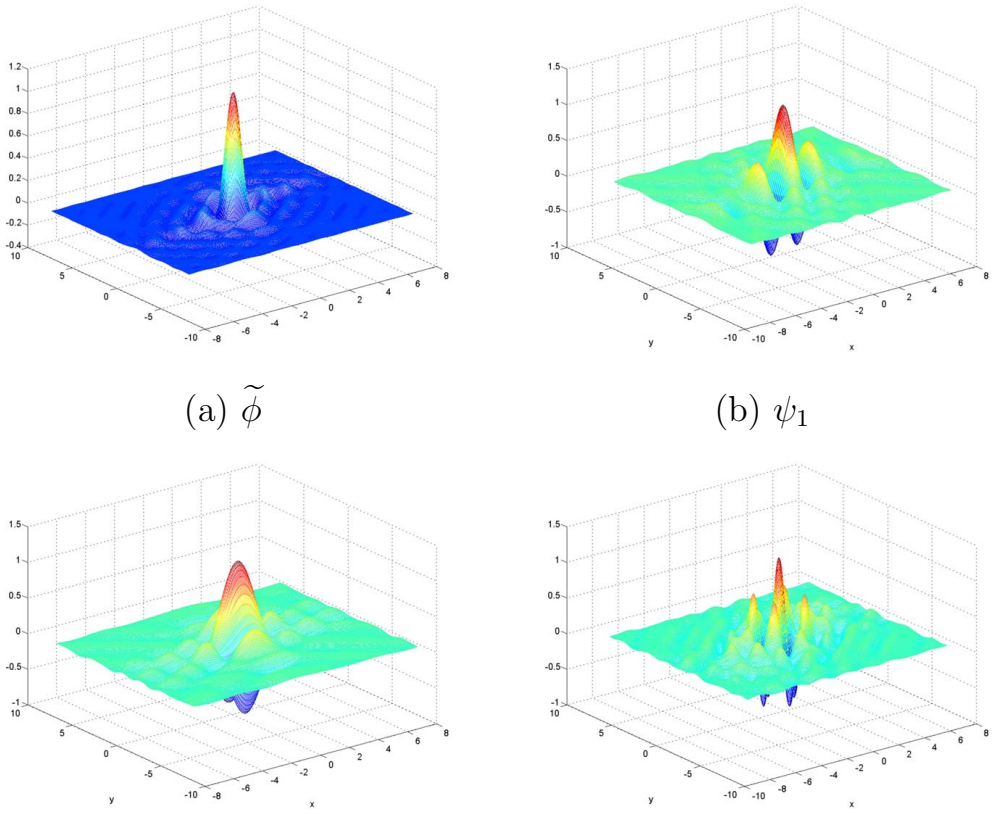

(a) $\widetilde{\phi}$ (b) ψ_1

(c) ψ_2 (d) ψ_3

Figure 4.2: Graphs of the refinable function and its associated orthonormal wavelets as introduced in Example 4.2. (a) Refinable function; and (b)–(d) the associated three orthonormal wavelets.

Chapter 5

Recovering Over/Under-exposed Regions of Digital Colour Photographs

This chapter constitutes the application part of this thesis. More precisely, by using wavelet tight frames (framelets) as the main tool, we propose a method for restoring digital colour photographs with over/under-exposed regions. As in the opening chapter of this thesis, we have introduced some related background on the origination of the over/under-exposed regions recovery problem. Now in this new chapter, we provide the detailed procedures for handling this problem. Firstly, we start with the rigorous formulation of over/under-exposed regions recovery problem and provide the basic scheme for solving this problem. Secondly, we briefly review some most related works. Thirdly, we present the detailed implementation and explanation for the proposed method. Finally, we show some numerical experiments and discussions for evaluation.

5.1 Problem formulation and the workflow

5.1.1 Problem formulation

At first glance, it seems that the over-exposure correction can be re-formulated as certain well studied image restoration task. For example, one might treat it as an image inpainting problem and use some existing image inpainting approach to directly recover the colour details of over-exposed regions. The missing colour information of over-exposed regions is then inferred either from its neighbouring regions or by some self-similarities existing in the image. However, by doing so, the overall brightness of the inpainted over-exposed regions will be in general equal to or slightly lower than that of their neighbouring well-exposed regions. As a result, the local contrast and the reflection shown in the area around the over-exposed regions look very artificial, since the over-exposed regions are supposed to be brighter than its neighbouring regions. The picture does not appear to be taken under some realistic lighting condition in real life. See Figure 5.1 for an illustration.

(a) (b) (c)

Figure 5.1: Demonstration of over-exposure correction by directly inpainting over-exposed regions. (a) The input photograph; (b) the result from inpainting the over-exposed regions using the wavelet-based inpainting method [9]; (c) the result from the proposed method.

(a) (b) (c)

Figure 5.2: Demonstration of over-exposure correction using existing HDR reconstruction and tone mapping techniques. (a) the input photograph; (b) the result obtained by directly using the tone mapping operator proposed in [40]; (c) the result obtained by firstly using the HDR reconstruction proposed in [58] to construct an HDR image, followed by the tone mapping process [40]; (d) the result from the proposed method.

One may also directly apply some tone mapping technique to remove the whiteness of the over-exposed regions by compressing the dynamic range. However, such an approach cannot recover the chromatic information and image details of the over-exposed regions. See Figure 5.1 (b) for an illustration. A better way is to first create an HDR image from the input LDR image and then apply the tone mapping technique to reconstruct an LDR image. However, most existing software based HDR reconstruction methods need to take multiple images with different exposure times as the input. The single-image based HDR reconstruction is much less reliable in practice. Moreover, most existing single-image based HDR techniques usually aim at creating an HDR image with its dynamic range much wider than the dynamic range allowed in LDR image. As a result, after using the tone mapping technique to compress such a hallucinated dynamic range back to the low dynamic range, the colour of those over-exposed regions still looks washed out. See Figure 5.2 (b) for an illustration.

In other words, the over/under-exposure correction is an image recovery problem different from many existing image recovery problems including inpainting,

HDR reconstruction and tone mapping. There are certain needs for developing a specific restoration method to correct over/under-exposure of the digital colour photographs taken by regular LDR cameras. In recent years, there have been a few methods proposed for over-exposure correction (see e.g. [72, 54, 45]). Both [72] and [54] are for recovering 'partial over-exposure', i.e. the colour of over-saturated regions is not completely white. The applicability of these two approaches is quite limited, as they usually fail to correct the over-exposed regions where only bright white is shown. The correction of fully over-exposed regions is first considered by Guo *et al.* in [45]. Suppose that colour is represented in CIELAB space $[L; a; b]$: L denotes the lightness value, and $[a; b]$ represents two chromatic values (see e.g. [64]). Guo *et al.* [45] decompose the problem of over-exposure correction into the following two sub-problems:

1. a tone mapping problem in the lightness channel L for lowering the lightness of the over-exposed regions;

2. an image inpainting problem in the two colour channels $[a; b]$ for recovering the colour and image details of the over-exposed region.

It is noted that lowering the lightness of the over-exposed region is a necessary step to show true colour of over-exposed regions, since the colour will appear white as long as L is close to the maximum value (i.e., 100). The method proposed by Guo *et al.* [45] shows much better performance on over-exposure correction than other generic colour restoration methods in [72, 54]. However, Guo *et al.*'s method is far from satisfactory, and there is still a lot of room for improvement: firstly, the lightness channel of the result is not fully utilized by only considering the compression of the dynamic range; secondly, the tone mapping technique used in [45] is designed for re-mapping the dynamic range of an HDR image to that of an LDR image which may erase shadow details in under-exposed regions; lastly, the

recovery of image details of the over-exposed regions by [45] is not very satisfactory.

5.1.2 Basic idea and the workflow

In this thesis, we propose another approach to better correct over/under-exposures in digital colour photographs. Our approach considers the simultaneous correction of both over-exposed and under-exposed regions, since they are often co-existing for scenes with very high dynamic range (see Figure 1.1 for an illustration). Different from [45], we propose to decompose the problem of over/under-exposure correction to the following three sub-problems:

1. an inpainting problem for recovering clipped values of over-exposed regions in lightness channel L;

2. a tone mapping problem for adjusting the inpainted lightness channel to fit the range allowed in LDR images;

3. an inpainting problem in two colour channels $[a; b]$ for recovering colour details in over-exposed regions.

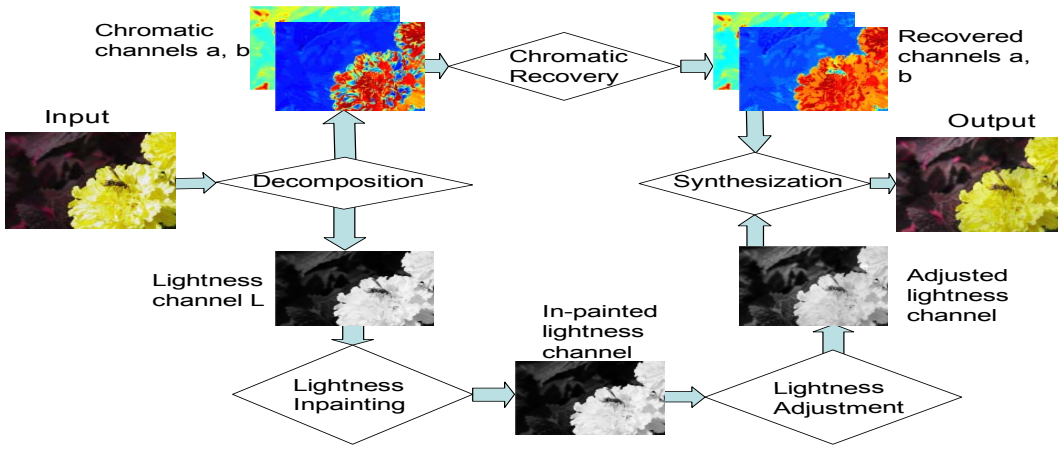

Figure 5.3: Workflow of the proposed method

The first sub-problem is about how to recover the lightness values of over/under-exposed pixels that are clipped to be inside the physical range $[0, 100]$ supported by LDR image. After the recovery, the range of the lightness channel will usually be slightly larger than the physical range (see Figure 5.8 (d)). Then the second sub-problem is about how to adjust the lightness of the whole image such that it fits the physical range while not destroying any visible image details with low lightness values. In our setting, such a tone mapping has an additional function, i.e. magnifying the lightness values of under-exposed pixels to increase the local contrast and seamlessly blend the corrected pixels back to the whole image. Recall that the colour of over-exposed regions is completely white since the lightness is set to the maximum. Thus, the third sub-problem is about how to recover the missing colour details of over-exposed regions from the information of its neighbouring well-exposed regions.

The proposed approach is applicable to photographs with both fully over-exposed regions and severely under-exposed regions. As shown in the experiments, there are several advantages of the proposed method over the existing ones, including more effective use of lightness range, better recovery of chromatic details in over-exposed regions, and better local contrasts of the under-exposed regions. See Figure 5.1 (c) and Figure 5.2 (d) for an illustration.

5.2 Review of Related works

Over-exposure and under-exposure happen when the dynamic range of a scene is higher than the dynamic range supported by the camera. As a result, the colour information of the over-exposed regions is completely lost by only showing white colour; or similarly the colour information of the under-exposed regions are hardly perceived by showing nearly black colour. The colour correction is a challenging

task, as the human perception of colour is a very profound process which is still not fully understood. In the past, there were many well-studied image restoration tasks that are related to the colour correction, including HDR reconstruction, tone mapping and inpainting. Until very recently, there have been some work focusing on over-exposure correction. In the following, we give a very brief review on some most related techniques.

Since the over/under-exposure happens due to the limitation of dynamic range allowed in LDR camera, one solution is to render an HDR image of the scene by using multiple LDR images taken under different exposure times (see e.g. [31, 53, 44, 43]). These multiple images based approaches either require costly additional hardware instruments or are only applicable to certain configurations. For example, when using multiple exposures, both the camera and the scene need to be static in order to avoid motion blurring. There have been some previous works on hallucinating an HDR image from a single LDR image. Wang *et al.* [69] recovered the missing details of the over-exposed regions of an LDR image by using some texture synthesis technique. In their approach, the user needs to manually input the locations of well-exposed regions that are similar to the over-exposed regions. Rempel *et al.* [58] proposed an approach to recover the lightness of the picture by increasing the upper bound of the dynamic range. The basic idea is to fit a smooth function on an over-exposed region and its neighbourhood. This method is mainly for recovering the lightness of the picture and the chromatic details are not recovered in their method.

The *tone mapping* technique is an inverse process of HDR creation. It is about synthesizing an LDR image out of an HDR image for regular display. The dynamic range of the HDR image needs to be compressed in order to fit the range allowed in LDR image. There have been plenty of tone mapping methods proposed by many researchers in the literature. Some methods use tone reproduction curves, such

as Gamma curve, to re-map the global lightness values (see e.g. [70, 48]). Some use more sophisticated spatially-varying local operators (see e.g. [40, 39, 50]) for tone mapping. In general, local tone mapping operators are more favorable than the global tone reproduction curves, as they perform better on preserving images details when compressing the dynamic range (see e.g. [40, 50]).

There have been an abundant literature on image inpainting, which is first proposed by [3] to recover damaged pixels from un-damaged pixels in images. There are many representative image inpainting approaches. One is the PDE-based variational approach which propagates information from un-damaged pixels to damaged pixels in the direction of the isophotest (see e.g. [3, 4]). One is treating the image inpainting problem as a linear inverse problem and solve it via some regularization methods. For example, the TV (total variation) based regularization [20, 21] and the wavelet tight frame based regularization [9, 14, 32] have been used for general image inpainting. Another one is the template-based approach which covers the image patches in the damaged regions by using similar patches from un-damaged regions (see e.g. [25, 37]).

There have been relatively few works on designing specific methods for over-exposure correction. Earlier works assume that only 'partial over-exposure' occurs in the input photograph. That is, at least one colour channel is not fully saturated among all three colour channels: red, green and blue. Zhang and Brainard [72] estimated the global ratios among three colour channels using well-exposed regions of the image. Then the saturated colour channels for over-exposed regions are recovered by applying the estimated ratios on unsaturated channels. Masood *et al.* [54] improved the results of [72] by using a spatially varying ratio function to recover the saturated colour channels of over-exposed regions. The applicability of these two approaches are quite limited, as many real-life digital colour photographs are mainly degraded by 'total over-exposure' (i.e. all three colour channels fully

saturated) rather than 'partial over-exposure'.

The over-exposure correction for fully over-exposed regions is first considered by Guo *et al.* in [45] with a much more sophisticated approach. There are two main components in Guo *et al.*'s approach: (i) applying some tone mapping technique to compress dynamic range of the given picture to make room for the recovered lightness of over-exposed regions; and (ii) estimating the colour of over-exposed pixels by image inpainting. In [45], the tone mapping technique proposed by Fattal *et al.* [40] is modified and adopted for dynamic range compression. The inpainting process in two colour channels $[a; b]$ is done via a modified version of the colourization method proposed by Levin *et al.* [49], in which the colour of the targeted pixel is propagated from its neighbouring similar pixels. The similarity of pixels are determined from their lightness and chromatic values.

5.3 The main algorithm

In this section, we give a detailed description on the proposed approach that follows the workflow illustrated in figure 5.3. It is seen that the lightness information and the chromatic information of pixels are processed in different modules. The main steps of our approach are outlined in the following.

Outline of the main algorithm

---

1. Converting the RGB channels of the given image I into the CIELAB channels $[L; a; b]$;

2. Inpainting the lightness channel L to reconstruct a new lightness channel $\widetilde{L}$ with its range beyond the limitation of LDR image

3. Adjusting the lightness channel $\widetilde{L}$ to fit the range allowed in LDR image and increase the local contrast of under-saturated regions. Denote the resulting lightness channel by L^*.

4. Recovering the missing chromatic details of the over-exposed regions in two chromatic channels $[a, b]$ to obtain the recovered chromatic channels $[a^*, b^*]$.

5. Synthesizing the new colour photograph using the three channels $[L^*; a^*; b^*]$.

Among the five major steps, Step 100 and Step 5 are standard colour conversion routines between RGB colour representation and CIELAB colour representation (see [64] for more details). The main components are Step 2, Step 3 and Step 4. The detailed discussion on Step 2 and Step 3 will be given in Section 5.3.1 and Section 5.3.2. Section 5.3.3 will cover the discussion of Step 4 as well as Step 5.

5.3.1 Inpainting in lightness channels L

In an LDR photograph with over-exposed pixels, the 'true' lightness values of those over-exposed pixels are clipped at the maximum value(i.e. 100). As a result, the over-exposed regions are white regions without any chromatic details. These over-exposed pixels are easy to detect by checking their lightness values. In practice, the colour of the pixels whose lightness values are close to 100 is indistinguishable from white in human perception. Similarly, the colour of the pixels whose lightness values close to 0 is nearly invisible in human perception. Thus we treat all pixels whose lightness values close to 100 or 0 as over/under-exposed pixels. The clipped region Γ for inpainting is then defined by

$$\Gamma := \{p : L(p) > K_1\} \cup \{p : L(p) < K_2\}, \tag{5.1}$$

where K_1 (close to 100), K_2 (close to 0) are two positive real numbers. See Figure 5.4 for an illustration of the result of our lightness inpainting method under different settings of K_1 and K_2. Based on the contour shape of inpainted lightness region, we set $K_1 = 98$ and $K_2 = 0.2$ through all experiments.

The goal of this section is then to develop an inpainting method for recovering the lightness values of over/under-exposed pixels in the set Γ, the set of those pixels with lightness values close to 100 or 0. It is observed that the part associated with each clipped lightness region for inpainting usually belongs to the surface made by the same material in physical world which should have the same surface reflection property. Thus, we may assume that the change of lightness within each individual clipped region is smooth, and assume as well that the transition between a clipped region and its neighbouring well-exposed regions is smooth. These two assumptions lead to the following minimization model for inpainting in lightness channel L:

$$\begin{aligned} \widetilde{L} = \text{argmin}_U & \frac{1}{2}\|\mathcal{D}_1 U\|_2^2 + \frac{\sigma}{2} \cdot \|\mathcal{D}_2 U\|_2^2 \\ & \text{subject to } U|_{\Gamma^c} = L|_{\Gamma^c}, \end{aligned} \tag{5.2}$$

where Γ^c denote the complement of the index set Γ given in (5.1), $\mathcal{D}_1$, $\mathcal{D}_2$ are the level-1 and level-2 framelet decomposition operator associated with the band-limited framelet system raised in Example 3.1, and $\sigma > 0$ is the weight assigned to the level-2 regularized term (whose value is set to 0.2 in all experiments).

In the following, we give a brief explanation on the model (5.2). It is known that the wavelet frame coefficients characterize the local variation of the signal. Thus, by minimizing the framelet coefficients of lightness channel, the solution tends to have smooth wavelet coefficients which in turn lead to lightness channel with smooth variations. In addition, the use of band-limited framelets in (5.2) is also quite helpful for characterizing the smooth variations of clipped regions, since band-limited framelets are infinitely smooth in spatial domain.

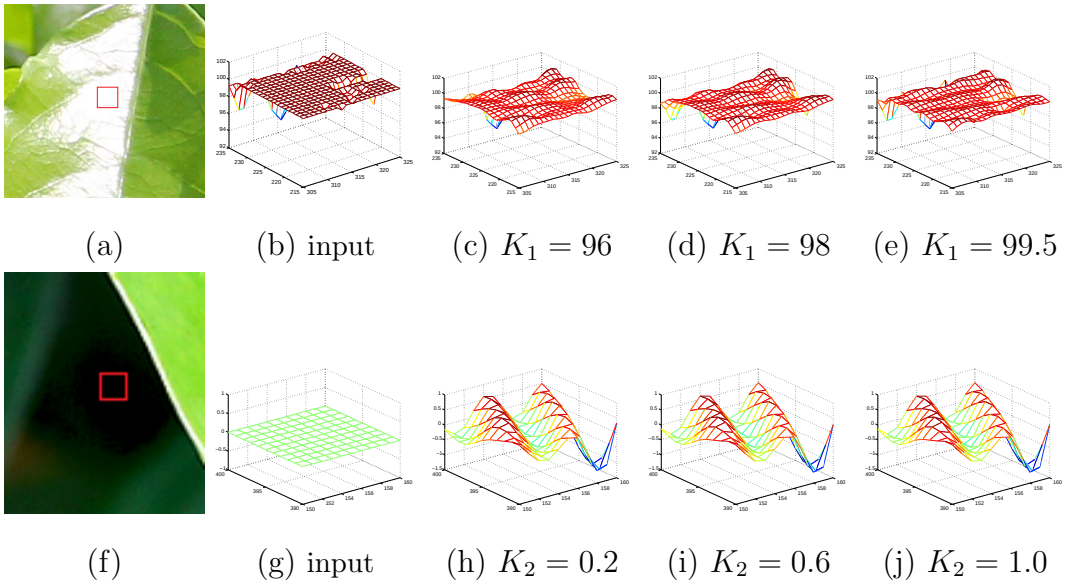

(a) (b) input (c) $K_1 = 96$ (d) $K_1 = 98$ (e) $K_1 = 99.5$

(f) (g) input (h) $K_2 = 0.2$ (i) $K_2 = 0.6$ (j) $K_2 = 1.0$

Figure 5.4: Demonstration of lightness of over/under-exposed region inpainted using different K_1 and K_2 as in (5.1). (a) The input image with over-exposed region marked out by red rectangle; (b)–(e) the contours of lightness of over-exposed region before and after inpainting; (f) the input image with under-exposed region marked out by red rectangle; (g)–(j) the contours of lightness of under-exposed region before and after inpainting.

The minimization model (5.2) is a least squares problem with linear constraints for which there exist many numerical solvers. More specifically, define

$$A := \mathcal{D}_1^T \mathcal{D}_1 + \sigma \mathcal{D}_2^T \mathcal{D}_2$$

and B the projection matrix that maps U to $U|_{\Gamma^c}$, then there exists a vector Λ of size $|\Gamma^c|$ such that the concatenated vector $V := (L^{*\top}, \Lambda^\top)^\top$ is exactly the solution of the following linear system:

$$DX = Y,$$

where $D := \begin{bmatrix} A & B^\top \\ B & 0 \end{bmatrix}$ and $Y := \begin{bmatrix} 0 \\ L|_{\Gamma^c} \end{bmatrix}$. See Figure 5.4 for an illustration of the inpainting in lightness channel using 2 levels of framelet decomposition.

5.3.2 Lightness adjustment

The range of the lightness channel $\widetilde{L}$ recovered by solving (5.2) would usually be slightly larger than the physical range of $[0, 100]$ of LDR images (see Figure 5.8 (d)). Also, the under-exposed regions are still of low contrast. Our next step is then to adjust the lightness channel to fit the dynamic range supported by LDR image. Such an adjustment should keep image details visible in well-exposed regions and increase the contrast of under-exposed regions. This is closely related to the tone mapping that converts an HDR image to an LDR image. Similar to some popular tone mapping methods (e.g. [39, 40]), the lightness adjustment in our approach is done in the logarithm domain of lightness channel:

$$\widetilde{R} := \log\left(\widetilde{L} + \delta\right), \tag{5.3}$$

where δ is some positive constant to guarantee that $\widetilde{L} + \delta > 0$. In experiments, we use

$$\delta = \begin{cases} 0.5, & \text{if } \min \widetilde{L} \geq 0; \\ -\min \widetilde{L} + 0.5, & \text{if } \min \widetilde{L} < 0. \end{cases}$$

Most widely-used tone mapping for adjusting lightness channel is to adjust the image edges of lightness channel, instead of directly adjusting the intensity values in lightness channel. During the adjustment, strong image edges and weak image edges are treated differently. The reason is that, despite the smaller magnitudes, weak image edges represent fine details. A straightforward compression will erase out these fine image details, and consequently the quality of the image will be noticeably degraded. Thus, to keep the visual quality of the input image, an effective lightness compression method should aggressively attenuate the strength of strong image edges while conservatively attenuate the strength of weak image edges.

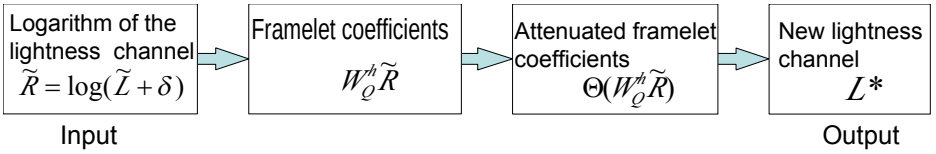

Figure 5.5: Flowchart of the lightness modification algorithm.

In our approach, we use the high-pass spline framelet coefficients as the measurement of image edges, as those framelet coefficients naturally encode the image gradients of different orders in a multi-scale fashion. In our implementation, the 2D tensor-product *piecewise linear spline framelet system* (see Example 2.3) is adopted. Recall that the piecewise linear spline framelet system is associated with a set of three masks $\{\tau_0, \tau_1, \tau_2\}$, whose Fourier coefficients form the following 3 discrete filters respectively:

$$h_0 = \frac{1}{4}[1 \quad 2 \quad 1],\ h_1 = \frac{\sqrt{2}}{4}[1 \quad 0 \quad -1],\ h_2 = \frac{1}{4}[1 \quad -2 \quad 1].$$

Then, the 2D tensor-product piecewise linear spline framelet system is simply associated with the following mask set

$$\{h_i \otimes h_j, 0 \leqslant i, j \leqslant 2\},$$

where $h_0 \otimes h_0$ is the refinement mask and others are wavelet masks. Specifically, piecewise linear spline framelets can capture both first-order and second-order derivative information of the image along different directions [11].

The basic procedure of the proposed lightness adjustment is to first calculate the Q levels of high-pass *piecewise linear spline* framelet coefficients $W_Q^h \widetilde{R}$ for the logarithm of lightness channel R, followed by the attenuation of $W_Q^h \widetilde{R}$ by applying an attenuation function Θ on $W_Q^h \widetilde{R}$. Then the adjusted lightness channel is reconstructed using the attenuated framelet coefficients $\Theta(W_Q^h \widetilde{R})$. See Figure 5.5 for the illustration of a flowchart of the lightness adjustment.

It is noted that the workflow of our proposed lightness adjustment is similar to the tone mapping technique in [40], except that ours is done in framelet domain and that one is done in finite difference domain. Another main difference between ours and the existing one lies in the design of the attenuation function, which plays an important role in the lightness adjustment. In the following, we first give a detailed discussion on the design of attenuation function, and then we present the numerical scheme of constructing lightness channel from the attenuated framelet coefficients of the logarithm of the input lightness channel.

Design of the attenuation function Θ

The attenuation function, which we denote as Θ, plays an important role in the lightness adjustment. The function Θ in our approach takes $W_Q^h \widetilde{R}$, i.e. the framelet coefficient of the logarithm of lightness channel, as the input. The basic principle is to attenuate more on framelet coefficients with large magnitude and attenuate less on framelet coefficients with small magnitude. For each image pixel p, a multi-scale measurement of strength of image edges centering at the pixel p is defined as

$$\vec{H}(p) = (H_1(p), H_2(p), \ldots, H_Q(p))^\top = (\|\vec{c}_1(p)\|_2, \|\vec{c}_2(p)\|_2, \ldots, \|\vec{c}_Q(p)\|_2)^\top,$$

where $\vec{c}_j$ denotes the level-j high-pass framelet coefficients centered at the pixel. Note that $\vec{c_j} \in \mathbb{R}^8$ for the linear spline framelet. In other words, the j-th element of $\vec{H}(p)$ measures the overall energy of R around the pixel p in all high-pass channels at the scale 2^{j-1}, for $j = 1, 2, \ldots, Q$. It is noted that at each scale 2^{j-1}, there are in total eight high-pass channels in a piecewise linear spline framelet system, which account for image gradients with different orders and orientations. After defining the multi-scale strength measurement of image edges for each pixel p, we propose the following discrete attenuation function $\Theta : W_H^1 R \mapsto \widetilde{C_1}$ pixel-wisely

that

$$\Theta\big(\vec{c}_1(p)\big) \mapsto \theta(p)\vec{c}_1(p), \tag{5.4}$$

where the weight $\theta(p)$ is some measurement of the overall strength of local image edges around the pixel p, which is defined as

$$\theta(p) = \Big[\prod_{j=1}^{Q} \frac{H_j(p)}{c' E(H_j)}\Big]^{\beta-1}, \tag{5.5}$$

where $E(H_j)$ is the average of $H_j(p)$ for all pixels p, that is, the average of the whole j-th level high-pass framelet channels. There are two parameters in (5.5), $c' > 0$ and $\beta \in [0, 1]$ which control the adjustment behaviour of the lightness channel. See Figure 5.7 for an illustration of how these two parameters change the lightness channel. In our implementation, we set $\beta = 0.88$ and $c' = 0.2$ for a 3-level piecewise linear framelet decomposition (i.e. $Q = 3$ in (5.5)).

As it is seen from the definition of Θ in (5.5), the degree of the attenuation on each framelet coefficient depends on its magnitude. The larger is the magnitude of the frame coefficient, the more attenuation is applied on it.

Construction of lightness channel from the attenuated framelet coefficients

Let $\widetilde{R}$ denote the logarithm of the lightness channel L defined by (5.3), $W_Q^h \widetilde{R}$ denote its *piecewise linear spline* framelet coefficient vector, and Θ denote the attenuation function applied on the framelet coefficient vector $W_Q^h \widetilde{R}$. Then, the goal is to construct a new lightness channel L^* from the attenuated framelet coefficient vector:

$$\widetilde{C_Q} = \Theta(W_Q^h \widetilde{R}) = \Theta\big(W_Q^h \log(\widetilde{L} + \delta)\big). \tag{5.6}$$

We propose to construct the new lightness channel L^* by setting

$$L^* := \exp(R^*), \tag{5.7}$$

with R^* to be the solution of the following minimization problem:

$$R^* := \text{argmin}_R \frac{1}{2}\|W_1^h R - \widetilde{C_1}\|_2^2 + \eta\|W_1^h R\|_1, \tag{5.8}$$

subject to $\sum_j R(j) = \sum_j \widetilde{R}(j)$, where $\widetilde{C_1}$ denotes the attenuated single-level framelet coefficient vector given by (5.6) with $Q = 1$ and η is the regularization parameter. There are two terms in the objective function of (5.8). The first is the fidelity term and the second is the sparsity prompting regularization term on framelet coefficient vector of the solution. The ℓ_1 norm related regularization term is for suppressing image noise while keeping sharp edges [14]. The reconstruction is not very sensitive to the value of regularization parameter η as long as η is reasonably small (e.g., when $\eta \leqslant 1 \times 10^{-3}$); see Figure 5.6 for an illustration of the results using different regularization parameters. In our implementation, η is set to 5×10^{-4}. It is noted that only single-level framelet coefficients are used for reconstruction of the lightness channel. The main reason is that in (5.8), the reconstruction from multi-level attenuated framelet coefficients tends to yield some undesirable effects like halos.

The adjusted lightness channel L^* obtained from (5.7) and (5.8) is usually severely squeezed. We thus re-scale it back to the physical range of the lightness channel of the original input image:

$$L^* \hookleftarrow \frac{L^* - \min(L^*)}{\max(L^*) - \min(L^*)}\big(\max(L) - \min(L)\big) + \min(L), \tag{5.9}$$

where L is the lightness channel of the original input photograph. The minimization model (5.8) can be effectively solved by the split Bregman method. The following is a detailed description of the solver. Empirically, two parameters μ and ρ are set to be 1×10^{-3} and 5×10^{-4} respectively in real implementation of the algorithm.

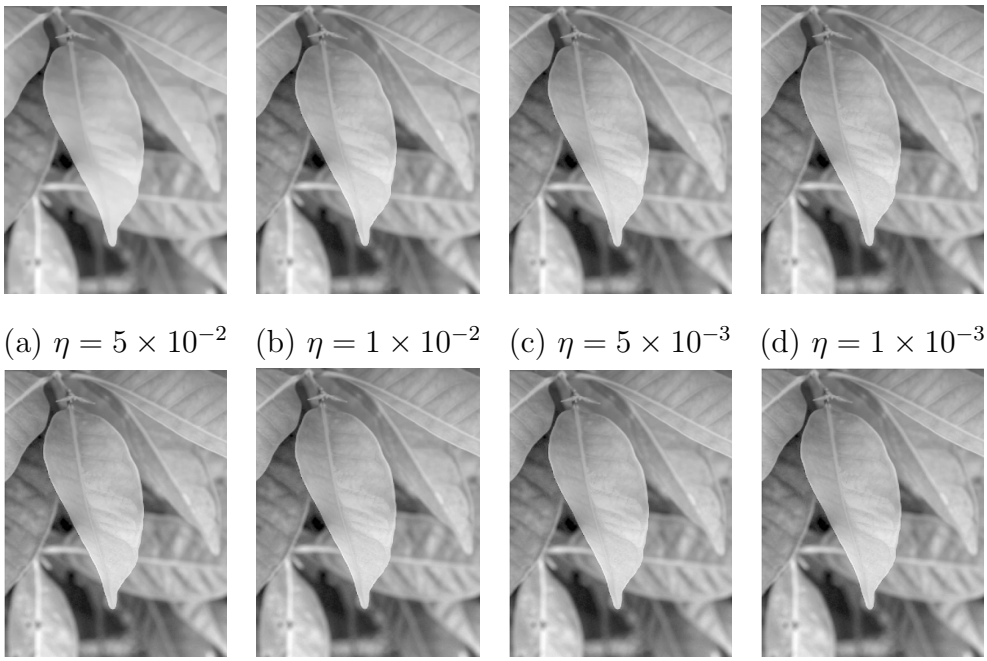

(a) $\eta = 5 \times 10^{-2}$ (b) $\eta = 1 \times 10^{-2}$ (c) $\eta = 5 \times 10^{-3}$ (d) $\eta = 1 \times 10^{-3}$

(e) $\eta = 5 \times 10^{-4}$ (f) $\eta = 1 \times 10^{-4}$ (g) $\eta = 5 \times 10^{-5}$ (h) $\eta = 1 \times 10^{-5}$

Figure 5.6: The results of lightness reconstruction with different η as in (5.8).

Algorithm 1. **Numerical algorithm for solving** (5.8)

---

1. Initialize $u^0, d^0, r^0,$ and c^0.

2. For $k = 0, 1, 2, \ldots$, generate u^{k+1} from u^k according to the following iteration:

   (a) $u^{k+1} \longleftarrow \arg\min_u \frac{1}{2}\|W_1^h u - C_1\|_2^2 + \frac{\mu}{2}\big\|\sum_j u(j) - \sum_j \widetilde{R}(j) + c^k\big\|_2^2 + \frac{\rho}{2}\big\|W_1^h u - d^k + r^k\big\|_2^2$;

   (b) $d^{k+1} \longleftarrow \mathcal{T}_{\eta/\rho}\big(W_1^h u^{k+1} + r^k\big)$;

   (c) $r^{k+1} \longleftarrow r^k + (W_1^h u^{k+1} - d^{k+1})$;

   (d) $c^{k+1} \longleftarrow c^k + (\sum_j u^{k+1}(j) - \sum_j \widetilde{R}(j))$;

   until $\|u^{k+1} - u^k\|_2 \leq \epsilon$ for some tolerance ϵ.

3. $R^* \longleftarrow u^{k+1}$.

The overall algorithm for inpainting and adjustment of the lightness channel is summarized in Algorithm 2. See Figure 5.8 for an illustration of the changes on the overall lightness and the distribution of lightness values after applying Algorithm 2 on a sample image.

Algorithm 2. **Inpainting and adjustment of the lightness channel**

Input: the original lightness channel L.

Output: the inpainted and adjusted lightness channel L^*

Steps:

1. Obtaining the inpainted lightness channel $\widetilde{L}$ from L by solving (5.2);
2. Converting $\widetilde{L}$ to its logarithm $\widetilde{R}$ via (5.3) and computing the associated framelet coefficients $W_1^h\widetilde{R}$;
3. adjusting the framelet coefficients $W_1^h\widetilde{R}$:
   (a) define the pixel-wise attenuation weights θ as (5.5) using a $Q(=3)$-level framelet decomposition $W_3^h\widetilde{R}$;
   (b) computing adjusted framelet coefficients $\Theta(W_1^h\widetilde{R})$ by applying Θ on $W_1^h\widetilde{R}$ as in (5.4).
4. Reconstructing a new lightness channel L^* from adjusted coefficients $\Theta(W_1^h\widetilde{R})$:
   (a) constructing R^* from $\Theta(W_1^h\widetilde{R})$ by solving (5.8), and then taking exponential of R^* to get the adjusted lightness channel L^*;
   (b) re-scaling the values of the adjusted lightness channel L^* as in (5.9).

5.3.3 Recovering the chromatic channels $[a;\ b]$

Clearly, for those over-exposed pixels as defined by (5.1) in Section 5.3.1, both chromatic channels $[a; b]$ are saturated such that the original chromatic information is erased. It thus becomes an inpainting problem in two chromatic channels on how to recover the erased chromatic information. Similar to the inpainting approach in the lightness channel stated in Section 5.3.1, the pixels for recovery are first identified and then recovered by an inpainting process.

The strategy of defining pixels for recovery in two chromatic channels is slightly different from that in the lightness channel. The visual perception of the colour in human is very complicated. A slight change in two chromatic channels may

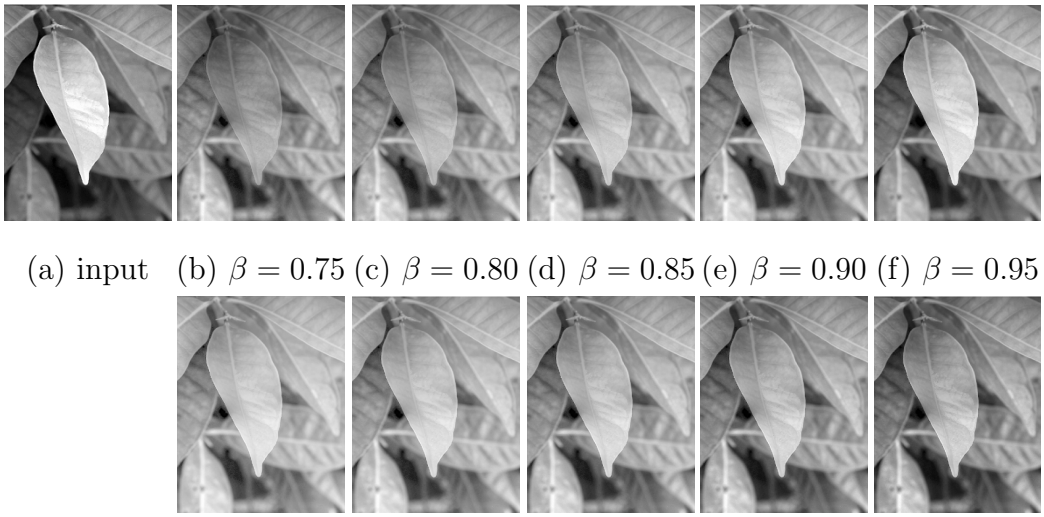

(a) input (b) $\beta = 0.75$ (c) $\beta = 0.80$ (d) $\beta = 0.85$ (e) $\beta = 0.90$ (f) $\beta = 0.95$

(g) $c' = 0.05$ (h) $c' = 0.10$ (i) $c' = 0.20$ (j) $c' = 0.40$ (k) $c' = 0.80$

Figure 5.7: The lightness adjustment using different β and c' as in (5.5). (a) The input; (b)–(f) the lightness adjustment results using different β and $c' = 0.2$; (g)–(k) the results using different c' and $\beta = 0.88$.

lead to a fairly large change in human colour perception. Thus, to avoid some rapid changes along the boundary between the over-exposed regions and the well-exposed regions, one good approach is to define a super-set of pixels for recovery. In other words, the set of pixels for recovery could contain not only those over-exposed pixels, but also all pixels whose lightness values are sufficiently large and whose chromatic values are sufficiently small in magnitude. Moreover, similar to [45], the assignment of pixels for recovery is done in a "soft" manner, instead of a"hard" manner as (5.1). More specifically, pixels for chromatic recovery should be

(i) of high lightness intensities (i.e., close to 100),

(ii) of inadequate chromatic information (i.e., both a, b values close to 0).

Based on the above argument, the likeliness measure of a pixel p being a pixel for recovery in two chromatic channels is defined by the following measurement as

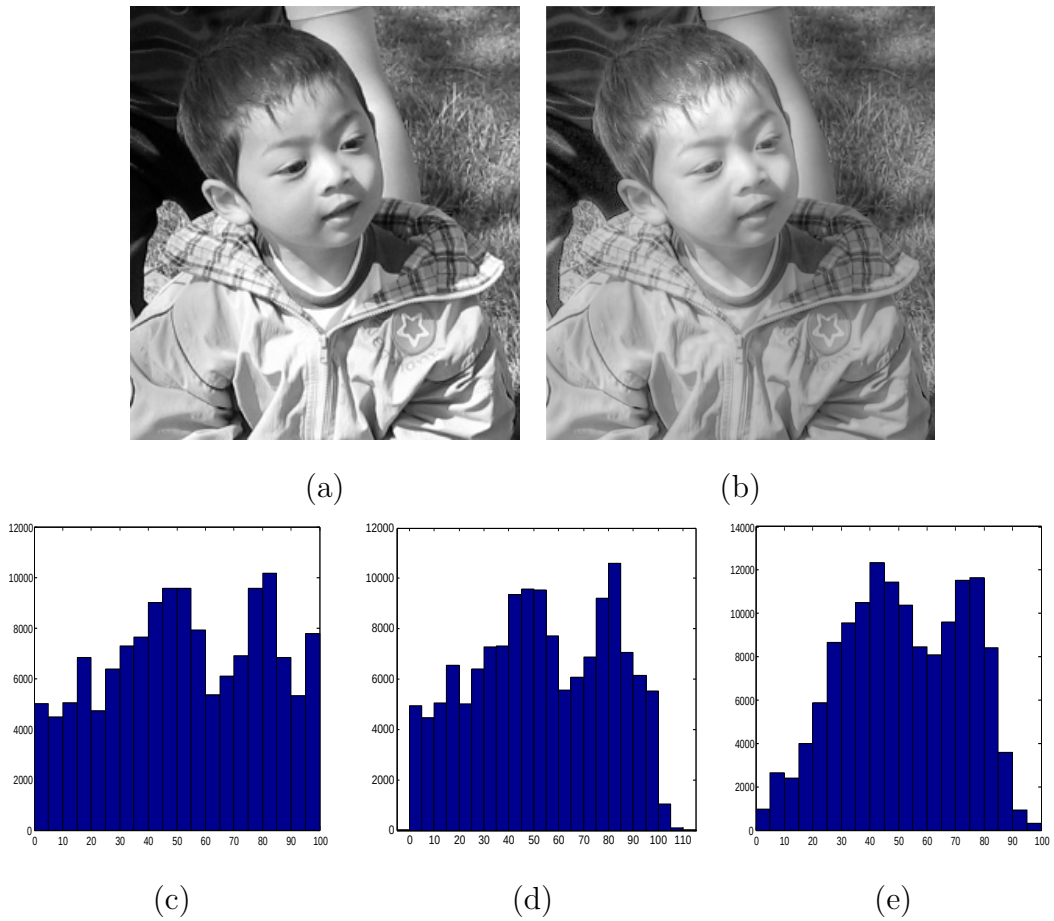

Figure 5.8: Illustration of lightness inpainting and adjustment by Algorithm 2. (a) The input lightness channel, (b) the lightness channel after inpainting and adjustment by Algorithm 2, (c) the histogram of the input lightness channel, (d) the histogram of the lightness channel after lightness inpainting; and (e) the histogram of the lightness channel after lightness inpainting and adjustment. It is seen from (d) that the lightness range of lightness channel is $[-5, 115]$ after applying lightness inpainting method, which goes beyond the physical range $[0, 100]$. Also, it is seen from (e) that the pixels of lightness close to 0 or 100 are fewer in the output of Algorithm 2.

proposed in [45]:

$$M(p) = \frac{1}{2}\Big(\tanh\big(\frac{1}{60}((L(p) - \ell_0) + (c_0 - \sqrt{a^2(p) + b^2(p)}))\big) + 1\Big), \tag{5.10}$$

where ℓ_0 and c_0 are two constants related to the values along the boundary of over-exposed regions. Same as in [45], the values of ℓ_0 and c_0 are set empirically to be 80 and 40 respectively in (5.10) in implementations. A pixel p is defined as a pixel for recovery in two chromatic channels if $M(p) > \tau$ for some pre-defined positive constant $\tau \in (0, 1)$, so the index set of pixels for chromatic recovery is determined via

$$\Omega = \{p : M(p) > \tau\}. \tag{5.11}$$

Since the value of τ in (5.11) is to determined the over-exposed regions that need chromatic recovery, thus it cannot be very large, otherwise the over-exposed regions would not be fully covered; the value of τ cannot be very small either, otherwise the detected region for chromatic recovery would be too large and some existing chromatic details would be erased. We suggest to set τ in (5.11) inside the range $[0.4, 0.7]$. See Figure 5.9 for an illustration of the results using different τ. In all experiments of this thesis, we simply set $\tau = 0.5$.

The appearance of two chromatic channels of natural images is quite different from that of the lightness channel. There are much more visible variations in two chromatic channels than the lightness channel, which account for the fine details of the photograph. Motivated by the successes of sparsity prior of natural greyscale images in wavelet tight frame for various image restoration tasks (e.g. [14, 32, 12]), we propose to use the ℓ_1 norm of wavelet tight frame coefficients as the sparsity prompting functional to regularize the inpainting process. The following minimization model is proposed for the recovery of the chromatic channel **a** (the same for the recovery of the channel **b**):

$$a^* = \text{argmin}_u \|\text{diag}(\lambda) W u\|_1, \quad \text{subject to } u|_{\Omega^c} = a|_{\Omega^c}, \tag{5.12}$$

(a) $\tau = 0.4$ (b) $\tau = 0.5$ (c) $\tau = 0.6$ (d) $\tau = 0.7$ (e) $\tau = 0.8$ (f) $\tau = 0.9$

Figure 5.9: Over/under-exposure correction using different τ as in (5.11). The input photograph is the one shown in Figure 5.2 (a). It is seen that if τ is set too large, e.g. $\tau = 0.8$ or 0.9, the colour shown on the recovered over-exposed regions is less vivid.

where Ω is the index set of the pixel for recovery, and Ω^c denotes its complement (see Figure 5.9). The diagonal matrix $\text{diag}(\lambda)$ is the weighting matrix whose diagonal elements are determined by the likeliness measure of the corresponding pixel being saturated in the channel **a**. Intuitively, the larger is the likeliness measure of the pixel being saturated in the channel **a**, the larger the associated weight should be. Thus, the assigned weights should be monotone increasing with respect to the likeliness measure $M(p)$ as defined in (5.10). Based on the empirical observations, in our implementation, the following weighting matrix is proposed to enhance the performance

$$\lambda(c_{j,k}(p)) = (M(p) + \frac{1}{5})^2 + \frac{2}{5}.$$

To better regularize images with edges of multiple orientations, we use the wavelet tight frame system consisting of two framelet systems. One is the standard 2D tensor product of 1D piecewise linear framelet; and the other is the 2D tensor product of 1D piecewise linear framelet rotated by 45 degree. It is empirically observed that such a two-system tight frame system propagates the chromatic information from the well-exposed pixels to pixels for recovery better than that

of a single tight frame system. The minimization (5.12) is the so-called *analysis*-based approach (see [67]), which, similar as (5.8), can also be efficiently solved by the split Bregman method.

Moreover, it is observed that a direct reconstruction of the colour photograph from the corrected $[L; a; b]$ channels will lead to some visual distortions on the colour of recovered pixels, due to the complex nature of how human perceive colour. Thus, we propose further adjustments on the two chromatic channels to keep the consistency of colour perception by normalizing the two chromatic channels as follows

$$a^* \longleftarrow \Big(\frac{L^*}{L}\Big)^{\frac{1}{2}} a^* \quad \text{and} \quad b^* \longleftarrow \Big(\frac{L^*}{L}\Big)^{\frac{1}{2}} b^*,$$

where L is the original lightness channel, L^* is the recovered lightness in (5.9). The final photograph is then synthesized from the three channels $[L^*; a^*; b^*]$. A detailed description of the numerical solver for (5.12) is given in Algorithm 3. Two parameters in Algorithm 3 is set as follows: $\mu = 0.4$ and $\rho = 0.5$. See Figure 5.10 for an illustration of the recovery of the two chromatic channels for a sample photograph.

Algorithm 3. **Numerical algorithm for recovering the chromatical channel** a (b)

---

1. Initialize $u^0, d^0, r^0,$ and c^0.

2. Let P_{Ω^c} denote the sample operator that only keeps the elements whose index in the set Ω^c. Then, for $k = 0, 1, 2, \ldots$, generate u^{k+1} from u^k according to the following iteration:

   (a) $u^{k+1} \longleftarrow \arg\min_u \frac{\mu}{2}\big\|P_{\Omega^c}(u - a) + c^k\big\|_2^2 + \frac{\rho}{2}\big\|Wu - d^k + r^k\big\|_2^2$;

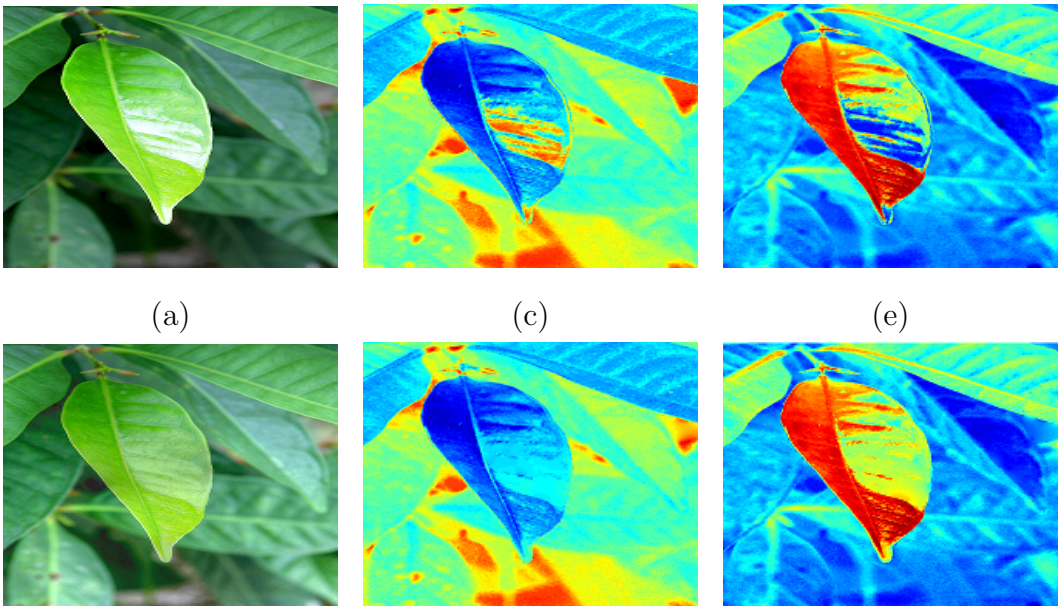

(a) (c) (e)

(b) (d) (f)

Figure 5.10: Illustration of chromatic recovery. (a) The input photograph; (b) the synthesized photograph after lightness inpainting, adjustment and colour recovery; (c) input a-channel; (d) recovered a-channel; (e) input b-channel; (f) recovered b-channel.

(b) $d^{k+1} \longleftarrow \mathcal{T}_{\lambda/\rho}\big(Wu^{k+1} + r^k\big)$;

(c) $r^{k+1} \longleftarrow r^k + (Wu^{k+1} - d^{k+1})$;

(d) $c^{k+1} \longleftarrow c^k + P_{\Omega^c}(u^{k+1} - a)$;

until $\|u^{k+1} - u^k\|_2 \leq \epsilon$ for some tolerance ϵ.

3. $a^* \longleftarrow \left(\frac{L^*}{L}\right)^{\frac{1}{2}} u^{k+1}$.

In the end, the proposed approach for correcting overall over/under-exposure in photograph is summarized in Algorithm 4.

Algorithm 4. **Wavelet tight frame based method for recovering over/under-exposed regions**

1. Converting the RGB channels of the given image I into the CIELAB channels $[L; a; b]$;

2. Inpainting and adjusting lightness channel L.

   (a) Recovering the lightness channel $\widetilde{L}$ by inpainting the lightness values of over/under-exposed regions with clipped pixels by solving the minimization problem in (5.2).

   (b) Adjusting the lightness channel $\widetilde{L}$ of high dynamic range to obtain the lightness channel L^* of low dynamic range without losing visible image details using Algorithm 2.

3. Recovering the missing chromatic details of the over-exposed regions in two chromatic channels $[a; b]$ by solving the minimization problem in (5.12) using Algorithm 3, and as a consequence obtaining the recovered chromatic channels $[a^*; b^*]$.

4. Synthesizing the new colour photograph using the three channels $[L^*; a^*; b^*]$.

5.4 Numerical experiments and discussions

The proposed algorithm for correcting over/under exposure is evaluated on several real photographs taken by a regular LDR camera. Some tested images are from

[45] and [40]. Some are captured by our own using a Canon DSLR camera. The average time for processing a colour image of size 500×800 is around 3 minutes by using MATLAB (version 7.10.0) implemented on a laptop PC with Intel T9400 CPU (2.53 GHz) and 4 GB RAM.

5.4.1 Experimental evaluation

The proposed method is compared against several other existing methods. The methods for comparison include two existing over-exposure correction methods: Masood *et al.*'s method [54], Guo *et al.*'s method [45]. These two methods are specifically designed for correcting over-exposure in photograph. Also, to illustrate the differences between the problem of over-exposure correction and other colour correction problems, we also include two other related colour correction methods in the comparison. One is the spline framelet based generic image inpainting method [14], and the other is the combination of the HDR reconstruction method [58] and the tone mapping method [40]. The results of those methods are either directly quoted from the referenced research articles or computed from the authors' implementation downloaded from the web. The results using the proposed method and four other methods are shown in Figure 5.11–5.14 for visual comparison.

In the test image shown in Figure 5.11 (a), several regions on the leaves appear to be over-exposed with very high reflection. In the result from Masood *et al.*'s method, some existing details are erased. In the result produced by the HDR plus tone mapping method, the lost chromaticity information within the over-exposed regions has not been restored as they still appear shine white. Cai *et al.*'s method restores the lost colour information of the over-exposed regions, but the repaired over-exposed leaves look slightly darker than their neighbourhoods. Such a reflection is not realistic in real life. In contrast, two over-exposure correction

method: Guo *et al.*'s method and ours do a better job on correcting over-exposure with realistic reflection. But the result from Guo *et al.*'s method appears to be a little bit too dim. The reason is that only tone mapping is done in Guo *et al.*'s method that will lower the overall brightness of the image. Our method does not have this problem and the result looks well-exposed.

In the image shown in Figure 5.12 (a), several regions on the boy's body are over-exposed. Masood *et al.*'s method partially recovers the damaged colour information, but it also degrades the visual quality of some well-exposed regions like the boy's cheek. In the result produced by Cai *et al.*'s inpainting method, the damaged chromatic information has been largely recovered. But the resulting image still suffers from the un-realistic local contrast on those repaired regions. In the result produced by the HDR plus tone mapping method, there is no significant improvement shown for those over-exposed regions. In contrast, our method and Guo *et al.*'s method both recover the damaged chromatic information in the over-exposed regions and preserve local lightness contrasts. Again the overall brightness of our result is better balanced than that from Guo *et al.*'s method. The results shown in Figure 5.13 and Figure 5.14 also are consistent with what we observed in Figure 5.11 and Figure 5.12.

In summary, the two related restoration methods are not very suitable for correcting over-exposure in photograph. The image inpainting method will recover the colour but will not produce correct brightness of over-exposed regions. As a result, the local contrast and the reflection in the area around over-exposed regions do not appear to be realistic with respect to natural light conditions. The combination of general-purpose HDR and tone mapping method is not suitable for correcting over-exposure neither. They are designed for dealing with large change on dynamic range, not for the case of over-exposure correction which only need about no more than 20% of change in dynamic range. Masood *et al.*'s method

(a) Input

(b) Masood *et al.* [54]

(c) Guo *et al.* [45]

(d) Cai *et al.* [14]

(e) HDR [58] + tone mapping [40]

(f) Our result

Figure 5.11

often cannot find correct colour of over-exposed regions, since their approach only considers the case of partial over-exposure. The best two performers are Guo *et al.*'s method and the proposed method. However, the results from Guo *et al.*'s method often seem to be the images taken with in-sufficient exposure time. The reason is that there is not any process similar to HDR reconstruction involved in their approach. In contrast, our approach produces well-exposed images.

5.4.2 Conclusions and future work

We present a new wavelet frame based approach for correcting pixels that are affected by over- and under-exposure in an input photograph. Numerical results on

(a) Input image from [45]

(b) Masood *et al.* [54]

(c) Guo *et al.* [45]

(d) Cai *et al.* [14]

(e) HDR [58] + tone mapping [40]

(f) Our result

Figure 5.12

(a) Input image from [45] (b) Masood *et al.* [54] (c) Guo *et al.* [45]

(d) Cai *et al.* [14] (e) HDR [58] + tone mapping [40] (f) Our result

Figure 5.13

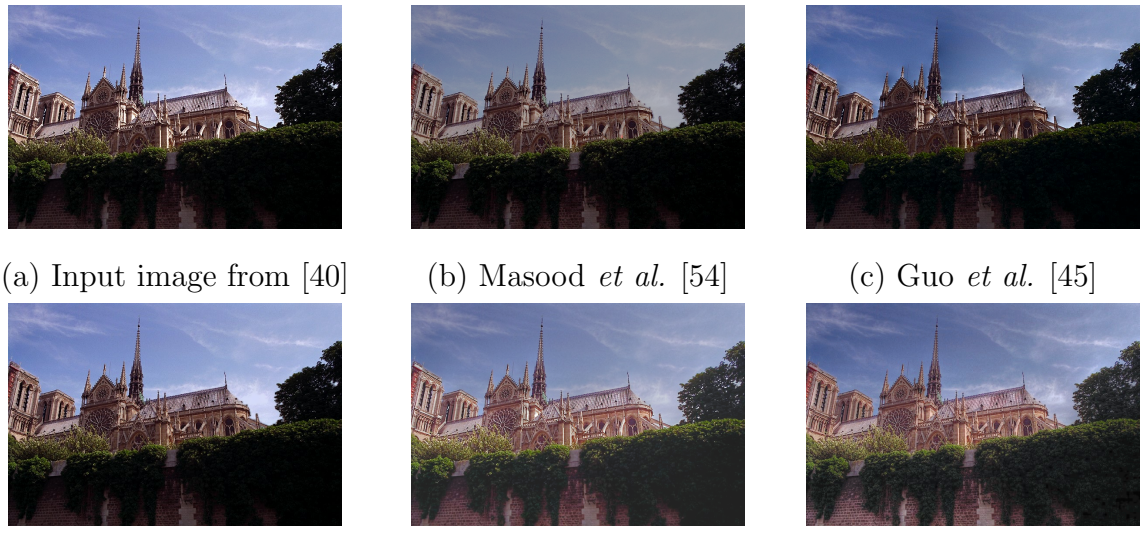

(a) Input image from [40] (b) Masood *et al.* [54] (c) Guo *et al.* [45]

(d) Cai *et al.* [14] (e) HDR [58] + tone mapping [40] (f) Our result

Figure 5.14

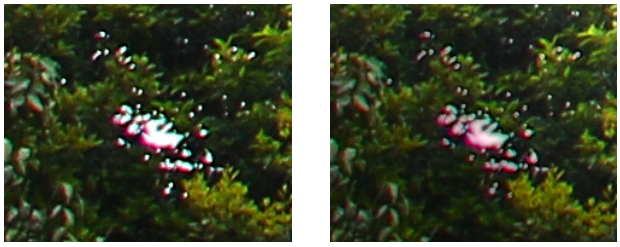

(a) (b)

Figure 5.15: Demonstration of the failure in the presence of chromatic aberration by our algorithm.

real photographs show that our algorithm can more efficiently improve the visual quality of both over-exposed and under-exposed regions of the input photograph than some existing methods. There are still a few issues remaining when dealing with certain types of over-exposure. One is chromatic aberration occurring near the boundary of over-exposed regions (see Figure 5.15). In the proposed approach, these aberrant values might be propagated into the over-exposed regions during the chromatic recovery procedure, consequently unfaithful colourized result might be produced. Another issue is the small halo-like artifacts shown in the image with over-exposure. Currently there is no mechanism in our approach for removing these halo-like artifacts. In the future, we will examine how to develop more robust recovery procedure to handle this chromatic aberration problem and suppress halo-like artifacts in photographs with over/under-exposure.

Bibliography

[1] J. J. Benedetto and S. Li, *The theory of multiresolution analysis frames and applications to filter banks*, Applied and Computational Harmonic Analysis, 5 (1998), pp. 389–427.

[2] J. J. Benedetto and J. R. Romero, *Measure and theoretic characterization of multiresolution frames in higher dimensions*, Journal of Applied Functional Analysis, 2 (2007), pp. 403–426.

[3] M. Bertalmio, G. Sapiro, V. Caselles, and C. Ballester, *Image inpainting*, in Proc. SIGGRAPH, 2000, pp. 417–424.

[4] M. Bertalmio, L. Vese, G. Sapiro, and S. Osher, *Simultaneous structure and texture image inpainting*, IEEE Transactions on Image Processing, 12 (2003), pp. 882–889.

[5] C. D. Boor, R. A. Devore, and A. Ron, *On the construction of multivariate (pre-)wavelets*, Constructive Approximation, 9 (1993), pp. 123–166.

[6] C. D. Boor, R. A. Devore, and A. Ron, *Approximations from shift-invariant subspaces of* $\mathrm{L}_2(\mathbb{R}^d)$, Transactions of American Mathematical Society, 341 (1994), pp. 787–806.

[7] C. D. Boor, K. Höllig, and S. D. Riemenschneider, *Box Splines*, Springer-Verlag, 1993.

[8] J. Cai, R. Chan, L. Shen, and Z. Shen, *Simultaneously inpainting in image and transformed domains*, Numerische Mathematik, 112 (2009), pp. 509–533.

[9] J. Cai, R. Chan, and Z. Shen, *A framelet-based inpainting algorithm*, Applied and Computational Harmonic Analysis, 24 (2008), pp. 131–149.

[10] ——, *Simultaneous cartoon and texture inpainting*, Inverse Problem and Imaging, 4 (2010), pp. 379–395.

[11] J. Cai, B. Dong, S. Osher, and Z. Shen, *Image restoration: total variation, wavelet frames, and beyond*, Journal of the American Mathematical Society, 25 (2012), pp. 1033–1089.

[12] J. Cai, H. Ji, C. Liu, and Z. Shen, *Framelet based blind image deblurring from a single image*, IEEE Transaction on Image Processing, 21 (2012), pp. 562–572.

[13] J. Cai, H. Ji, F. Shang, and Z. Shen, *Inpainting for compressed images*, Applied and Computational Harmonic Analysis, 29 (2010), pp. 368–381.

[14] J. Cai, S. Osher, and Z. Shen, *Split Bregman methods and frame based image restoration*, Multiscale Modeling and Simulation, A SIAM Interdisciplinary Journal, 8 (2009), pp. 337–369.

[15] J. Cai and Z. Shen, *Framelet based deconvolution*, Journal of Computational Mathematics, 28 (2010), pp. 289–308.

[16] A. Chai and Z. Shen, *Deconvolution: A wavelet frame approach*, Numerische Mathematik, 106 (2007), pp. 91–104.

[17] R. H. Chan, T. F. Chan, L. Shen, and Z. Shen, *Wavelet algorithms for high-resolution image reconstrction*, SIAM Journal on Scientific Computing, 24 (2003), pp. 1408–1432.

[18] R. H. Chan, S. D. Riemenschneider, L. Shen, and Z. Shen, *High-resolution image reconstrction with displacement errors: A framelet approach*, International Journal of Imaging Systems and Technology, 14 (2004), pp. 91–115.

[19] R. H. Chan, L. Shen, and Z. Shen, *A framelet based approach for image inpainting*, Research Report 4, (2004), p. 325.

[20] T. F. Chan and J. Shen, *Mathematical models for local non-texture inpaintings*, SIAM Journal on Applied Mathematics, 62 (2002), pp. 1019–1043.

[21] T. F. Chan, J. Shen, and H. M. Zhou, *Total variation wavelet inpainting*, J. Math. Imaging Vision, 25 (2006), pp. 107–125.

[22] W. Chen and S. S. Goh, *Band-limited refinable functions for wavelets and framelets*, Applied and Computational Harmonic Analysis, 28 (2010), pp. 338–345.

[23] R. R. Coifman and D. L. Donoho, *Translation invariant de-noising*, Wavelets and Statistics, A. Antoniadis and G. Oppenheim, Eds. New York: Springer-Verlag, 103 (1992), pp. 125–150.

[24] P. L. Combettes and V. R. Wajs, *Signal recovery by proximal forward-backward splitting*, Multiscale Modeling and Simulation, 4 (2006), pp. 1168–1200.

[25] A. Criminisi, P. Patrick, and T. Kentaro, *Region filling and object removal by exemplar-based image inpainting*, IEEE Transactions on Image Processing, 13 (2004), pp. 1200–1212.

[26] I. Daubechies, *Orthonormal bases of compactly supported wavelets*, Communications on Pure and Applied Mathematics, 41 (1988), pp. 909–996.

[27] I. Daubechies, *Ten Lectures on Wavelets*, SIAM, 1992.

[28] I. Daubechies, B. Han, A. Ron, and Z. Shen, *Framelets: MRA-based constructions of wavelet frames*, Applied and Computational Harmonic Analysis, 14 (2003), pp. 1–46.

[29] I. Daubichies, A. Grossmann, and Y. Meyer, *Painless nonorthogonal expansions*, Journal of Mathematical Physics, 27 (1986), pp. 1271–1283.

[30] K. David, *A First Course in Fourier Analysis*, Prentice Hall, 2000.

[31] P. E. Debevec and J. Malik, *Recovering high dynamic range radiance maps from photographs*, ACM SIGGRAPH, (1997), pp. 369–378.

[32] B. Dong, H. Ji, J. Li, and Z. Shen, *Wavelet frame based blind image inpainting*, Applied and Computational Harmonic Analysis, 32 (2012), pp. 268–279.

[33] B. Dong and Z. Shen, *Pseudo-splines, wavelets and framelets*, Applied and Computational Harmonic Analysis, 22 (2007), pp. 78–104.

[34] ——, *MRA-based wavelet frames and applications*, vol. 19, IAS/Park City Mathematics Series, 2010.

[35] D. Donoho and M. Ramondo, *A fast wavelet algorithm for image deblurring*, The Australian & New Zealand Industrial and Applied Mathematics Journal, 46 (2005), pp. 29–46.

[36] D. L. Donoho, *De-noising by soft-thresholding*, IEEE Transactions on Information Theory, 41 (1995), pp. 613–627.

[37] I. Drori, D. Cohen-Or, and H. Yeshurun, *Fragment-based image completion*, in Proc. SIGGRAPH, 2003.

[38] R. J. Duffin and A. C. Schaeffer, *A class of non-harmoic fourier series*, Transactions of American Mathematical Society, 72 (1952), pp. 341–336.

[39] F. Durand and J. Dorsey, *Fast bilateral filtering for the display of high-dynamicrange images*, ACM Transactions on Graphics, 21 (2002), pp. 257–266.

[40] R. Fattal, D. Lischinski, and M. Werman, *Gradient domain high dynamic range compression*, ACM Transactions on Graphics, 21 (2002), pp. 249–256.

[41] T. Goldstein and S. Osher, *The split Bregman iteration for* L*1-regularized problems*, SIAM Journal of Imaging Sciences, 2 (2009), pp. 323–343.

[42] R. C. Gonzalez and R. E. Woods, *Digital Image Processing*, Prentice Hall, 2 ed., 2002.

[43] M. Granados, B. Ajdin, M. Wand, C. Theobalt, H. P. Seidel, and H. Lensch, *Optimal hdr reconstruction with linear digital cameras*, in Proc. CVPR, 2010.

[44] M. Grossberg and S. Nayar, *High dynamic range from multiple images: which exposures to combine?*, Color and Photometric Methods in Computer Vision, (2003), pp. 1–8.

[45] D. Guo, Y. Cheng, S. Zhuo, and T. Sim, *Correcting over-exposure in photographs*, in Proc. CVPR, 2010.

[46] B. Han, *On dual wavelet tight frames*, Applied and Computational Harmonic Analysis, 4 (1997), pp. 380–413.

[47] H. Holschneider, R. Kronland-Martinet, J. Morlet, and P. Tchamitchian, *A real-time algorithm for signal analysis with the help of the wavelet transform*, in Wavelets, Time-Frequency Methods and Phase Space, Springer-Verlag, Berlin, 1989, pp. 289–297.

[48] G. W. Larson, H. Rushemier, and C. Piatko, *A visibility matching tone reproduction operator for high dynamic range scenes*, IEEE transactions on Visulization and Computer Graphics, 3 (1997), pp. 291–306.

[49] A. Levin, D. Lischinski, and Y. Weiss, *Colorization using optimization*, in SIGGRAPH, 2004.

[50] Y. Li, L. Sharan, and E. H. Adelson, *Compressing and Companding High Dynamic Range Images with Subband Architectures*, in SIGGRAPH, 2005.

[51] S. Mallat, *Multiresolution approximations and wavelet orthonormal bases of $L_2(R)$*, Transations of the American Mathematical Society, 315 (1989), pp. 69–87.

[52] ——, *A Wavelet Tour of Signal Processing*, Academic Press Incorporation, San Diego, CA, 2nd ed., 1998.

[53] S. Mann and R. W. Picard, *On being undigital with digital cameras: Extending dynamic range by combining differently exposed pictures*, in Proceedings of IS&T, 1995, pp. 442–448.

[54] S. Z. Masood, J. Zhu, and M. F. Tappen, *Automatic correction of saturated regions in photographs using cross-channel correlation*, in Computer Graphics Forum (CGF), International Journal of Eurographics Association, 28(7), 2009.

[55] Y. Meyer, *Principle d'incertitude, bases hilbertiennes et algèbres d' opérateurs*, Séminaire Bourbaki, 662 (1986).

[56] ——, *Wavelets and Operators,* Translated by D. H. Salinger, Cambridge Studies in Advanced Mathematics, Cambridge University Press, 1992.

[57] K. N. Plataniotis and A. N. Venetsanopoulos, *Color Image Processing and Applications*, Springer-Verlag, Berlin, 2000.

[58] A. Rempel, M. Trentacoste, H. Seetzen, H. Young, W. Heidrich, L. Whitehead, and G. Ward, *Ldr2hdr: on-the-fly reverse tone mapping of legacy video and photographs*, ACM Transactions of Graphics, 26 (2007).

[59] S. D. Riemenschneider and Z. Shen, *Box-splines, cardinal series and wavelets*, Approximation Theory and Fundamental Analysis, 71 (1990), pp. 133–149.

[60] ——, *Wavelets and pre-wavelets in low dimensions*, Journal of Approximation Theory, (1992), pp. 18–38.

[61] A. Ron and Z. Shen, *Frames and stable bases for shift-invariant subspaces of $L_2(R^d)$*, Canadian Journal of Mathematics, 47 (1995), pp. 1051–1094.

[62] ——, *Affine systems in $L_2(R^d)$: the analysis of the analysis operator*, Journal of Functional Analysis, 148 (1997), pp. 408–447.

[63] L. Rudin, S. Osher, and E. Fatemi, *Nonlinear total variation based noise removal algorithms*, Phys. D, 60 (1992), pp. 259–268.

[64] J. Schanda, ed., *Colorimetry: Understanding the CIE System*, John Wiley & Sons Inc., 2007.

[65] I. J. Schoenberg, *Cardinal interpolation and spline functions*, tech. report, University of Wisconsin–Madison, 1968.

[66] L. Shen and Z. Shen, *Compression with time-frequency localization filters*, Wavelets and Splines, Athens, G.Chen, M. Lai eds, Nashboro Press, (2006), pp. 428–443.

[67] Z. Shen, *Wavelet frames and image restorations*, in Proceedings of the International Congress of Mathematicians, vol. 4, 2010, pp. 2834–2863.

[68] Z. Shen, K. C. Toh, and S. Yun, *An accelerated proximal gradient algorithm for frame-based image restoration via the balanced approach*, SIAM Journal on Imaging Sciences, 4 (2011), pp. 573–596.

[69] L. Wang, L. Wei, K. Zhou, B. Guo, and H. Shum, *High dynamic range image hallucination*, in EGSR, 2007.

[70] G. J. Ward, *A contrast-based scalefactor for luminance display*, Graphics Gems IV, P.S Heckbert, Ed. Academic Press Professional, (1994), pp. 415–421.

[71] Z. Xu, *Multivariate F-splines and fractional box splines*, Journal of Fourier Analysis and Applications, 15 (2009), pp. 723–738.

[72] X. Zhang and D. H. Brainard, *Estimation of saturated pixel values in digital color imaging*, J. Opt. Soc. Am. A, 21 (2004), pp. 2301–2310.

LOW DIMENSIONAL BAND-LIMITED FRAMELETS AND THEIR APPLICATIONS IN COLOUR IMAGE RESTORATION

HOU LIKUN

NATIONAL UNIVERSITY OF SINGAPORE

2013

Low dimensional band-limited wavelets, framelets and a framelet based method for over/under-exposure correction **Likun Hou**

2013